Prifysgol Abertawe
Swansea University

The implications of costly airflows for space-use and movement decisions in birds

Emmanouil Lempidakis

Supervised by:

Prof. Emily L.C. Shepard, Prof. Andrew N. Ross, Prof. Rory P. Wilson, Prof. Adrian Luckman.

Submitted to Swansea University in fulfilment of the requirements for the Degree of Doctor of Philosophy

Swansea University

2022

Abstract

The behavioural ecology of flight has largely considered how birds respond to mean flow conditions, but it is the gusty or extreme airflows that are likely to be particularly challenging. This thesis addresses this, examining the strategies birds use to negotiate turbulence over land, and exceedingly strong winds at sea. I first develop a method for sensing turbulence at fine scales using data collected onboard the animals themselves, taking homing pigeons (*Columba livia*) as model flapping fliers. Fine scale variation in the flight altitude and body displacement emerged as effective proxies of turbulence. I then assess the impact of freestream turbulence on flapping fliers and find that pigeons adapted their wingbeat kinematics (frequency and amplitude) to increase their flight stability in response to turbulence, but did so without a clear increase in flight effort. In my final two chapters I examine the responses of two seabird species to strong winds, first at sea, and then on land. Specifically, I investigate how streaked shearwaters (*Calonectris leucomelas*) respond to tropical cyclones, and how common guillemots (*Uria aalge*) select their breeding cliffs in relation to airflow conditions. I find that shearwaters fly towards the eye of the storm. This tendency increases with cyclone intensity and may enable birds to avoid strong onshore winds and reduce the associated risks of forced landings and/ or injury. Finally, computational fluid dynamics models reveal that guillemots select breeding cliffs that are sheltered from wind and storm conditions, rather than from the mean wind alone, or heat stress. This model of habitat selection could also predict habitat use across islands. Overall, this highlights the varied and sometimes surprising capacities of birds to cope with extreme and variable airflows and operate in areas that are, as yet, inaccessible to aircraft.

Declarations and statements

DECLARATION

This work has not previously been accepted in substance for any degree and is not being concurrently submitted in candidature for any degree.

Signed .....  .. (candidate)

Date ..... 26/03/22.....

STATEMENT 1

This thesis is the result of my own investigations, except where otherwise stated. Where correction services have been used, the extent and nature of the correction is clearly marked in a footnote(s).

Other sources are acknowledged by footnotes giving explicit references. A bibliography is appended.

Signed .....  ... (candidate)

Date ..... 26/03/22.....

STATEMENT 2

I hereby give consent for my thesis, if accepted, to be available for photocopying and for inter-library loan, and for the title and summary to be made available to outside organisations.

Signed .....  (candidate)

Date ..... 26/03/22.....

Table of contents

Acknowledgments

In life no one is self-made. Likewise while this thesis is my own work the support and contribution of others have been essential for implementing it. Not only in a professional level but also in a personal. However, before I start thanking people individually, I would like to thank everyone that unintentionally I might have missed. Please know that I am grateful to you all and please forgive me if I have not mentioned you here. Your contribution has been important!

Having said that, I could have not started this section in any other way other than thanking Professor Emily L.C. Shepard. I remember when the first days of my PhD someone asked me who is my supervisor and after my answer said: "you are lucky that Emily is your supervisor, she is one of the very good ones". What I did not realise at the time, I had the pleasure to keep seeing throughout these five years that I have been working with Emily. Emily is a remarkable scientist, a caring mother, a wonderful wife, and a special friend besides a supervisor, or a supervisor like supervisors should be. She is the hardest working person I know, and she always leads by example and sets the standards for the rest of us. Without her I would simply have not been where I am today, and I would have not materialised this thesis. I fully understand that this must have been said a lot, but it has been said a lot because it is true. This is the role that special people play in our lives. I am and I will always be grateful to her for everything that she has done for me, from guidance, advice, and support, to even funding extensions, all beyond what I would have ever hoped. Her input to all my chapter has been vital and there are no words that can describe how grateful I am, and no words can be enough to describe all that she has done for me.

Second, I need to thank another special person, Professor Andrew N. Ross. I first met Andrew in my PhD interview through Skype, and it was love at the first site. I cannot understand how this happened but from the first time that I looked at Andrew I knew that he is one of the kindest people I have ever met. I had the privilege to work with Andrew closely all these five years and I had so much fun working with him every week. It is necessary to say that his knowledge and understanding of the aerial environment and its processes guided me in the implementation of all my chapters.

Third, I believe acknowledgements in our lab cannot be written without thanking Professor Rory P. Wilson. I wonder if there is anything left to say about Rory that has not been said before. I first met Rory when I was working with him for my master's thesis and he is the first person who has ever made me truly feel good about myself. His wisdom is second

to none and his excitement is infectious, and I had the pleasure to experience these also in my PhD. Emily, Andrew and Rory are just people that you simply do not want to live without! The day you offered me this PhD is the day I learned how happiness truly feels. For this I will always be grateful!

Following this, I need to thank Professor Adrian Luckman. Adrian was my first supervisor during my master's thesis, and he has always been available for me to help and to listen, especially during the period when Emily was on maternity leave. He has only shown sincere caring to me and always tried to help in every way possible. From anxiety levels to spatial analysis. Thank you Adrian, I will always be grateful for what a remarkable person you are.

Special thanks need also to be given to Professor Luca Börger for always being warm and for all his support especially with statistical modelling.

Then I need to thank all the people in the Swansea laboratory for animal movement. Those that have been with me during my entire PhD and those that have visited us for a shorter period. It has been such a pleasure being there with you all. Special thanks have to go to my friend Dr Baptiste Garde who I had the pleasure to work with the most and even live with during our collaboration with the Max Planck institute in Germany. Baptiste is a dear friend that I dearly miss. Then of course I need to thank Dr James Redcliffe, Dr Lloyd Hopkins, Dr Will Kay, Dr Richard Gunner, and Dr Gwen Wilson for being my friends and for making my life better. This brings me to my favourite person in the lab, the ever hard working Dr Mark Holton. Mark has helped me tremendously with logger handling and processing in DDMT but has also been a friend to chat about all the silly things I do like to talk about sometimes.

But as mentioned during this PhD I had the pleasure to collaborate with wonderful people in the Max Planck institute for animal behaviour during my visits in Germany. I would like to thank you all for being so welcoming and kind, for all your efforts to help me, and your hospitality. I had the privilege to especially receive these from Kami Safi, Micha Quetting, Heidi Schmid, and Bernhard Banzer with which I worked with the most. Micha Heidi and Bernhard have supported me throughout my data collection for chapters 2 and 3 and Micha made me feel welcomed by even accommodating me in his own home. But even when I was in Germany for data analysis only, Kami opened his lab for me, he offered his wisdom on my work, and spent time with me in fruitful and joyful conversations.

As this section is getting closer to an end, I would like to thank my parents for their support all these years. We had good and dark times and I know that you always had the best intentions and only love for me. For this I am grateful!

Finally, I need to thank the person who has helped me the most not only to change my life but even to survive it as he has been my friend through many dangers. That person is my therapist Dr Yannis Fronimos. This thesis is dedicated to him because I used to know nothing else other than fear and conflict in my life, and he has helped me to find peace, take leaps of faith and more than anything else to know myself and my story.

In conclusion I would like to finish this section the way I started it. I want to thank everyone who has been part of my story and who I am. No one is self-made in life, we all grow with others and learn from others and how beautiful is science for being built in this same way.

Funding

This PhD was funded by the European Research Council under the European Union's Horizon 2020 research and innovation program (grant 715874 to E. L. C. Shepard) and a Max Planck Sabbatical Fellowship (to E. L. C. Shepard).

Fieldwork for chapters 1 and 2 was also supported by the Deutsche Forschungsgemeinschaft (DFG, German Research Foundation) under Germany's Excellence Strategy – EXC 2117 (grant 422037984 to M. Wikelski).

Fieldwork conducted in the Sea of Japan by contributing authors was funded by Grants-in-Aid for Scientific Research from the Japan Society of the Promotion of Science (24681006, 16H01769, 16H06541, 16K21735, 21H05294 to K. Yoda).

Ethics statements and approvals

Personal

Ethical permissions for the tagging and handling of homing pigeons (*Columba livia*), for chapters 1 and 2 in Germany, were granted by the Swansea University AWERB, issue number IP-1718-23 and the Regierungspräsidium Freiburg, Baden-Württemberg, Germany, permit number G-17/92.

Contributing authors

Ethical permissions for the capture and tagging of streaked shearwaters (*Calonectris leucomelas*), for chapter 4 in the Sea of Japan, were provided by the Animal Experimental Committee of Nagoya University (GSES08–18) and the Ministry of the Environment Government of Japan.

Disclaimer and author contributions

Chapter 5 has been published, and chapters 2 and 4 have been submitted for publication in peer-reviewed journals (see chapter title pages for details). The contribution of co-authors in each chapter are listed below.

Chapter 2: Estimating fine-scale changes in turbulence using the movements of a flapping flier.

The study was conceived by Emily L.C. Shepard (ELCS), Emmanouil Lempidakis (EL), Michael Quetting (MQ) and Martin Wikelski (MW). Data collection was carried out by EL and Baptiste Garde (BG) and the ultralight was flown by MQ. EL undertook the data analysis with input from Andrew N. Ross (ANR) and ELCS. The estimation of turbulence strength from the ultrasonic anemometer was implemented with code written by ANR. The text was first drafted by EL with input from ELCS. All authors commented on the final draft.

Chapter 3: Turbulence affects the flight kinematics of an obligate flapping flier.

The study was conceived by ELCS, EL, ANR and MW. Data collection was carried out by EL and BG and overseen by MQ. EL undertook the data analysis with input from ANR and ELCS. The estimation of wingbeat frequency and amplitude was implemented with code provided by BG and edited by EL. The text was first drafted by EL with input from ELCS.

Chapter 4: Pelagic seabirds reduce risk by flying into the eye of the storm.

The study was conceived and designed by ELCS, EL, ANR and Ken Yoda (KY). Data collection was conducted by KY, Sakiko Matsumoto (SM), and Shiho Koyama (SK). EL undertook the data analysis with input from ANR and ELCS, and Ichiro Takeuchi (IT) advised on the implementation of statistical models. The text was first drafted by EL with input from ELCS. ANR and KY commented on the final draft.

Chapter 5: Airflow modelling predicts seabird breeding habitat across islands.

The study was conceived and designed by ELCS, EL and ANR. EL undertook the data analysis with input from ANR and ELCS. Statistical modelling was overseen by Luca Börger (LB). The text was first drafted by EL with input from ELCS. ANR and LB commented on the final draft.

List of figures and tables

List of abbreviations

3D	Three dimensional
ABG	Altitude above ground
AIC	Akaike information criterion
AOC	Area under the curve
ASL	Altitude above sea level
BIC	Bayesian information criterion
BP	Bird position in relation to the eye of a storm, with 0^o indicating a position in front of the eye and 180^o behind the eye of a storm ($0 – 360^o$)
CFD	Computational fluid dynamics
CI	Confidence intervals
C_p	Specific heat capacity
CRW	Crosswind component
DD	Daily Diary
DDMT	Daily Diary Multiple Trace software
DEM	Digital elevation model
DSM	Digital surface model
ECMWF	European Centre for Medium-Range Weather Forecasts
EDF	Estimated degrees of freedom
ERA5	ECMWF Reanalysis 5^{th} generation
f	Time series frequencies
FD	The direction to which a bird is flying ($0 – 360^o$)
FDL	Flight direction in relation to the closest location on land, with 0^o indicating a flight towards land and 180^o flight away from land ($0 – 360°$)

FDS	The direction to which a bird is flying in relation to the location of the eye of a storm (0 – 360º)
fs(f)	Log power spectrum
g	Gravitational acceleration
GAM	Generalised additive model
GAMM	Generalised additive mixed-effect model
GPS	Global positioning system
h	Boundary layer depth
HWC	Headwind component
IBTrACS	International Best Track Archive for Climate Stewardship (US NOAA)
ID	Identity
IQR	Interquartile range statistic
JMA	Japan meteorological agency
L	Latent heat of vaporisation of water
LD	The direction that a bird would have to fly to travel straight to the closest location of land (0 – 360°)
LES	Large eddy simulations
LHF	Surface latent heat
LiDAR	Light detection and ranging
MeanU	Mean wind speed
MED	Median statistic
OA	Overall accuracy
p	Surface pressure
RANS	Reynolds averaged Navier-Stokes
re	Random effect
Ref.df	Maximum available degrees of freedom

SA	Storm angle. The direction a bird would have to travel to fly straight to the eye of a storm (0 – 360º)
SD	Storm direction. The direction to which a storm is travelling (0 – 360°)
SHF	Instantaneous surface sensible heat flux
SI	Straightness index
Skew	Skewness statistic
sqrt	Square-root
T	Surface temperature
ti	Tensor product interaction
TI	Turbulence intensity
TKE	Turbulence kinetic energy
ts	Thin plate regression spline
TSS	True skill statistic
u^*	Shear velocity
U_2	Vertical wind component
UAV	Unmanned aerial vehicle
VAR	Variance statistic
VeSBA	Vectorial static body acceleration
V_z	Climb rate
w^*	Convective velocity
ΔAIC	Delta Akaike information criterion
ε	Dissipation rate of turbulence eddies
θ	Potential temperature
θ_v	Virtual temperature
ρ	Air density

Chapter 1: General introduction

In February 2022, storm Eunice hit the UK, generating gusts of 92 miles per hour in Swansea and up to 122 miles per hour in England (provisionally the highest ever recorded). Over 20 million people were advised to stay indoors, as the storm was forecast to cause a danger to human life. As the winds increased to storm strength it was clear that birds follow different rules: gulls, corvids, and pigeons were all still flying, and what is more, many of them, even pigeons, were soaring above the trees and houses. It is not just their responses to extreme winds that highlights the remarkable flight performance of birds; some operate in strong turbulence, with great frigate birds (*Fregata minor*) soaring hundreds of metres within cumulus clouds (Weimerskirch et al., 2016), in which birds can encounter highly turbulent conditions. But perhaps most challenging of all is the negotiation of strong and/ or turbulent airflows when birds are flying close to ground. Here, there is little room for error, as collision with the land is often fatal. And yet while large numbers of birds collide with buildings (Nichols et al., 2018), apparently oblivious to surfaces that are reflective in the day and dazed by lights at night (Elmore et al., 2021), there are only a few records of birds injuring themselves during landing or take-off in the natural environment (Shepard et al., 2019). Equally, while vagrants do appear either ahead of or following storms, they tend to be few in number (e.g. Van Bemmelen and Wielstra, 2008). Birds must therefore possess strategies that enable them to respond to extreme and variable flight conditions safely. While these strategies may ultimately have important consequences for fitness, we know intriguingly little about them.

Responses to wind: moving beyond the mean

Birds show a wide range of behaviours in response to changes in mean wind speed. This is primarily because wind can have a profound impact on the ability of birds to make progress in a desired direction, and hence the cost of covering a unit distance i.e. the costs of transport (Hedenström, 1993). As a result, birds show well-documented changes in airspeed in relation to the wind conditions to reduce their flight costs, which can be predicted using a framework adopted from aeronautical engineering (Hedenström, 1993). A range of studies (e.g. Liechti et al., 1994, Pennycuick et al., 2013) have shown that birds tend to follow these predictions, with birds increasing their airspeed in headwinds and reducing it with wind assistance. Although, this simple relationship is further complicated by factors such as whether birds are flying in flocks, and their movement objective (Hedenström and Åkesson, 2016).

Birds also adapt their flight path in relation to wind. Wind speed and direction change vertically and many birds adjust their flight altitude to exploit tail winds or minimise the headwind component. This has been observed in birds undertaking relatively short foraging trips (e.g. Krüger and Garthe, 2001), as well as long migrations(e.g. Dokter et al., 2011) Large-scale patterns of wind circulation also influence migration routes (Kranstauber et al., 2015), with birds sometimes deviating from the shortest route in order to benefit from tail-wind assistance. The length of migration flight legs and stopovers can also be adjusted according to the availability of favourable winds (Liechti, 2006). Even when birds are not adapting their course to take advantage of tailwinds, they must still respond to the wind vector in order to compensate for wind drift to reach their goal. Compensation for wind drift is a complex task requiring adjustment of heading and speed (McLaren et al., 2014) and it can be seen not only during migration but also during the daily commute back to a central place (i.e. colony) (Goto et al., 2017). Yet the appearance of vagrants after storms suggests that in extreme winds, birds cannot always achieve it.

While the effects of the mean wind condition on flight are relatively well documented, we know far less about how birds are impacted by the flow variability around the mean i.e. the turbulence (Shepard et al., 2016). More specifically, turbulence is a measure of the chaotic variability in the flow's pressure and wind speed/ direction. Turbulence is common in nature (Zhiyin, 2015), and laboratory studies suggest that turbulence can have a substantial impact on flight energetics and control (Ravi et al., 2015). It is possible that birds also vary their flight path in relation to turbulence. In the aviation industry, aircraft are often forced to increase flight altitude or to make detours to avoid clear air turbulence (Storer et al., 2019). For volant animals that mainly occupy lower altitudes than commercial airlines, the relevant forms of turbulence are mainly a result of surface heating (thermal updraughts) and/or the interaction of wind with the land surface and the topography causing mechanical turbulence. Where there is an upward component to turbulence e.g. the rising air in thermal updrafts, birds can use this to gain altitude or stay aloft without flapping, as exemplified by large soaring animals (Williams et al., 2020). But mechanically-driven turbulence is less likely to be associated with energetic benefits, in fact, birds are predicted to increase their wingbeat frequency to reduce the impact of gustiness on their flight. Recent studies using numerical simulations or wind tunnel experiments have shown a variety of responses of wing kinematics and body adjustments (Ortega-Jimenez et al., 2014, Ravi et al., 2015, Sapir et al., 2011) suggesting that the effects of turbulent eddies on flight performance likely vary with body size, speed, flight style and the severity and scale of turbulence (Shepard et al., 2016).

Nonetheless, whether and how birds adjust their flight kinematics and flight route in relation to turbulence in the wild has yet to be examined.

Overall, despite the fundamental importance of wind and turbulence to animal flight, the majority of ecological studies have focused on the effects of mean flows and sustained conditions. Our understanding of responses to extreme winds is hampered by the rarity of these events. In contrast, the challenges of studying responses to turbulence in nature relate to the lack of environmental information at fine scales. Animal movement can now be tracked with ultra-high frequency and resolution (e.g. Brighton et al., 2017, Gunner et al., 2021): Accelerometers enable us to track fine scale changes in wing kinematics with sub-second resolution (e.g. Elliott et al., 2014, O'Mara et al., 2019, Williams et al., 2020) and GPS observations are now recorded at frequencies as high as 1 to 5 Hz, documenting animal tracks during daily activities such as foraging, in detail (Brighton et al., 2017). Clearly movement needs to be tracked with a sampling rate of hours to days to resolve behaviours over the annual cycle (Egevang et al., 2010), but questions such as how birds respond to rapid changes in wind strength and direction, and how they negotiate highly unstable flows, need high resolution data on both the movement of the animals themselves and the environment they are moving through. There is therefore a clear need for fine-scale data on the aerial environment that more closely matches the scale at which animals experience it.

Tools to quantify the dynamic aerial environment

The tools available to the biological community for quantifying the aerial environment vary in scale, cost, and complexity and their application depends on the available resources, expertise, and the particular scientific questions that need to be addressed. In recent decades, advances in global reanalyses and computational fluid dynamics (CFD) have provided us with an exciting toolset, and the former are now widely used by behavioural ecologists.

Global reanalyses

Global reanalyses first appeared in the 1990's and since then a number of products have been freely available (i.e. ERA5, ERA-Interim, and the Japanese 55-year Reanalysis (JRA55)). Global reanalyses are produced by combining real observations and a global circulation forecast model with an assimilation scheme, in order to estimate an extensive set of environmental variables (Fujiwara et al., 2017). Specifically, for every time step a short-range weather forecast model is used to predict the state of the Earth system. The initial conditions for this model are provided by the forecast model of the previous time step and the produced estimates are constrained by the real observations that are available for the current time step.

These observations come from many different sources, for example weather stations, satellites, ships, buoys, radiosondes and aircrafts, and in different forms including digitised old paper historical records. The process of combining the previous short-range forecast with the latest real observations to set-up and run the short-range forecast of the current time step is called analysis and when this process is repeated for an extended period back in time the complete product is called a reanalysis or a “map without gaps" of essential climate variables of the Earth system (Hersbach et al., 2020).

Of particular interest to avian ecologists are the wind speed and direction, gustiness, temperature, air density, and heat fluxes close to the surface or at multiple levels in the atmosphere. As different parts of the Earth system coexist, an environmental variable of one system (i.e. land or ocean) can influence one or more variables of another system (i.e. the atmosphere). To ensure that this is taken into account, reanalyses use coupled assimilation where variables from one system are allowed to interact with variables from other systems (Hersbach et al., 2020). As their name suggests, global reanalysis models provide global spatial coverage, with different reanalyses being produced at different spatial and temporal resolutions. Reanalyses also cover different time periods extending back several decades, with ERA5, for example, providing historical data as far back as the 1950s, with a temporal resolution of one hour and a spatial resolution of 30 km (Hersbach et al., 2018, Hersbach et al., 2020). The available information can be divided into different levels of the atmosphere with ERA5 offering data for a smaller set of parameters (i.e. wind strength) at 37 pressure levels. Consequently, the aerial environment above different ecosystems, whether they are terrestrial or aquatic, can be represented at kilometre scales that are relevant for many questions relating to animal flight.

Computational Fluid Dynamics

Computational fluid dynamics can be broadly defined as a branch of fluid mechanics that employs numerical equations and computer algorithms to simulate the motion of a fluid, in this case the air’s motion, and its interaction with a surface, such as a part of a landscape or a mixture of land and water. The main numerical equations used to describe the air’s motion are usually taken to be the Navier–Stokes equations because air is a viscous fluid. In general, the spatial domain of the model has to be discretised into a regular or irregular mesh, with the latter being more suitable for the complex air motion over a landscape (Pope, 2004) and appropriate algorithms must be set to solve the governing numerical equations. To perform a simulation, initial conditions that describe the state of the simulation at the beginning must be

defined, as well as the boundary conditions, which describe how air behaves at the boundaries of the model's domain. Finally, simulations are completed either after a given number of time steps (transient solver) or when convergence is reached (steady-state solver). While it is possible to solve the Navier–Stokes equations analytically, for example for laminar flow and when all the length scales of the fluid's motion can be resolved in the model's grid (direct numerical simulations), in most cases the extent of the model's domain and the flow's complexity require the use of a turbulence model (Lesieur and Metais, 1996).

Main computational fluid dynamics approaches (RANS/LES)

CFD models are split into two main approaches for modelling turbulence: Reynolds-Averaged Navier-Stokes (RANS) models and the Large-eddy simulations (LES) models. LES is particularly useful in modelling a wide range of length and time scales of turbulent eddies as these cascade from large to small in the atmosphere, down to the smallest significant scale, the Kolmogorov scale (Frisch and Kolmogorov, 1995). In LES, while the larger turbulent eddies that contain most of the energy of the air's motion are resolved, the effects of the smaller turbulent eddies are parametrised and modelled using a sub-grid scale to represent the small scale motion (Lesieur and Metais, 1996, Pope, 2004). In contrast, RANS models average out the small-scale phenomena below a certain threshold. In general, the RANS models also produce less accurate results, especially when the airflow is dominated by large scale unsteady motions, which are the most responsible for turbulent mixing (Pope, 2004, Zhiyin, 2015). However, RANS models can be computationally cheaper, and depending on the study, can be implemented on a personal computer.

Comparison of different tools

The global coverage of reanalyses datasets, the large range of environmental variables they offer, and the simplicity in acquisition makes them very attractive tools for investigating the impact of the physical environment on animal flight when (i) the fine scales offered by CFD are not necessary, (ii) a CFD model would be too complex to run, or (iii) the extent of the movement, in space or time, is large for CFD. Global reanalyses can also provide us with reconstructed historical data. Therefore, it is not surprising that global reanalyses have been used most frequently by the biological community. However, reanalyses also incorporate uncertainties, both from the observational inputs and the circulation models themselves. For example, the performance of all modern reanalyses in describing surface winds lack accuracy compared to ERA5 when comparisons are made with in situ measurements (Ramon et al., 2019), but ERA5 is also known to under represent wind strength in extreme conditions

(Malakar et al., 2020). Nonetheless, both approaches have their strengths, and can even be used in combination, with reanalyses providing the initial and boundary conditions for CFD models.

When higher resolution and more accurate representation of the real world are required, CFD models represent the most appropriate choice. CFD models are flexible and can be used to run either (i) a real case scenario where a high-resolution model layer(s) is nested within a regional coarse resolution model(s) in two or more layers, or (ii) an idealised scenario, where for example the terrain is considered level and nesting is not necessary. However, choosing between RANS and LES can be difficult. The greatest advantage of RANS is the lower computational cost to simulate complex turbulent flow. This currently makes them the most widespread application in engineering (Thé and Yu, 2017). While RANS typically run faster than LES and provide a sufficient level of accuracy, LES models are essential for resolving highly complex flows. In recent decades, the exponential increase in computer power means that the necessary demands of LES, and CFD in general, are less prohibitive for modelling highly complex flow over large realistic landscapes (Pope, 2004). Ultimately, the most appropriate method depends on the cost and the desired level of accuracy, which in turn depends on the level to which small spatiotemporal phenomena need to be resolved (Kochkov et al., 2021).

Ecological applications of Global reanalyses and CFD

Global reanalyses have been used extensively in ecological studies. For example, to map the use of soaring flight in relation to updraught availability at a European scale (Scacco et al., 2019), to link in-flight energy savings to convection (Shamoun-Baranes et al., 2016), and to show that migrating birds spend more time searching for updraughts when these are scarcer (Vansteelant et al., 2017). Other studies that have utilised global reanalyses to estimate airspeed and to associate it with wind support, were able to show that the fastest airspeeds in dynamic soaring flight occur with cross-winds (Richardson et al., 2018), and that the power costs of flapping flight increase with headwinds (O'Mara et al., 2019).

There have been far fewer applications of CFD in avian ecology, but the examples are diverse, demonstrating the large potential of this toolset. For example, RANS have been used at fine scales e.g. modelling the interaction of wind with the flapping wing of a Canada goose (*Branta canadensis*) and estimating the energy savings of flight in a v-formation (Maeng et al., 2013), as well as landscape scales e.g. modelling the nocturnal passerine migration over complex topography, which demonstrated the strong selection of favourable winds (Aurbach

et al., 2018), and modelling airflows around entire islands (Goddard et al., 2022), to estimate how this affects the ability of birds to land at their nests (Shepard et al., 2019). Unfortunately despite the great potentials of LES in ecology (Nathan et al., 2005), I am only aware of one study that has made use of LES in association with bird movement (see below) (Shannon et al., 2002).

CFD has also been used to assess flow selection in fish, enabling researchers to estimate flow characteristics over large scales and in inaccessible locations (e.g. due to current velocity). For instance, CFD models have been applied in natural and engineered river systems to evaluate the influence of turbulence, flow velocity and rate, and the interaction between flow regimes and river morphology, on fish habitat and passage suitability (Daneshvar et al., 2017). Booker (2003) identified suitable fish refugia in two urban river systems that offered protection from extreme velocities at high flows and showed that natural habitat offers better refugia than modified systems. Kolden et al. (2016) also modelled the flow conditions in natural and modified pools and found significant differences in turbulence kinetic energy (TKE) and current velocity between natural and white-water park systems, suggesting that the former offer better refugia. Haro et al. (2015) assessed the flow velocity in rivers with low and high flow rates to simulate the impact of dam removal on connectivity and found that the size and number of challenging passage zones increased from low to high flow, and from larger to smaller fish. In a similar way CFD should be able to inform us how airflow conditions affect habitat selection in birds, particularly for areas of high use, such as territories and breeding sites.

A new tool for quantifying the aerial environment: bird-borne sensors

In the last few decades, ecologists have also started using data from animal-borne sensors to quantify changes in the physical environment with high resolution, including in locations that anthropogenic platforms cannot reach (Jetz et al., 2022, Wilmers et al., 2015). A key advantage to this approach is the potential to acquire high-resolution information on time-varying flows at the scale of the animal motion. This is likely to be particularly useful for the aerial environment, which is extremely variable across spatial and temporal scales (Shepard et al., 2016). To date, this approach has also been used more widely in aquatic environments (e.g. Charrassin et al., 2008, Roquet et al., 2014), but the use of animal-borne sensors has been validated for both the estimation of the wind vector and thermal updraught intensity and distribution (Bohrer et al., 2012, Goto et al., 2017, Weinzierl et al., 2016). For instance, thermal updraught intensity measured from the climb rate of soaring American white pelicans

(*Pelecanus erythrorhynchos*) showed good agreement with results from LES simulations (Shannon et al., 2002). Satellite estimates of ocean surface winds were also correlated with those derived from fine-scale changes in groundspeed in three species of dynamic soaring birds (Yonehara et al., 2016). This demonstrates the potential of bird-borne platforms as a complimentary tool to sense the aerial environment, although a key limitation is that it can only be applied where animals move, requiring other techniques to assess the conditions in other areas, including those they may actively avoid.

Objectives and chapter summary

The aim of my thesis is to investigate how birds respond to challenging airflows, specifically, chaotic variations in wind speed and direction and exceedingly strong winds. The first two data chapters focus on turbulence; how it can be measured and how birds respond. The final two data chapters investigate how seabirds respond to strong winds, first at sea, where I examine movements in relation to cyclones, and then on land, where I assess whether airflows can predict breeding habitat selection.

The thesis starts by recognising the limited utilisation of animal-borne sensors as a tool for quantifying the aerial environment (Bohrer et al., 2012, Goto et al., 2017, Weinzierl et al., 2016). Yet anyone who has flown can recognise when an aircraft hits a particularly turbulent patch, simply from the bumpiness of the ride. In chapter 2, I use metrics derived from the solo-flight of homing pigeons (*Columba livia*) and from the flight of an ultralight, to assess whether body displacement can be used as a proxy for turbulence intensity over complex terrain. Specifically, I derive metrics of displacement from acceleration and barometric pressure sensors attached to pigeons and an ultralight following some distance behind the birds. The ultralight was also equipped with a tri-axial anemometer to provide independent estimates of turbulence along the flight path, allowing me to compare the performance of different turbulence proxies. In order to examine whether the best proxy can provide general insight into turbulence levels, irrespective of how turbulence is generated, I then compare the best proxy to estimates of convective and mechanically driven turbulence (using reanalysis data). Finally, I use the best proxy to predict turbulence strength across the pigeon flight paths to identify fine scale hot- and cold-spots of turbulence across the study area under different wind conditions.

Very few studies have addressed how flapping fliers are affected by, and respond to, turbulence. Most studies have used hummingbirds (Ortega-Jimenez et al., 2014, Ravi et al., 2015), which are excellent models as they will hover in front of a feeder, allowing their

wingbeat kinematics (i.e. frequency and amplitude) to be quantified in different conditions. However, the "freestream turbulence" in the natural environment is fundamentally different to turbulence generated in laboratory conditions, as for example freestream turbulence also has an upward component. Furthermore, laboratory studies are limited in what they can tell us about how animals respond in terms of adjusting their flight speed and flight path. In chapter 3, I use the estimates of turbulence from bird-borne sensors to assess how turbulence affects the flight effort (wingbeat frequency and amplitude), speed and route choice of homing pigeons, using an expanded tracking dataset from chapter 2. If turbulence does represent a cost to flapping fliers, as expected, this should be reflected in an increase in wingbeat frequency for a given flight speed and an increase in the variability of wingbeat frequency and amplitude, which, together represent strategies to improve flight stability (Ortega-Jimenez et al., 2014, Ravi et al., 2015). I then consider how turbulence affects track properties, from fine-scale tortuosity (which is also associated with increased cost, relative to straight line travel) to overall route choice. Pigeons are a model species for chapters 2 and 3 as they will return to their loft in a range of conditions. I therefore released birds in two different seasons and at different times of day to maximise the range of turbulence levels that they encountered.

Turbulence is not the only aspect of the aerial environment that presents challenges for flying animals. Strong winds can also levy costs, which vary with flight morphology, style and flight type. For most flapping fliers, flight costs increase with the headwind component (Hedenström, 1993, O'Mara et al., 2019), whereas costs decrease with wind speed for dynamic soaring birds (Furness and Bryant, 1996, Richardson, 2011). However, there is little information on how birds using either flight strategy respond to extreme winds (though see Hass et al., 2012, Weimerskirch and Prudor, 2019). Flying animals are only able to operate independently of the wind i.e. fly against headwinds and minimise drift, when their airspeed exceeds the wind speed (Liechti, 2006). Winds that are similar in strength to maximum flight speeds are therefore risky in terms of a bird's ability to control its trajectory and prevent collisions with the substrate. Chapter 4 addresses how a dynamic-soaring seabird routes its flight path in relation to cyclones, using data from streaked shearwaters (*Calonectris leucomelas*) foraging in the Sea of Japan over an 11 year period. I focus on the responses to the 5 strongest storms that differ in magnitude, path, and duration and use environmental data from storm tracks and the latest global reanalysis (ERA5) to examine how birds move in relation to the eye of the storm. This allow me to identify whether these dynamic-soaring birds avoid storms, are attracted to them or ignore them. Finally, I examine how birds

modulate their distance to land, which represents a potential danger to these seabirds during storms due to the specific risks of collision, stranding and predation (Yoda et al., 2021, Yoda et al., 2017). This is particularly pertinent for these streaked shearwaters, as the Sea of Japan is enclosed, offering limited options for circumnavigation of large typhoons.

Clearly seabirds have to operate close to land when they leave and approach their nests, and the wind field surrounding these areas can have important consequences for flight control. In fact, strong winds have recently been shown to reduce the ability of auks to land at their breeding cliffs (Shepard et al., 2019). Wind speed at the nesting site is also pertinent for other reasons, including heat loss (of adults and chicks). Despite this, wind is rarely incorporated into studies of habitat selection, even for seabirds, which nest in exposed areas. In chapter 5, I use CFD to estimate a wide range of airflow variables around the cliffs of Skomer Island, UK and investigate how these vary between breeding and non-breeding sites. I then extend my analysis to assess habitat quality and assess whether airflows can predict the distribution of the largest and densest colonies, rather than just the presence/ absence of breeding birds. Finally, I demonstrate the application of CFD in species distribution modelling, by taking the best-fitting model of habitat selection and seeing how well it predicts the distribution of breeding birds on the neighbouring island of Skokholm. I focus on the habitat selection of the common guillemot (*Uria aalge*), as there is a known relationship between landing ability and wind speed (Shepard et al., 2019). Overall, this allowed to me assess (i) the role of CFD in providing insight into the breeding distributions of seabirds, in comparison to a simpler model based on orientation, and (ii) whether breeding habitat selection in guillemots is driven by landing performance, thermal considerations and/ or exposure to storm conditions.

Finally, in chapter 6, I revisit my findings in light of the questions they raise about how birds respond to challenging airflows. This is a broad topic, and responses are likely to vary with morphology as well as the biological and geographical context. Nonetheless, I hope that the examples in this thesis may ultimately help researchers develop a framework to predict when extreme or variable flows are likely to be problematic for flying birds.

References

Aurbach, A., Schmid, B., Liechti, F., Chokani, N. & Abhari, R. 2018. Complex behaviour in complex terrain-modelling bird migration in a high resolution wind field across mountainous terrain to simulate observed patterns. *Journal of theoretical biology,* 454**,** 126-138.

Bohrer, G., Brandes, D., Mandel, J. T., Bildstein, K. L., Miller, T. A., Lanzone, M., Katzner, T., Maisonneuve, C. & Tremblay, J. A. 2012. Estimating updraft velocity components over large spatial scales: contrasting migration strategies of golden eagles and turkey vultures. *Ecology letters,* 15**,** 96-103.

Booker, D. 2003. Hydraulic modelling of fish habitat in urban rivers during high flows. *Hydrological processes,* 17**,** 577-599.

Brighton, C. H., Thomas, A. L. & Taylor, G. K. 2017. Terminal attack trajectories of peregrine falcons are described by the proportional navigation guidance law of missiles. *Proceedings of the National Academy of Sciences,* 114**,** 13495-13500.

Charrassin, J.-B., Hindell, M., Rintoul, S. R., Roquet, F., Sokolov, S., Biuw, M., Costa, D., Boehme, L., Lovell, P. & Coleman, R. 2008. Southern Ocean frontal structure and sea-ice formation rates revealed by elephant seals. *Proceedings of the National Academy of Sciences,* 105**,** 11634-11639.

Daneshvar, F., Nejadhashemi, A. P., Woznicki, S. A. & Herman, M. R. 2017. Applications of computational fluid dynamics in fish and habitat studies. *Ecohydrology & Hydrobiology,* 17**,** 53-62.

Dokter, A. M., Liechti, F., Stark, H., Delobbe, L., Tabary, P. & Holleman, I. 2011. Bird migration flight altitudes studied by a network of operational weather radars. *Journal of the Royal Society Interface,* 8**,** 30-43.

Egevang, C., Stenhouse, I. J., Phillips, R. A., Petersen, A., Fox, J. W. & Silk, J. R. 2010. Tracking of Arctic terns Sterna paradisaea reveals longest animal migration. *Proceedings of the National Academy of Sciences,* 107**,** 2078-2081.

Elliott, K. H., Chivers, L. S., Bessey, L., Gaston, A. J., Hatch, S. A., Kato, A., Osborne, O., Ropert-Coudert, Y., Speakman, J. R. & Hare, J. F. 2014. Windscapes shape seabird instantaneous energy costs but adult behavior buffers impact on offspring. *Movement Ecology,* 2**,** 1-15.

Elmore, J. A., Hager, S. B., Cosentino, B. J., O'Connell, T. J., Riding, C. S., Anderson, M. L., Bakermans, M. H., Boves, T. J., Brandes, D. & Butler, E. M. 2021. Correlates of bird

collisions with buildings across three North American countries. *Conservation Biology,* 35**,** 654-665.

Frisch, U. & Kolmogorov, A. N. 1995. *Turbulence: the legacy of AN Kolmogorov*, Cambridge university press.

Fujiwara, M., Wright, J. S., Manney, G. L., Gray, L. J., Anstey, J., Birner, T., Davis, S., Gerber, E. P., Harvey, V. L. & Hegglin, M. I. 2017. Introduction to the SPARC Reanalysis Intercomparison Project (S-RIP) and overview of the reanalysis systems. *Atmospheric Chemistry and Physics,* 17**,** 1417-1452.

Furness, R. W. & Bryant, D. M. 1996. Effect of wind on field metabolic rates of breeding northern fulmars. *Ecology,* 77**,** 1181-1188.

Goddard, K., Craig, K., Schoombie, J. & le Roux, P. 2022. Investigation of ecologically relevant wind patterns on Marion Island using Computational Fluid Dynamics and measured data. *Ecological Modelling,* 464**,** 109827.

Goto, Y., Yoda, K. & Sato, K. 2017. Asymmetry hidden in birds' tracks reveals wind, heading, and orientation ability over the ocean. *Science advances,* 3**,** e1700097.

Gunner, R. M., Holton, M. D., Scantlebury, M. D., van Schalkwyk, O. L., English, H. M., Williams, H. J., Hopkins, P., Quintana, F., Gómez-Laich, A. & Börger, L. 2021. Dead-reckoning animal movements in R: a reappraisal using Gundog. Tracks. *Animal Biotelemetry,* 9**,** 1-37.

Haro, A., Chelminski, M. & Dudley, R. W. 2015. Computational fluid dynamics–habitat suitability index (CFD–HSI) modelling as an exploratory tool for assessing passability of riverine migratory challenge zones for fish. *River research and applications,* 31**,** 526-537.

Hass, T., Hyman, J. & Semmens, B. 2012. Climate change, heightened hurricane activity, and extinction risk for an endangered tropical seabird, the black-capped petrel Pterodroma hasitata. *Marine Ecology Progress Series,* 454**,** 251-261.

Hedenström, A. 1993. Migration by soaring or flapping flight in birds: the relative importance of energy cost and speed. *Philosophical Transactions of the Royal Society of London. Series B: Biological Sciences,* 342**,** 353-361.

Hedenström, A. & Åkesson, S. 2016. Ecology of tern flight in relation to wind, topography and aerodynamic theory. *Philosophical Transactions of the Royal Society B: Biological Sciences,* 371**,** 20150396.

Hersbach, H., Bell, B., Berrisford, P., Biavati, G., Horányi, A., Muñoz Sabater, J., J, N., Peubey, C., Radu, R., Rozum, I., Schepers, D., Simmons, A., Soci, C., Dee, D. & Thépaut, J.-N. 2018. ERA5 hourly data on single levels from 1979 to present.

Hersbach, H., Bell, B., Berrisford, P., Hirahara, S., Horányi, A., Muñoz-Sabater, J., Nicolas, J., Peubey, C., Radu, R. & Schepers, D. 2020. The ERA5 global reanalysis. *Quarterly Journal of the Royal Meteorological Society,* 146**,** 1999-2049.

Jetz, W., Tertitski, G., Kays, R., Mueller, U., Wikelski, M., Åkesson, S., Anisimov, Y., Antonov, A., Arnold, W. & Bairlein, F. 2022. Biological Earth observation with animal sensors. *Trends in Ecology & Evolution,* 37**,** 293-298.

Kochkov, D., Smith, J. A., Alieva, A., Wang, Q., Brenner, M. P. & Hoyer, S. 2021. Machine learning–accelerated computational fluid dynamics. *Proceedings of the National Academy of Sciences,* 118.

Kolden, E., Fox, B., Bledsoe, B. & Kondratieff, M. 2016. Modelling whitewater park hydraulics and fish habitat in Colorado. *River Research and Applications,* 32**,** 1116-1127.

Kranstauber, B., Weinzierl, R., Wikelski, M. & Safi, K. 2015. Global aerial flyways allow efficient travelling. *Ecology letters,* 18**,** 1338-1345.

Krüger, T. & Garthe, S. 2001. Flight altitudes of coastal birds in relation to wind direction and speed. *Atlantic Seabirds,* 3**,** 203-216.

Lesieur, M. & Metais, O. 1996. New trends in large-eddy simulations of turbulence. *Annual review of fluid mechanics,* 28**,** 45-82.

Liechti, F. 2006. Birds: blowin'by the wind? *Journal of Ornithology,* 147**,** 202-211.

Liechti, F., Hedenström, A. & Alerstam, T. 1994. Effects of sidewinds on optimal flight speed of birds. *Journal of theoretical Biology,* 170**,** 219-225.

Maeng, J.-S., Park, J.-H., Jang, S.-M. & Han, S.-Y. 2013. A modeling approach to energy savings of flying Canada geese using computational fluid dynamics. *Journal of theoretical biology,* 320**,** 76-85.

Malakar, P., Kesarkar, A., Bhate, J., Singh, V. & Deshamukhya, A. 2020. Comparison of reanalysis data sets to comprehend the evolution of tropical cyclones over North Indian Ocean. *Earth and Space Science,* 7**,** e2019EA000978.

McLaren, J. D., Shamoun-Baranes, J., Dokter, A. M., Klaassen, R. H. & Bouten, W. 2014. Optimal orientation in flows: providing a benchmark for animal movement strategies. *Journal of the Royal Society Interface,* 11**,** 20140588.

Nathan, R., Sapir, N., Trakhtenbrot, A., Katul, G. G., Bohrer, G., Otte, M., Avissar, R., Soons, M. B., Horn, H. S. & Wikelski, M. 2005. Long-distance biological transport processes through the air: can nature's complexity be unfolded in silico? *Diversity and Distributions,* 11**,** 131-137.

Nichols, K. S., Homayoun, T., Eckles, J. & Blair, R. B. 2018. Bird-building collision risk: An assessment of the collision risk of birds with buildings by phylogeny and behavior using two citizen-science datasets. *PloS one,* 13**,** e0201558.

O'Mara, M. T., Scharf, A. K., Fahr, J., Abedi-Lartey, M., Wikelski, M., Dechmann, D. K. & Safi, K. 2019. Overall dynamic body acceleration in straw-colored fruit bats increases in headwinds but not with airspeed. *Frontiers in Ecology and Evolution,* 7**,** 200.

Ortega-Jimenez, V. M., Sapir, N., Wolf, M., Variano, E. A. & Dudley, R. 2014. Into turbulent air: size-dependent effects of von Kármán vortex streets on hummingbird flight kinematics and energetics. *Proceedings of the Royal Society B: Biological Sciences,* 281**,** 20140180.

Pennycuick, C. J., Åkesson, S. & Hedenström, A. 2013. Air speeds of migrating birds observed by ornithodolite and compared with predictions from flight theory. *Journal of the Royal Society Interface,* 10**,** 20130419.

Pope, S. B. 2004. Ten questions concerning the large-eddy simulation of turbulent flows. *New journal of Physics,* 6**,** 35.

Ramon, J., Lledó, L., Torralba, V., Soret, A. & Doblas-Reyes, F. J. 2019. What global reanalysis best represents near-surface winds? *Quarterly Journal of the Royal Meteorological Society,* 145**,** 3236-3251.

Ravi, S., Crall, J. D., McNeilly, L., Gagliardi, S. F., Biewener, A. A. & Combes, S. A. 2015. Hummingbird flight stability and control in freestream turbulent winds. *The Journal of experimental biology,* 218**,** 1444-1452.

Richardson, P. L. 2011. How do albatrosses fly around the world without flapping their wings? *Progress in Oceanography,* 88**,** 46-58.

Richardson, P. L., Wakefield, E. D. & Phillips, R. A. 2018. Flight speed and performance of the wandering albatross with respect to wind. *Movement ecology,* 6**,** 1-15.

Roquet, F., Williams, G., Hindell, M. A., Harcourt, R., McMahon, C., Guinet, C., Charrassin, J.-B., Reverdin, G., Boehme, L. & Lovell, P. 2014. A Southern Indian Ocean database of hydrographic profiles obtained with instrumented elephant seals. *Scientific data,* 1**,** 1-10.

Sapir, N., Horvitz, N., Wikelski, M., Avissar, R., Mahrer, Y. & Nathan, R. 2011. Migration by soaring or flapping: numerical atmospheric simulations reveal that turbulence kinetic energy dictates bee-eater flight mode. *Proceedings of the Royal Society B: Biological Sciences,* 278**,** 3380-3386.

Scacco, M., Flack, A., Duriez, O., Wikelski, M. & Safi, K. 2019. Static landscape features predict uplift locations for soaring birds across Europe. *Royal Society open science,* 6**,** 181440.

Shamoun-Baranes, J., Bouten, W., Van Loon, E. E., Meijer, C. & Camphuysen, C. 2016. Flap or soar? How a flight generalist responds to its aerial environment. *Philosophical Transactions of the Royal Society B: Biological Sciences,* 371**,** 20150395.

Shannon, H. D., Young, G. S., Yates, M. A., Fuller, M. R. & Seegar, W. S. 2002. Measurements of thermal updraft intensity over complex terrain using American white pelicans and a simple boundary-layer forecast model. *Boundary-Layer Meteorology,* 104**,** 167-199.

Shepard, E., Cole, E.-L., Neate, A., Lempidakis, E. & Ross, A. 2019. Wind prevents cliff-breeding birds from accessing nests through loss of flight control. *Elife,* 8**,** e43842.

Shepard, E. L., Ross, A. N. & Portugal, S. J. 2016. Moving in a moving medium: new perspectives on flight. The Royal Society.

Storer, L. N., Williams, P. D. & Gill, P. G. 2019. Aviation turbulence: dynamics, forecasting, and response to climate change. *Pure and Applied Geophysics,* 176**,** 2081-2095.

Thé, J. & Yu, H. 2017. A critical review on the simulations of wind turbine aerodynamics focusing on hybrid RANS-LES methods. *Energy,* 138**,** 257-289.

Van Bemmelen, R. & Wielstra, B. 2008. Vagrancy of Brünnich's Guillemot Uria lomvia in Europe. *Seabird,* 21**,** 16-31.

Vansteelant, W. M., Shamoun-Baranes, J., McLaren, J., van Diermen, J. & Bouten, W. 2017. Soaring across continents: decision-making of a soaring migrant under changing atmospheric conditions along an entire flyway. *Journal of Avian Biology,* 48**,** 887-896.

Weimerskirch, H., Bishop, C., Jeanniard-du-Dot, T., Prudor, A. & Sachs, G. 2016. Frigate birds track atmospheric conditions over months-long transoceanic flights. *Science,* 353**,** 74-78.

Weimerskirch, H. & Prudor, A. 2019. Cyclone avoidance behaviour by foraging seabirds. *Scientific reports,* 9**,** 1-9.

Weinzierl, R., Bohrer, G., Kranstauber, B., Fiedler, W., Wikelski, M. & Flack, A. 2016. Wind estimation based on thermal soaring of birds. *Ecology and Evolution,* 6**,** 8706-8718.

Williams, H. J., Shepard, E., Holton, M. D., Alarcón, P., Wilson, R. & Lambertucci, S. 2020. Physical limits of flight performance in the heaviest soaring bird. *Proceedings of the National Academy of Sciences,* 117**,** 17884-17890.

Wilmers, C. C., Nickel, B., Bryce, C. M., Smith, J. A., Wheat, R. E. & Yovovich, V. 2015. The golden age of bio-logging: How animal-borne sensors are advancing the frontiers of ecology. *Ecology,* 96**,** 1741-1753.

Yoda, K., Okumura, M., Suzuki, H., Matsumoto, S., Koyama, S. & Yamamoto, M. 2021. Annual variations in the migration routes and survival of pelagic seabirds over mountain ranges. *Ecology***,** e03297-e03297.

Yoda, K., Yamamoto, T., Suzuki, H., Matsumoto, S., Müller, M. & Yamamoto, M. 2017. Compass orientation drives naïve pelagic seabirds to cross mountain ranges. *Current Biology,* 27**,** R1152-R1153.

Yonehara, Y., Goto, Y., Yoda, K., Watanuki, Y., Young, L. C., Weimerskirch, H., Bost, C.-A. & Sato, K. 2016. Flight paths of seabirds soaring over the ocean surface enable measurement of fine-scale wind speed and direction. *Proceedings of the National Academy of Sciences,* 113**,** 9039-9044.

Zhiyin, Y. 2015. Large-eddy simulation: Past, present and the future. *Chinese journal of Aeronautics,* 28**,** 11-24.

Chapter 2: Estimating fine-scale changes in turbulence using the movements of a flapping flier.

The content of this chapter is in review in "Proceedings of the Royal Society B" as:

Lempidakis, E., Ross, A.N., Quetting, M., Garde, B., Wikelski, M., Shepard, E.L.C.

Abstract

Most animals using the aerosphere flap with wing-like structures and need to respond to aerial turbulence. Yet little is known about how flying animals do this because quantifying turbulence at fine scales is exceedingly difficult. Recently, data from animal-borne sensors have been used to quantify wind and updraft strength, providing a new prospect for sensing the environment at scales that animals experience it. We tested whether fine-scale changes in altitude and body acceleration measured onboard solo-flying pigeons (as model flapping fliers) can be used as proxies for turbulence. A range of pressure and acceleration proxies performed well when tested against independent turbulence measurements from a tri-axial anemometer mounted onboard an ultralight flying the same route, with stronger turbulence causing increasing vertical displacement. The best proxy for turbulence also varied with reanalysis estimates of both convective velocity and wind shear. The near linear relationship between proxies and turbulence levels suggests this approach should be widely applicable, providing insight into how turbulence changes in space and time. Furthermore, pigeons were able to fly in conditions of strong turbulence that were unsafe for the ultralight.

Introduction

The impact of atmospheric turbulence on flying animals represents an important frontier (Bomphrey and Godoy-Diana, 2018, Laurent et al., 2021, Quinn et al., 2017), as the effects on flight energetics and route selection are far less studied than those of wind (Hedenström and Alerstam, 1995, Liechti, 2006). Turbulence is broadly defined as a measure of rapid changes in wind velocity at small scales and is driven by mechanical forcing or surface heating. Within the boundary layer, and at the usual altitudes at which animals fly, turbulence is influenced by both processes, depending on the strength of the wind and heat fluxes (instability), the altitude above ground, land cover, and topography. Thermal-driven turbulence has a strong upward component, which a range of birds exploit to their reduce flight costs through thermal soaring (Sapir et al., 2011, Williams et al., 2020), particularly in species adapted to soaring flight, where the distribution of thermal updrafts can influence movement paths from local to regional scales (Bohrer et al., 2012, Treep et al., 2016).

Much less is known about the impact of gustiness, which is associated with both thermal- and mechanically driven turbulence. Nonetheless, this can impact flight control (Cheney et al., 2020, Ravi et al., 2015) and flight costs (Bowlin and Wikelski, 2008, Mallon et al., 2016, Tucker, 1972). As such, gustiness should be relevant for birds irrespective of their flight style and body mass. In fact, it should be most relevant for animals flying close to the ground, where an inability to respond to fine-scale changes in the wind could ultimately result in a collision. Indeed, it has been suggested that these risks explain why gulls soaring above buildings increased their distance to the buildings with increasing wind strength (Shepard et al., 2016).

Despite the potential importance of turbulence in animal movement, quantifying spatially and temporally explicit changes in gustiness over fine scales remains challenging (Lieber et al., 2021). Most weather stations do not report turbulence strength or vertical wind velocity, and when in situ measurements are made, conditions at a single location near the surface are often not representative of those at higher altitudes or along an entire flight track. Reanalyses models provide estimates of vertical velocity and turbulence strength with excellent spatial coverage however, the temporal and spatial resolutions tend to be relatively coarse, at best hourly and in the order of tens of kilometres respectively. Reanalyses models therefore cannot resolve changes in fine-scale gustiness that birds would experience along their flight path (Treep et al., 2016).

Large eddy simulation models (LES) can also be used to realistically assess the conditions associated with flight (i.e. for modelling convective velocity *w**, Shannon et al. (2002)) over a wide range of terrains and conditions. LES can produce fine-scale predictions by nesting a high resolution model within a lower resolution regional model(s). However, the computational costs tend to constrain their application according to the combination of the study area size, desired temporal/ spatial resolution, complexity and available computational resources (Nathan et al., 2005, Stoll et al., 2020).

Remote sensing solutions, namely LiDAR, are also capable of measuring near-surface changes in turbulence over seconds and tens of meters, by scanning at different angles to infer to the three velocity components. In most cases, turbulence is quantified by the vertical velocity of a vertically pointed LiDAR. The critical limitation of LiDAR for ecologists is the availability and expense of such sensing equipment, which mean that measurements tend to be made in specific locations in association with meteorological research programmes and often do not have wide spatial coverage depending on the instrument and scanning pattern (Newman et al., 2016). LiDAR also incorporates errors depending on atmospheric stability and scanning method, and often assumes that the 3-D flow is horizontally homogeneous (an assumption usually not valid, i.e. over complex terrain).

Recently, researchers have shown that the movements of the birds themselves can be used to quantify wind and thermal strength (Goto et al., 2017, Shannon et al., 2002). Indeed, large tracking datasets mean that these Lagrangian approaches can be used to quantify conditions over substantial areas (Scacco et al., 2019). It is clear from flying in aircraft that turbulence causes changes in altitude and body motion, suggesting that high-frequency data from animal-attached loggers could also be used to provide insight into the level of turbulence experienced by animals in flight. Indeed, Laurent et al. (2021) showed that the vertical displacements of the body accelerations of a single 5 kg golden eagle (*Aquila chrysaetos*) were similar to those of the motions of the turbulent air.

Our aim was to establish whether fine-scale movements recorded using animal-attached data loggers can be used as proxies for turbulence in flapping fliers. As this is the predominant type of flight used by birds, the ability to extract information on turbulence from onboard loggers would represent a powerful technique allowing researchers to monitor the aerial environment. On the one hand flapping fliers tend to be smaller than those that rely on gliding flight, potentially making their movements more sensitive to the movements of the air. But against this, the motion of the wings could compensate for much of the turbulence

spectrum, resulting in little displacement of the body. In order to investigate this, we flew an ultralight at the same time and in the same area as homing pigeons (*Columba livia Linnaeus*). The birds and the ultralight were equipped with high-frequency data-loggers recording altitude and body acceleration, and the ultralight was also instrumented with a tri-axial anemometer to provide independent estimates of turbulence. We used the resulting data to assess (1) the performance of a range of flight metrics based on changes in pressure (altitude) and body acceleration as turbulence proxies, and (2) whether the predictive power of the proxies varied according to whether data were collected onboard the fixed wing aircraft or flapping fliers.

Materials and methods

Data collection

Data were collected near Radolfzell in Germany (47°44'42.76"N, 8°57'59.39"E) within an area of 36.6 km^{-2} characterised by a narrow valley between two forested hills (Fig. 1C,D). Flight data were collected over six days in July 2018, eight days in April 2019 and nine days in July 2019. This ensured that we sampled a wide range of convective conditions, as well as wind strengths and directions. Data were also collected during morning and afternoon sessions, as turbulence and wind strength tended to be higher in the afternoons. Wind speed was logged at the pigeon release site every five seconds using a Kestrel 5500 anemometer (Kestrel instruments, USA) stationed 5 m above ground.

Pigeons were brought from the loft to the release site by car; a straight-line distance of 5.7 km (see Garde et al. (2021) for details). Both the pigeons and the ultralight were equipped with a "Daily Diary" logger (Wildbyte Technologies, Swansea University, UK), recording tri-axial acceleration and barometric pressure (using Bosch pressure sensor BMP280 with a relative accuracy of ±0.12 hPa, equivalent to ±1 m), and a GiPSy-5 GPS logger (Technosmart, Rome, Italy). The two tags were connected to the same battery and integrated in a single 3D printed housing (Garde et al., 2021). The Daily Diary tag was programmed to take the time from the GPS logger in order to time-synchronise the two datasets. The combined system was attached to the back of ten pigeons using a Velcro patch attached to the down feathers with cyanoacrylate glue (Fig. 1A) (Biro et al., 2002). The total unit had an approximate mass of 18 g, accounting for < 4.5% of the mean pigeon body mass (455 g). One logger was also attached to the front of the ultralight frame (Fig. 1B). The

ultralight had a mass of 173 kg, including the pilot and petrol, and a wingspan of 12 m. Tags were programmed to record barometric pressure at 20 Hz and acceleration at 200 Hz, with the

exception of flights in 2018 where measurements were taken at 4 Hz and 40 Hz, respectively. The GPS sampled locations at 1 Hz except for the flights in April 2019, where sampling frequency was 5 Hz. For consistency, these flights were subsampled to 1 Hz.

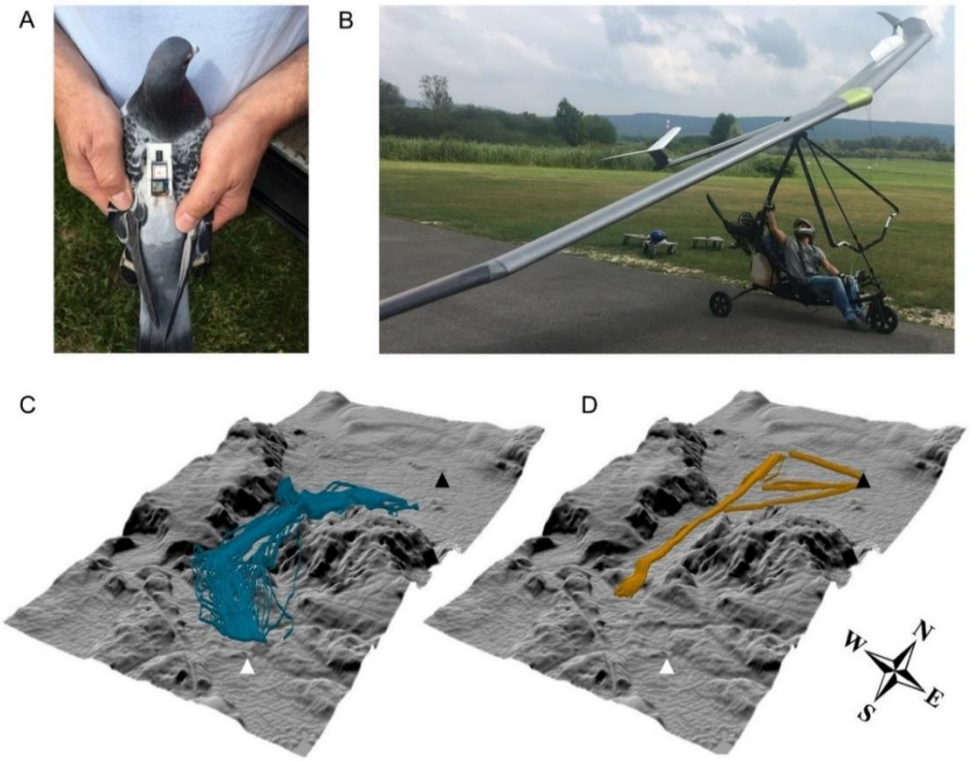

Figure 1. The logging platforms used in this study and corresponding flight tracks. A) The combined logger unit used on the pigeon's back, B) the ultralight, C) pigeon tracks and D) ultralight flight legs. Black and white triangles indicate the location of the release site and the loft, respectively. The parts of the tracks where pigeons performed orientation circles near the release site or loft, and the ultralight flight legs that did not form a straight line, were removed from the analysis, producing pigeon and ultralight flights with mean durations of ~293 and ~155 seconds respectively.

Prior to our trials pigeons had been flown with dummy loggers from the release site > 30 times to remove changes associated with route learning. We released six pigeons on a given day from the same release site, with 11-13 minutes between each release. Pigeons were released to fly solo so that any turbulence they encountered was the result of environmental conditions and not other birds (Usherwood et al., 2011). Birds were released when the ultralight reached the release site, to ensure that both the bird and the ultralight were flying in the same conditions. Once the bird was released, the ultralight flew a straight track from North to South (Fig. 1D), which largely coincided with the main pigeon flight route (Fig. 1C), with the Ultralight remaining behind the focal bird at all times. The ultralight maintained a

fixed altitude and speed during the flight, before returning to the release site for the next release.

While every attempt was made to maintain the same Ultralight path, on three days in July 2019, the pilot flew a triangular path close to the release site and before the valley because of mechanical difficulties and/ or unsafe wind conditions. This triangular path was split into two or three sections to extract flight legs that formed a relatively straight line. This reduced the effect of the ultralight's motion on the ultrasonic anemometer measurements (see below). The result of this process was 42 shorter flight legs (~ 40-60 seconds long) included in a total of 88 flights where a Daily Diary logger was attached on the ultralight. Forty two more flights were included in the analysis of turbulence (see below) where only ultrasonic anemometer data were available. These additional flights were only included in the comparison between the estimated turbulence and the pilot's rating of turbulence (see below). Data were collected with approval from the Animal Welfare Ethical Review Body of Swansea University (approval number: IP-1718-23) and the Regierungspräsidium Freiburg (reference number:G-17/92).

Turbulence estimation

A triaxial ultrasonic anemometer (uSonic-3 CLASS A, Supplementary information Fig. S1) was mounted on the front of the ultralight and programmed to record at 20 Hz. The three wind components were used to estimate the overall turbulence strength for each flight leg, and this, in turn, was used to examine the performance of fine-scale turbulence proxies (see data analysis). Turbulence intensity can be defined as the wind speed fluctuations relative to the mean wind speed. However, measurements made by the ultrasonic anemometer also included a contribution from the motion of the ultralight itself. Full estimation and subtraction of the ultralight's contribution requires high resolution measurements of the orientation and acceleration of the platform, however this is a complex process requiring very accurate measurements synchronised with the wind speed data (Canut et al., 2016, Prytherch et al., 2015, Schulz et al., 2005). This approach is required for calculating turbulent fluxes. Since our aim was to provide a qualitative measure of changes in turbulence levels, we developed a simpler approach using the anemometer measurements alone.

Our assumption was that the motion of the ultralight was largely confined to particular frequencies, which we identified using the turbulence power spectrum. The log power spectrum density of the root mean square of the three velocity components is predicted to follow a -5/3 slope for homogeneous, isotropic turbulence. This holds over a wide range of

frequencies (the whole inertial subrange) as energy cascades from low to high frequencies (larger to smaller scale eddies) until it is dissipated through viscosity (Stull, 1988). Our spectra were heavily contaminated by the ultralight's motion, especially at lower and higher frequencies. Nonetheless, it should be possible to identify a range of frequencies where contamination from the ultralight motion is small and this slope can be fitted.

Visual inspection of the log power plots revealed that frequencies between ~ $10^{-2.3}$ and 10^{0} (~0.05 to 1 seconds) were typically the least contaminated in the inertial subrange, and the most appropriate for fitting the ideal -5/3 power law (Supplementary information Fig. S2). Our method automatically fitted the -5/3 line within this range of frequencies and objectively selected the subrange with the best fit for each ultralight leg (that with the lowest root mean square error), subject to the subrange spanning at least half a decade.

The constant of proportionality of this fit is directly related to the eddy dissipation rate, which is equal to the rate of turbulence production at large scales (assuming the turbulence is statistically stationary), and hence provides a measure of turbulence. This follows because energy in the inertial subrange is not generated or lost, but rather cascades from larger to smaller scales. Indeed, this proportionality is often used in meteorology to estimate the dissipation rate from ultrasonic anemometers (e.g. Oncley et al., 1996), and similar approaches have been used to measure clear air turbulence using the eddy dissipation rate from aircraft (Huang et al., 2019, Kim et al., 2020). We therefore took the proportionality of the fit for the power law relationship (between the power and the frequency$^{(-5/3)}$ as a measure of the turbulent energy.

We also compared turbulence estimates from the ultralight anemometer with a qualitative assessment of turbulence made by the pilot on a scale of 0 – 5 (0: no turbulence and 5 highest turbulence). This is analogous to the turbulence observations that are routinely provided verbally by pilots in the form of pilot reports (PIREPs). Here, the turbulence level is determined by a pilot's subjective experience of the aircraft response to turbulence (Kim et al., 2020). Computations of our qualitative measure of turbulence strength were conducted in Python version 2.7.15 (Van Rossum, 2007) (see supplementary material for the code).

Data analysis

Estimates of turbulence from the anemometer on the ultralight were used to assess the performance of potential turbulence proxies based on pressure and acceleration measurements on both flying bodies. We predicted that turbulence would cause vertical displacements in flying bodies that should be evident in the barometric pressure data. To assess this we

smoothed the pressure values over two seconds and calculated the mean pressure difference per second. We also calculated the pressure fluctuations by subtracting pressure smoothed over 30 s (after testing different windows) from the raw values.

We also tested the performance of acceleration-based proxies, which could have advantages over pressure-based metrics because they can capture lateral, as well as vertical, displacements. For this we used the vectorial static body acceleration (VeSBA), calculated as the root mean square of the three smoothed acceleration channels, smoothed over two seconds (Wilson et al., 2013). Smoothing is a simple, but commonly used, way of removing much of the high frequency "dynamic" component of the acceleration and isolating the "static" or gravitational component. VeSBA should equal 1.0 *g* for a body flying straight and level and maintaining a constant velocity. Departures from 1 *g* can occur when the flying body is acted on by an external force, such as turbulence, which can cause (primarily) vertical and lateral displacements. We therefore predicted that increasing turbulence would result in greater displacements from a straight and level flight path, producing a positive correlation between VeSBA and turbulence intensity. We calculated the fluctuations in VeSBA by subtracting 1.0 *g* from VeSBA values.

In order to account for the difference in resolution between turbulence (one estimate per flight leg), VeSBA and pressure (measured with sub-second resolution and then smoothed), we calculated four metrics for each quantity per flight leg: the interquartile range (IQR), median, variance and the sum of all absolute values normalised by the flight's leg sample size (SUM), as a measure of the area under the curve (AOC). The SUM and the median were used to identify the magnitude of each measured quantity, and the interquartile range and the variance indicated the level of variability per flight. This process resulted in a set of 18 metrics including statistics from the fluctuations, the smoothed and non-smoothed VeSBA and pressure.

The statistical modelling tested 18 models based on pigeon flight and 18 models based on ultralight flight using a single flight metric of VeSBA or pressure as the single predictor, and the ground truth estimate of turbulence from the ultrasonic anemometer as the response variable. The same set of 18 metrics was tested for each flying body to assess the performance of each metric to act as proxy of turbulence and to compare the performance of proxies between the two flying bodies.

The performance of all metrics in predicting turbulence strength were evaluated with generalised additive effect models with gaussian errors (GAM, package "mgcv" version:

1.8.31, Wood (2017)). This allowed us to test for linear and non-linear relationships across the large set of models. Each ultralight flight leg (n=88) was associated with the turbulence measured within it, while each pigeon flight (n=66) was assigned the turbulence estimate of the closest ultralight flight in time (range: 0.2 – 107 minutes, with closest ultralight flight for two pigeon flights being greater than one hour). One model was run for each single metric and models were ranked by their predictive ability in terms of Akaike's Information Criterion (AIC). We assessed if different loggers had an effect on the models by having a trend to register higher or lower pressure or VeSBA variabilities and whether some pigeons tended to fly more or less stable by running the same models as generalised additive mixed effect models (GAMMs) with the addition of tag ID or pigeon ID (in the case of the pigeon models) as a random effect (intercept). All models included the date and the mean coordinates of each flight, using the corARMA and corSpatial functions (nlme package version: 3.1.148, Pinheiro et al. (2007)) to account for temporal and spatial autocorrelation respectively. The final models were evaluated for outliers, uniformity, over/ under-dispersion and spatial/ temporal autocorrelation using the DHARMa package version: 0.3.3.0 (Hartig and Hartig, 2017). All statistical analysis was conducted in RStudio version: 1.2.5 (RStudio Team, 2015) and the R programming language version: 3.6 (R Core Team, 2020).

As an additional ground-truthing step we assessed whether our best turbulence proxies were correlated with estimates of the convective velocity (w*) and the shear velocity (u*), using data from the global reanalysis ERA5 (Hersbach et al., 2018) (see Supplementary information for the estimation of convective and shear velocities).

Results

In several cases birds did not return to the loft immediately, but waited until other flockmate(s) were released, before flying back together. These flights, as well as others with incomplete or errroneous data were excluded. A total of 66 pigeon flights were used to estimate turbulence proxies after excluding the non-solo flights and pigeon flights for which the ultralight pilot did not fly either because of mechanical problems or because the conditions in the valley were not safe and hence turbulence was not measured. A total of 88 ultralight flights were used for analysis after excluding flights for which the ultrasonic anemometer did not record any data or did not measure data for all the flights of a given day because of low battery.

Our method of fitting the -5/3 power law line to the turbulence spectrum from the anemometer gave linear fitting errors > 0.2 (root mean square) for 24% of the ultralight

flights. This suggests that (i) the mean flow and/ or strength of the turbulence changed over the length of the flight leg, and/ or (ii) the part of the power spectra selected for analysis still contained some contamination from the motion of the ultralight. Nonetheless, there was a positive relationship between the anemometer estimates of turbulence and the pilots turbulence score on a given day (Pearson correlation coefficient = 0.73, t = 12.111, df = 128, p-value < 2.2e-16) (Linear fit: adj. R^2 = 0.53, n = 130 (Supplementary information Fig. S3).

Performance of turbulence proxies (i) pigeon flight data

A positive linear/ near-linear relationship was identified between the anemometer estimates of turbulence and the pigeon -based proxies in almost all of the top models in terms of AIC (Table 1, Supplementary information Fig. S4), which included both pressure- and VeSBA-based proxies. The top two models were proxies of pressure fluctuations, while three models of mean pressure difference per second (SUM, IQR and variance) followed in the top 10 models. Pressure proxies ranked higher than VeSBA proxies and had the highest R^2, with only three proxies based on VeSBA included in the top 10 models. Overall, AIC scores differed between models and the Adj. R^2 values ranged between 0.21-0.41). Neither tag ID nor pigeon ID was significant.

Table 1. Top 10 pigeon proxy models ranked by AIC. "IQR", "VAR", "MED", "SUM" are used to indicate that the model is the interquartile range, variance, median and area under the curve of each property. The estimated degrees of freedom (EDF) indicate the extent to which relationships are linear, with values closer to 1 describing a linear fit and closer to 2 curvilinear.

Model	**P-value**	**EDF**	**Adj. R^2**	**Dev.Expl.**	**AIC**	**ΔAIC**
Raw pressure fluctuations_ IQR	<0.001	1.57	0.41	0.43	176.59	-
Raw pressure fluctuations_SUM	<0.001	1.13	0.40	0.41	177.33	0.74
Raw pressure fluctuations_ MED	<0.001	1.20	0.38	0.39	179.58	2.99
Raw pressure fluctuations_VAR	<0.001	1.71	0.34	0.36	184.81	8.21
Mean pressure difference per s_SUM	<0.001	1.70	0.30	0.32	188.26	11.67
Mean pressure difference per s_IQR	<0.001	1.80	0.29	0.31	189.01	12.42
Mean pressure difference per s_VAR	<0.001	1.80	0.27	0.29	191.31	14.72
VeSBA fluctuations_VAR	<0.001	1.75	0.27	0.29	191.31	14.72
VeSBA_VAR	<0.001	1.40	0.22	0.24	195.28	18.69
VeSBA fluctuations_SUM	<0.001	1.00	0.21	0.22	195.65	19.06

Performance of turbulence proxies (ii) ultralight flight data

Proxies from metrics recorded on the ultralight performed less well than metrics from pigeon movements, with the R^2 from the top model being 0.33 (Supplementary information Table S1), compared to a maximum of 0.41 in the pigeon flight models. Nonetheless, similar to the pigeon proxies, models of pressure ranked higher than models of VeSBA. As with the pigeon models, all pressure summary statistics were included in the top 10 models. However, models of mean pressure difference per second ranked higher than models of pressure fluctuations, with the model that ranked 1st in the pigeon models, ranking 7th place in the ultralight models. Tag ID was significant, which was unsurprising as the same tag was used for all flight legs of the same day, and a small number of tags were used on the ultralight compared to the pigeons.

Positive near linear relationships were identified in the top 2 of the 10 best models for pigeon- and ultralight- based proxies (Fig. 2). While the majority of pigeon-based proxies had an approximately linear relationship with turbulence this varied between the pigeon and ultralight proxies, with more non-linear relationships predicted for the ultralight, although many of these non-linear relationships were strongly influenced by very high/ low proxy values where there were few data points (Fig S4, S5).

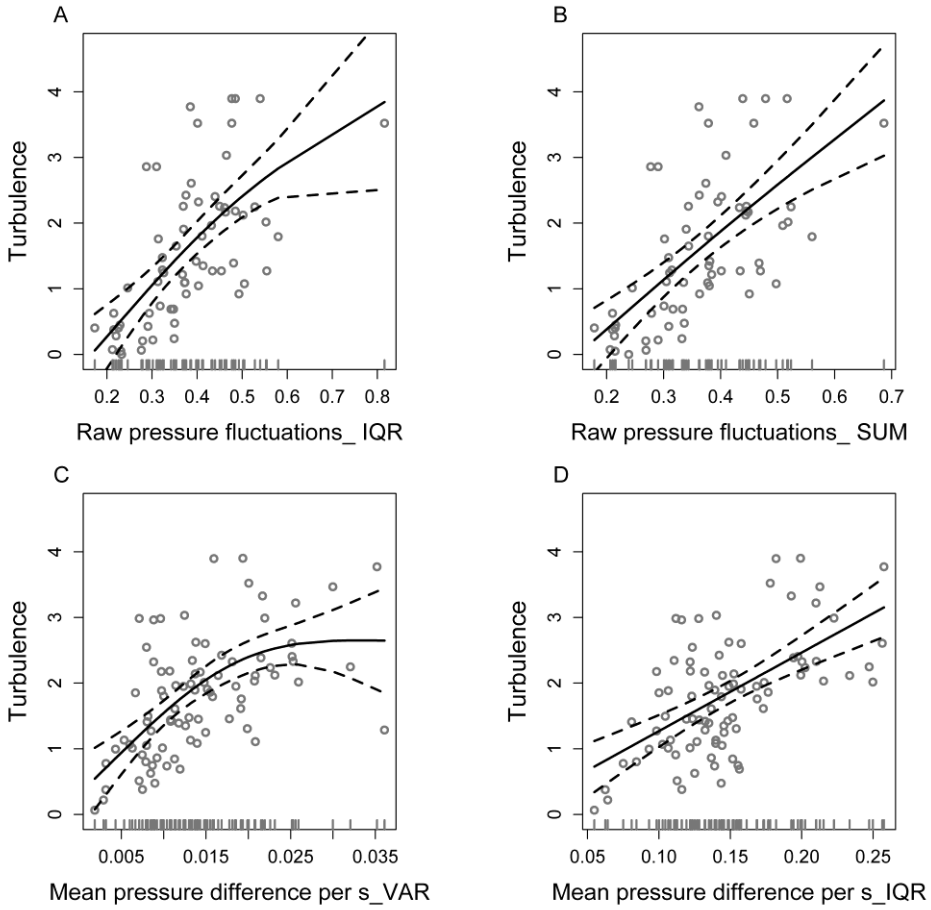

Figure 2. Turbulence predicted from (A, B) pigeon movement metrics and from (C, D) ultralight movement metrics, per flight. The top two models based on each aerial body are presented, with black solid curve indicating the predicted fit (dashed curves 95% confidence intervals) and grey points the raw observations.

Comparing pigeon flight turbulence proxies with thermal and mechanical turbulence

The best pigeon proxy in terms of both R^2 and AIC (raw pressure fluctuations IQR) was positively correlated with both the hourly convective velocity (w^*) and shear velocity (u^*) (Spearman correlation coefficients: 0.58, S= 2104.96, p-value= 2.68513674e-07 and 0.59, S= 20534.33, p-value= 1.46388147e-07, for w^* and u^* respectively). The latter, in turn, increased with the ERA5 wind speed (Fig. 3).

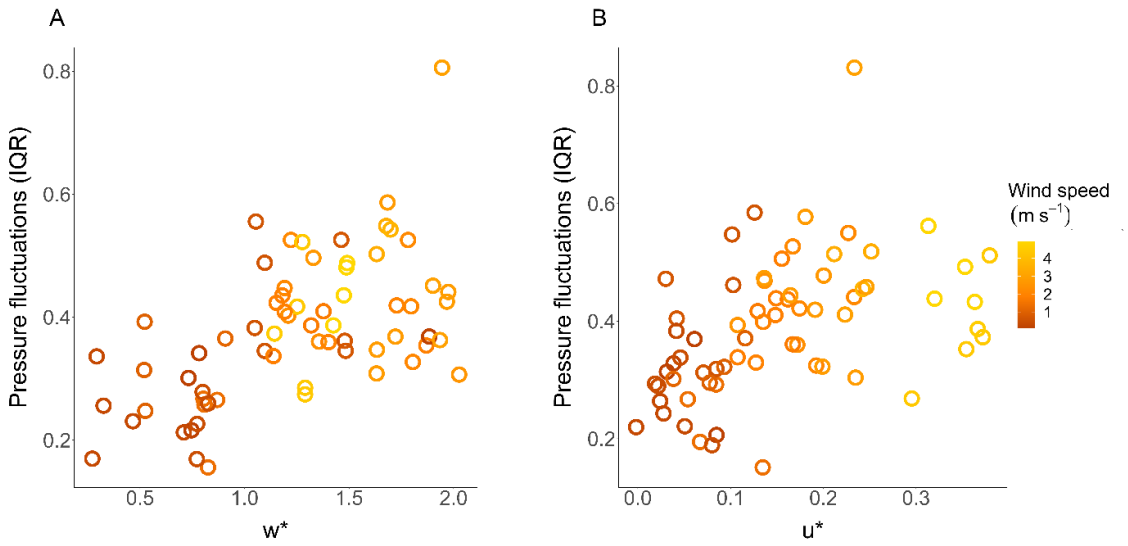

Figure 3. Comparison of the best pigeon turbulence proxy (the inter-quartile range of the raw pressure fluctuations) with (A) thermal uplift and (B) shear velocity (n=66 flights).

Mapping the turbulence using the same proxy summarised over 15 second sections of the flight path, revealed spatial patterns in turbulence (Fig. 4) that also varied with wind direction. Predicted turbulence was particularly high in the inlet and the outlet of the valley in Easterly winds (Fig. 4 A and B), whether or not overall turbulence was high. This pattern was also seen in the measured turbulence and corroborated by the pilot's experience. Nonetheless, the valley inlet and outlet were not particularly turbulent in Northerly or Southerly winds (Fig. 4 D) when turbulence conditions were weak. Furthermore, birds appeared to avoid the southerly end of the valley in Northerly/ Southerly winds when the mean turbulence was high (Fig. 4C).

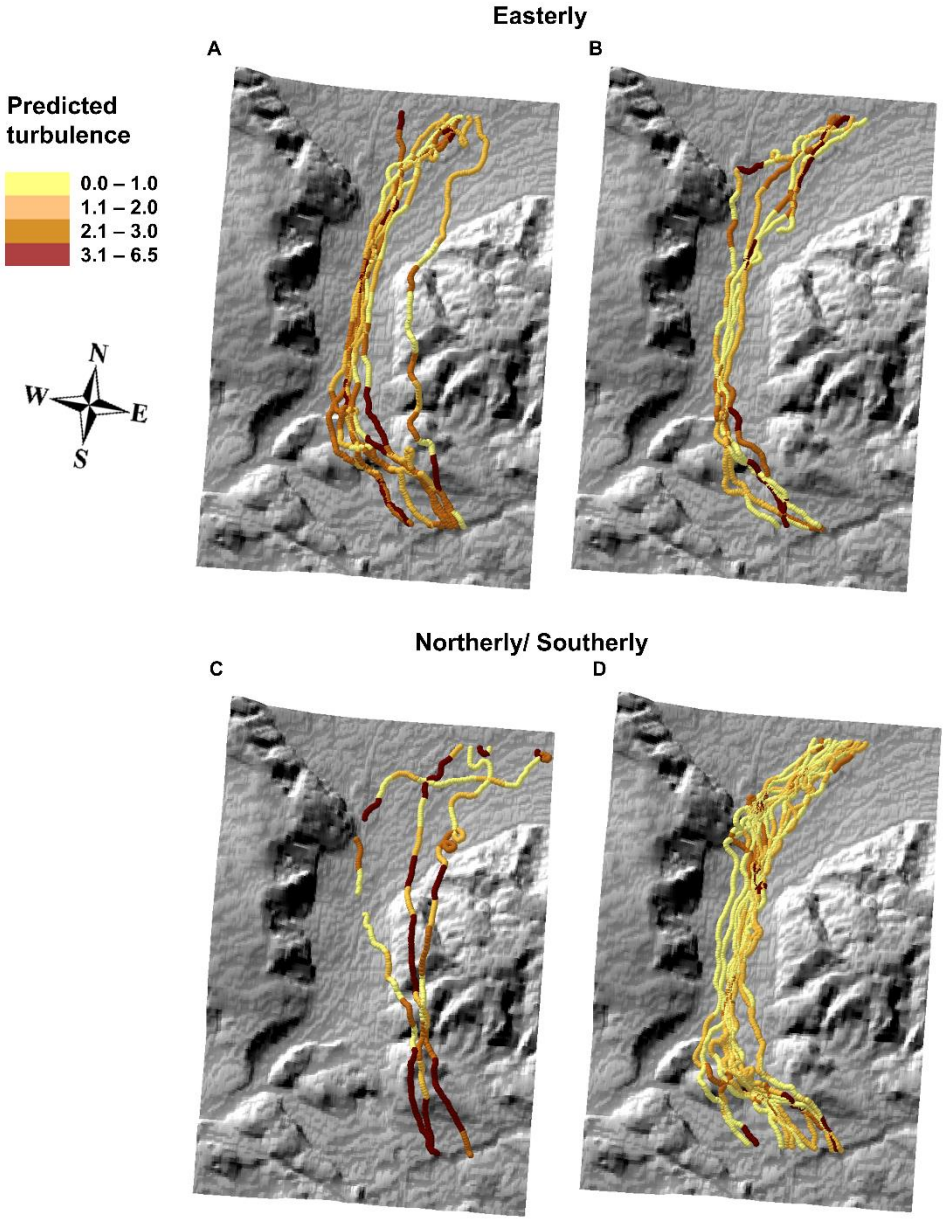

Figure 4. Spatial variation in turbulence as predicted from the fluctuations in pressure recorded onboard pigeons (specifically the interquartile range). Predictions were made for A) highly turbulent conditions (mean ≥ 3.0 per flight, mean wind speed = 2.9 m s^{-1}, n = 7 flights) and B) low turbulence (mean ≤ 1.5 per flight, mean wind speed = 1.3 m s^{-1}, n = 5 flights), both in Easterly winds and C) high turbulence (mean wind speed = 2.7 m s^{-1}, n = 3 flights) and D) low turbulence (mean wind speed = 1.7 m s^{-1}, n = 12 flights), in Northerly or Southerly winds.

Discussion

Previous studies have demonstrated that animal movement can be used to quantify the strength of thermal updrafts (Shannon et al., 2002, Treep et al., 2016, Weinzierl et al., 2016)

and determine the wind vector (Goto et al., 2017), at scales and in locations that are not possible using traditional meteorological approaches. Here we demonstrate that the fine-scale displacements of a flapping flier can also predict turbulence at the scale of a few hundred metres. Our primary estimates of turbulence were derived from an ultrasonic anemometer onboard an ultralight, which will have their own measurement error (e.g. from contamination of the three velocity components by the aircraft's motion). Nonetheless, the good agreement between turbulence estimates from the anemometer measurements, the pilot's scores, reanalysis data and proxy values, gives confidence in our overall approach and demonstrates that simple proxies can be employed to assess turbulence strength at fine scales. Our proxies are similar in concept to those developed for aviation (Kim et al., 2020), demonstrating the widespread utility of measurements derived from onboard accelerometers and pressure sensors.

The fact that turbulence generally followed an approximately- linear relationship with the proxies (particularly for birds but also in some cases for the ultralight proxies), means that relative changes in turbulence should be straightforward to approximate. The simple relationship is also in line with previous work that identified a linear correlation between the turbulence spectrum and the spectral composition of acceleration recorded onboard a golden eagle in gliding flight (Laurent et al., 2021).

Pressure proxies performed better than VeSBA proxies for both the pigeon and ultralight data, despite the fact that the variability in both proxies was positively correlated. In fact, the seven best pigeon proxies in terms of AIC were models of pressure, suggesting that turbulence caused more pronounced vertical than lateral displacements in these birds (as VeSBA will be sensitive to both, whereas pressure-based proxies relate to changes in the vertical axis alone).

Turbulence appeared to cause greater displacements for pigeons in flight than for the ultralight, as proxies derived from the ultralight flight did not perform quite as well. This will primarily be due to the substantial differences in mass and wing loading between the two systems, with a given eddy accelerating the larger ultralight to a lesser extent. Mean airspeeds of the ultralight and pigeon were similar (21.5 and 19.9 m s^{-1} respectively), but the objectives are likely to have differed as the pilot aimed to maintain a constant airspeed and straight and level flight, therefore compensating for turbulence along the flight path. Nonetheless it is likely that the pilot's ability to achieve this varied with the scale of the eddies, which may also have affected the performance of pressure and VeSBA proxies recorded on the ultralight.

Although the pilot aimed to maintain constant speed and altitude, the ability to do this might have varied with conditions and indeed he reported that he was able to respond to the large scale turbulence better, which might have led to a bias in the ultralight proxies that it is hard to quantify.

While we have not tested how pigeons respond to turbulence in terms of their kinematics and speed selection, it is clear that turbulence causes substantial variability in their vertical movements over fine scales, and that this increases with turbulence intensity. The motion of the pigeons' wings therefore did not dampen out all the turbulence that the birds encountered. (Combes and Dudley, 2009, Ortega-Jimenez et al., 2014, Ravi et al., 2015b). Variability in the pigeon trajectories has previously been interpreted as protean behaviour, with it conferring potential benefits as a predator avoidance strategy for solo-flying birds (Garde et al., 2021). These explanations are not necessarily mutually exclusive. The study by Garde et al. (2021) used a subset of our data (29 of 66 flights) that were performed under relatively weak turbulence intensities, with mean and maximum values of 0.9 and 2.5, compared to 1.6 and 4.7 in the current study. They also reported a lower variance in climb rate (mean and maximum 0.9 and 2.0 m s^{-1} per flight, compared to 1.6 and 6.7 reported here). Therefore, while some of the variability in pigeon flight behaviour reported by Garde et al. (2021) may be due to turbulence, it is likely there is still a baseline level of variability in birds flying solo and in low turbulence that could represent an anti-predator response. In both cases, what remains unknown is the power costs associated with variation in the flight trajectory.

The behaviour of the birds themselves, including the route selection, can provide insight into the likely costs or benefits of turbulence. Mapping changes in our pigeon-based proxies (estimated over 15 seconds) along the flight paths revealed patterns in turbulence that varied in both space and time. The high levels of turbulence intensity at the inlet and the outlet of the valley in strong Easterly winds are likely the result of wind shear, with the valley itself being more sheltered by the forested hill to the East. While predicted turbulence was lower overall in weaker winds, the strong turbulent features at the inlet and the outlet of the valley generally persisted, which might help explain why birds tended to fly the valley route. High turbulence was also predicted over the forested hill when wind direction changed to Northerly. This is consistent with wind travelling over an extended level terrain before the mouth of the valley where it is accelerated by the hill with high turbulence over the hill itself (although sample size is small in these conditions). These results also agree with the spatial

variability in turbulence strength experienced by the pilot. Overall, this demonstrates the capacity of our proxies to estimate fine scale turbulence over a complex terrain.

Widespread use of tracking technology means that pressure and acceleration data are increasingly available from animals instrumented with data loggers and that these can provide meteorological insight that is logistically difficult and costly to acquire from traditional platforms such as aircraft. Uncrewed aerial vehicles (UAVs) should provide also tractable platforms for the estimation of turbulence (Shannon et al., 2002), particularly in regions where birds do not fly. Nonetheless, planes and UAVs have their own limitations: In our study there were two days when the turbulence and wind made it unsafe for the pilot to fly the whole route. It is therefore notable that pigeons flew under these conditions, demonstrating that birds can reach areas that are inaccessible to light aircraft (the limitations are likely to be even more acute for UAVs). In some ways this is analogous to the case where seal-borne sensors are used to measure temperature and salinity below the ice, providing invaluable information on oceanographic processes in locations where ship-based studies are infeasible and satellite access is restricted (Charrassin et al., 2008, Roquet et al., 2014). However, our specific case raises intriguing questions about the behavioural, biomechanical (Cheney et al., 2020) and navigational capacities of birds, and other flying animals, that enable them to negotiate an aspect of the flight environment that remains dangerous for aircraft.

References

Biro, D., Guilford, T., Dell'Omo, G. & Lipp, H.-P. 2002. How the viewing of familiar landscapes prior to release allows pigeons to home faster: evidence from GPS tracking. *Journal of Experimental Biology,* 205**,** 3833-3844.

Bohrer, G., Brandes, D., Mandel, J. T., Bildstein, K. L., Miller, T. A., Lanzone, M., Katzner, T., Maisonneuve, C. & Tremblay, J. A. 2012. Estimating updraft velocity components over large spatial scales: contrasting migration strategies of golden eagles and turkey vultures. *Ecology letters,* 15**,** 96-103.

Bomphrey, R. J. & Godoy-Diana, R. 2018. Insect and insect-inspired aerodynamics: unsteadiness, structural mechanics and flight control. *Current opinion in insect science,* 30**,** 26-32.

Bowlin, M. S. & Wikelski, M. 2008. Pointed wings, low wingloading and calm air reduce migratory flight costs in songbirds. *PloS one,* 3**,** e2154.

Canut, G., Couvreux, F., Lothon, M., Legain, D., Piguet, B., Lampert, A., Maurel, W. & Moulin, E. 2016. Turbulence fluxes and variances measured with a sonic anemometer mounted on a tethered balloon. *Atmospheric Measurement Techniques,* 9**,** 4375-4386.

Charrassin, J.-B., Hindell, M., Rintoul, S. R., Roquet, F., Sokolov, S., Biuw, M., Costa, D., Boehme, L., Lovell, P. & Coleman, R. 2008. Southern Ocean frontal structure and sea-ice formation rates revealed by elephant seals. *Proceedings of the National Academy of Sciences,* 105**,** 11634-11639.

Cheney, J. A., Stevenson, J. P., Durston, N. E., Song, J., Usherwood, J. R., Bomphrey, R. J. & Windsor, S. P. 2020. Bird wings act as a suspension system that rejects gusts. *Proceedings of the Royal Society B,* 287**,** 20201748.

Combes, S. A. & Dudley, R. 2009. Turbulence-driven instabilities limit insect flight performance. *Proceedings of the National Academy of Sciences,* 106**,** 9105-9108.

Garde, B., Wilson, R. P., Lempidakis, E., Börger, L., Portugal, S. J., Hedenström, A., Dell'Omo, G., Quetting, M., Wikelski, M. & Shepard, E. L. 2021. Fine-scale changes in speed and altitude suggest protean movements in homing pigeon flights. *Royal Society open science,* 8**,** 210130.

Goto, Y., Yoda, K. & Sato, K. 2017. Asymmetry hidden in birds' tracks reveals wind, heading, and orientation ability over the ocean. *Science advances,* 3**,** e1700097.

Hartig, F. & Hartig, M. F. 2017. DHARMa: Residual Diagnostics for Hierarchical (Multi-Level Mixed) Regression Models. R package version 0.3.3.

Hedenström, A. & Alerstam, T. 1995. Optimal flight speed of birds. *Philosophical Transactions of the Royal Society of London. Series B: Biological Sciences,* 348**,** 471-487.

Hersbach, H., Bell, B., Berrisford, P., Biavati, G., Horányi, A., Muñoz Sabater, J., J, N., Peubey, C., Radu, R., Rozum, I., Schepers, D., Simmons, A., Soci, C., Dee, D. & Thépaut, J.-N. 2018. ERA5 hourly data on single levels from 1979 to present.

Huang, R., Sun, H., Wu, C., Wang, C. & Lu, B. 2019. Estimating eddy dissipation rate with QAR flight big data. Applied Sciences, 9, 5192.

Kim, S.-H., Chun, H.-Y., Kim, J.-H., Sharman, R. D. & Strahan, M. 2020. Retrieval of eddy dissipation rate from derived equivalent vertical gust included in Aircraft Meteorological Data Relay (AMDAR). Atmospheric Measurement Techniques, 13, 1373-1385.

Laurent, K. M., Fogg, B., Ginsburg, T., Halverson, C., Lanzone, M. J., Miller, T. A., Winkler, D. W. & Bewley, G. P. 2021. Turbulence explains the accelerations of an eagle in natural flight. *Proceedings of the National Academy of Sciences,* 118.

Lieber, L., Langrock, R. & Nimmo-Smith, W. A. M. 2021. A bird's-eye view on turbulence: seabird foraging associations with evolving surface flow features. *Proceedings of the Royal Society B,* 288**,** 20210592.

Liechti, F. 2006. Birds: blowin'by the wind? *Journal of Ornithology,* 147**,** 202-211.

Mallon, J. M., Bildstein, K. L. & Katzner, T. E. 2016. In-flight turbulence benefits soaring birds. *The Auk: Ornithological Advances,* 133**,** 79-85.

Nathan, R., Sapir, N., Trakhtenbrot, A., Katul, G. G., Bohrer, G., Otte, M., Avissar, R., Soons, M. B., Horn, H. S. & Wikelski, M. 2005. Long-distance biological transport processes through the air: can nature's complexity be unfolded in silico? *Diversity and Distributions,* 11**,** 131-137.

Newman, J. F., Klein, P. M., Wharton, S., Sathe, A., Bonin, T. A., Chilson, P. B. & Muschinski, A. 2016. Evaluation of three lidar scanning strategies for turbulence measurements. *Atmospheric Measurement Techniques,* 9**,** 1993-2013.

Oncley, S. P., Friehe, C. A., Larue, J. C., Businger, J. A., Itsweire, E. C. & Chang, S. S. 1996. Surface-layer fluxes, profiles, and turbulence measurements over uniform terrain under near-neutral conditions. Journal of Atmospheric Sciences, 53, 1029-1044.

Pinheiro, J., Bates, D., DebRoy, S., Sarkar, D. & Team, R. C. 2007. Linear and nonlinear mixed effects models. *R package version,* 3**,** 1-89.

Prytherch, J., Yelland, M. J., Brooks, I. M., Tupman, D. J., Pascal, R. W., Moat, B. I. & Norris, S. J. 2015. Motion-correlated flow distortion and wave-induced biases in air–

sea flux measurements from ships. *Atmospheric Chemistry and Physics,* 15**,** 10619-10629.

Quinn, D. B., Van Halder, Y. & Lentink, D. 2017. Adaptive control of turbulence intensity is accelerated by frugal flow sampling. *Journal of The Royal Society Interface,* 14**,** 20170621.

R Core Team 2020. R: A language and environment for statistical computing.

Ravi, S., Crall, J. D., McNeilly, L., Gagliardi, S. F., Biewener, A. A. & Combes, S. A. 2015. Hummingbird flight stability and control in freestream turbulent winds. *Journal of Experimental Biology,* 218**,** 1444-1452.

Roquet, F., Williams, G., Hindell, M. A., Harcourt, R., McMahon, C., Guinet, C., Charrassin, J.-B., Reverdin, G., Boehme, L. & Lovell, P. 2014. A Southern Indian Ocean database of hydrographic profiles obtained with instrumented elephant seals. *Scientific data,* 1**,** 1-10.

RStudio Team 2015. RStudio: Integrated Development Environment for R. Boston, MA.

Sapir, N., Horvitz, N., Wikelski, M., Avissar, R., Mahrer, Y. & Nathan, R. 2011. Migration by soaring or flapping: numerical atmospheric simulations reveal that turbulence kinetic energy dictates bee-eater flight mode. *Proceedings of the Royal Society B: Biological Sciences,* 278**,** 3380-3386.

Scacco, M., Flack, A., Duriez, O., Wikelski, M. & Safi, K. 2019. Static landscape features predict uplift locations for soaring birds across Europe. *Royal Society open science,* 6**,** 181440.

Schulz, E. W., Sanderson, B. & Bradley, E. F. 2005. Motion correction for shipborne turbulence sensors. *Journal of Atmospheric and Oceanic Technology,* 22**,** 55-69.

Shannon, H. D., Young, G. S., Yates, M. A., Fuller, M. R. & Seegar, W. S. 2002. Measurements of thermal updraft intensity over complex terrain using American white pelicans and a simple boundary-layer forecast model. *Boundary-Layer Meteorology,* 104**,** 167-199.

Shepard, E. L., Williamson, C. & Windsor, S. P. 2016. Fine-scale flight strategies of gulls in urban airflows indicate risk and reward in city living. *Philosophical Transactions of the Royal Society B: Biological Sciences,* 371**,** 20150394.

Stoll, R., Gibbs, J. A., Salesky, S. T., Anderson, W. & Calaf, M. 2020. Large-eddy simulation of the atmospheric boundary layer. *Boundary-Layer Meteorology,* 177**,** 541-581.

Stull, R. B. 1988. *An introduction to boundary layer meteorology,* Springer Science & Business Media.

Treep, J., Bohrer, G., Shamoun-Baranes, J., Duriez, O., de Moraes Frasson, R. P. & Bouten, W. 2016. Using high-resolution GPS tracking data of bird flight for meteorological observations. *Bulletin of the American Meteorological Society,* 97**,** 951-961.

Tucker, V. A. 1972. Metabolism during flight in the laughing gull, Larus atricilla. *American Journal of Physiology-Legacy Content,* 222**,** 237-245.

Usherwood, J. R., Stavrou, M., Lowe, J. C., Roskilly, K. & Wilson, A. M. 2011. Flying in a flock comes at a cost in pigeons. *Nature,* 474**,** 494-497.

Van Rossum, G. Python Programming Language. USENIX annual technical conference, 2007. 36.

Weinzierl, R., Bohrer, G., Kranstauber, B., Fiedler, W., Wikelski, M. & Flack, A. 2016. Wind estimation based on thermal soaring of birds. *Ecology and Evolution,* 6**,** 8706-8718.

Williams, H. J., Shepard, E., Holton, M. D., Alarcón, P., Wilson, R. & Lambertucci, S. 2020. Physical limits of flight performance in the heaviest soaring bird. *Proceedings of the National Academy of Sciences,* 117**,** 17884-17890.

Wilson, J. W., Mills, M. G., Wilson, R. P., Peters, G., Mills, M. E., Speakman, J. R., Durant, S. M., Bennett, N. C., Marks, N. J. & Scantlebury, M. 2013. Cheetahs, Acinonyx jubatus, balance turn capacity with pace when chasing prey. *Biology letters,* 9**,** 20130620.

Wood, S. N. 2017. *Generalized additive models: an introduction with R*, CRC press.

Chapter 2: Supplementary Information

Figure S1. Triaxial ultrasonic anemometer attached to the front part of the ultralight.

.

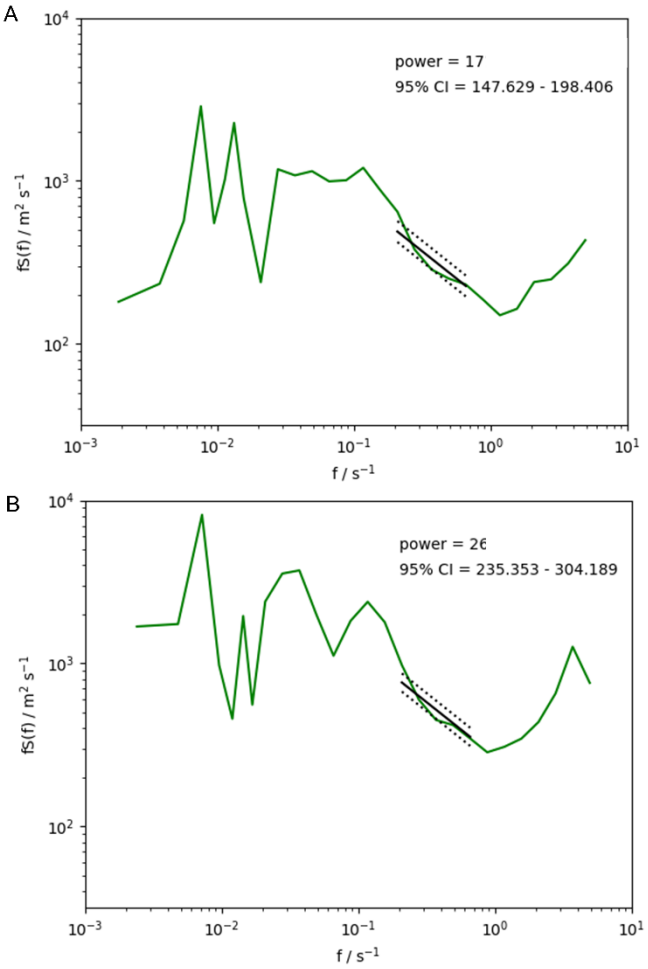

Figure S2. Two examples of the linear fit of the -5/3 slope on the ultrasonic anemometer log power spectrum. The log power spectrum ("fs(f)") is given over the time series frequencies ("f"). Error ("err") indicates the goodness of the linear fit.

Convective and shear velocity estimation

We examined the relationship between our best turbulence proxy (see below) and the convective velocity (w_*) and the shear velocity (u_*), using data from the global reanalysis ERA5 (Hersbach et al., 2018). While shear velocity was directly retrieved from ERA5, w_* can be estimated to a good approximation using the following equations:

$$w_* = \left(\frac{g\overline{(w'\theta'_v)}_0 h}{\theta_v}\right)^{\frac{1}{3}} \quad (1)$$

where h is the depth of the boundary layer from ERA5 (m) and g is the gravitational acceleration (9.81 m s^{-1}). In addition,

$$\overline{(w'\theta'_v)}_0 = \frac{SHF}{\rho C_p} + 0.61\theta_v \frac{LHF}{L}, \quad (2)$$

where SHF and LHF are the instantaneous surface sensible heat flux and surface latent heat flux from ERA5 (watts m^{-2}), ρ is the air density, C_p is the specific heat capacity = 1004 J kg^{-1}, and L is the latent heat of vaporisation of water = 2,260,000 J kg^{-1}.

Virtual temperature θ_v in equations 1 and 2 can be replaced with the potential temperature θ given by:

$$\theta = T\left(\frac{p}{p_0}\right)^{-R_d/C_p} \quad (3)$$

where p_0 = 1000 hPa, p is the surface pressure in hPa, $-R_d/C_p$ = -2/7 (to a good approximation), and T is the surface temperature at 2 m above ground from ERA5. All temperatures are in Kelvin.

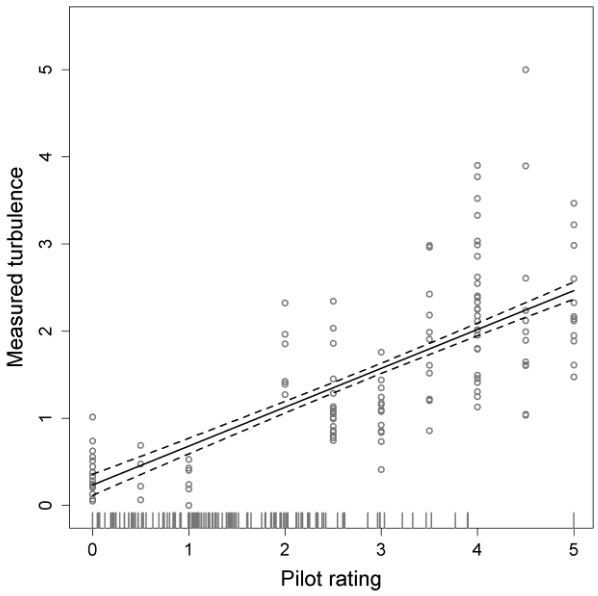

Figure S3. The turbulence measured by the ultrasonic anemometer per flight was positively correlated with the pilot's rating of turbulence per day (adj. $R^2 = 0.53$, n = 130). Solid line indicates the linear fit (with dashed lines: ± 1 standard error).

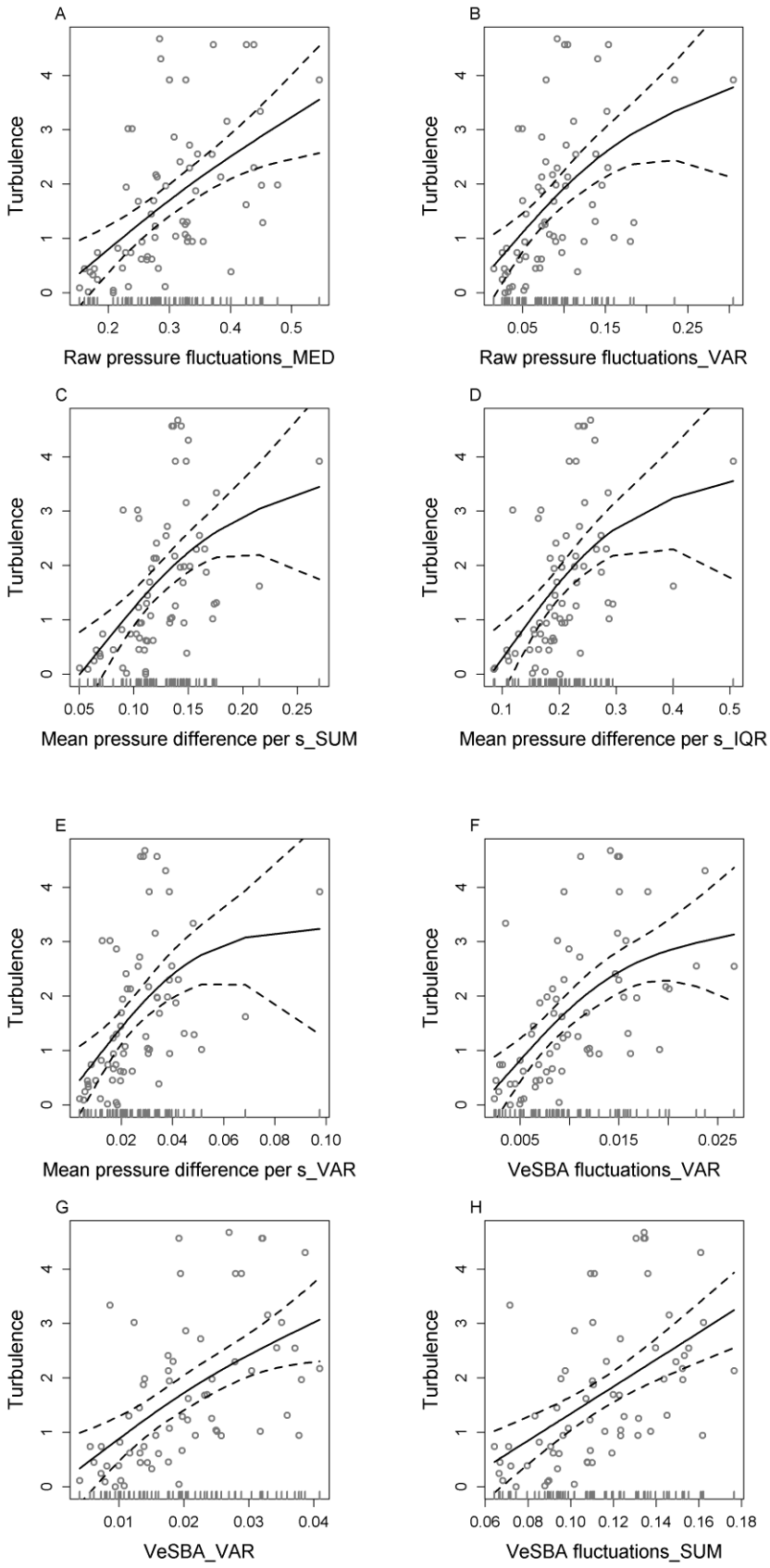
A
Turbulence
Raw pressure fluctuations_MED
B
Turbulence
Raw pressure fluctuations_VAR
C
Turbulence
Mean pressure difference per s_SUM
D
Turbulence
Mean pressure difference per s_IQR
E
Turbulence
Mean pressure difference per s_VAR
F
Turbulence
VeSBA fluctuations_VAR
G
Turbulence
VeSBA_VAR
H
Turbulence
VeSBA fluctuations_SUM

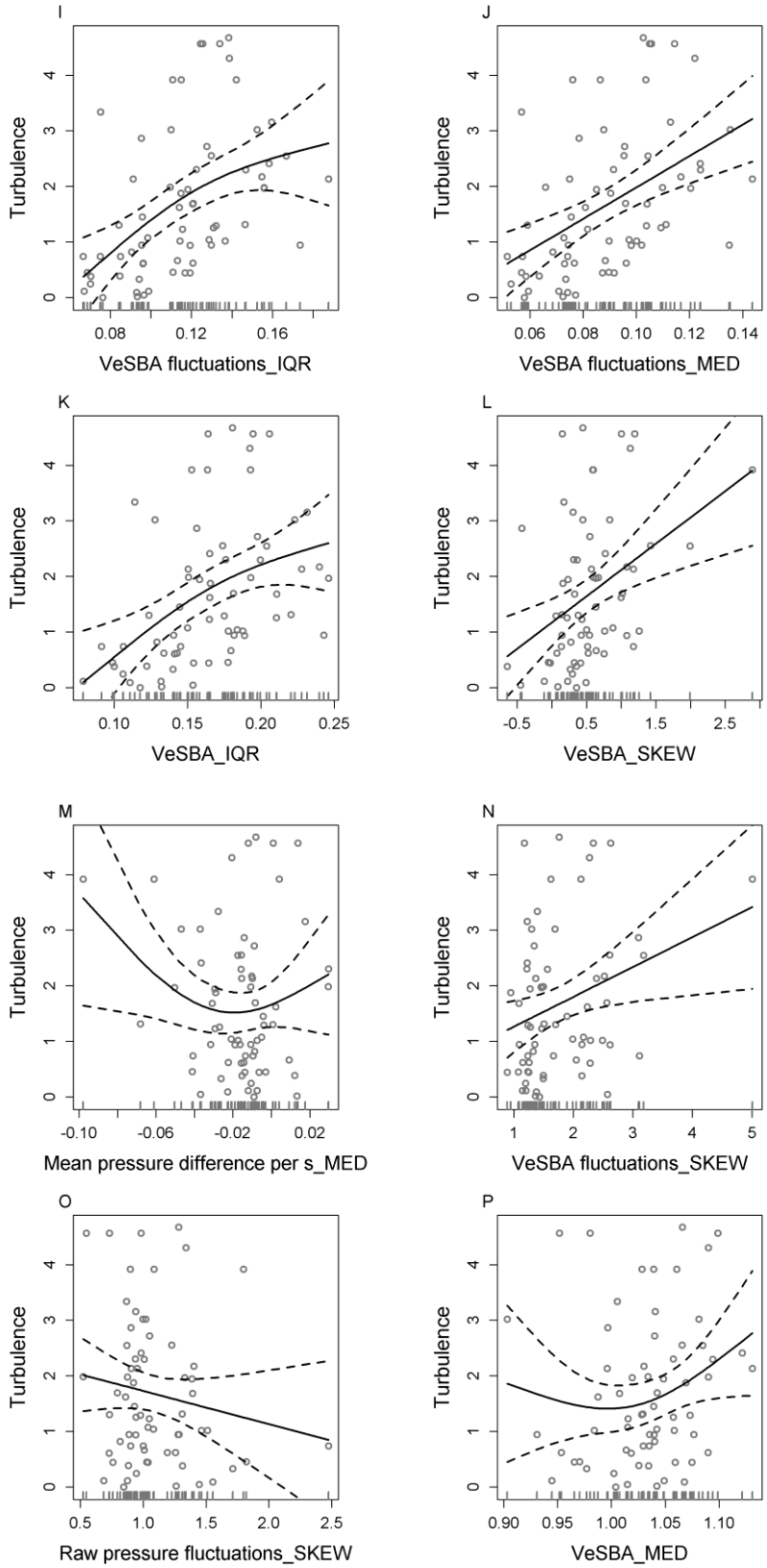

Figure S4. Pigeon-based proxies ranked from 3rd to 18th. The 16 models ranked below second place are presented in rank order. Black solid curves indicate the predicted fit (dashed curves 95% confidence intervals) and grey points the raw observations.

Table S1. Top 10 ultralight proxy models ranked by AIC. “IQR”, “VAR”, “MED”, “SUM” are used to indicate that the model is the interquartile range, variance, median and area under the curve of each property. The estimated degrees of freedom (EDF) indicate the extent to which relationships are linear, with values closer to 1 describing a linear fit and closer to 2 curvilinear.

Model	**P-value**	**EDF**	**Adj. R^2**	**Dev.Expl.**	**AIC**	**ΔAIC**
Mean pressure difference per s_VAR	<0.001	1.86	0.33	0.35	207.28	-
Mean pressure difference per s_IQR	<0.001	1.00	0.31	0.32	209.68	2.40
Mean pressure difference per s_SUM	<0.001	1.95	0.31	0.33	210.24	2.97
Raw pressure fluctuations_ SUM	<0.001	1.95	0.31	0.33	210.29	3.01
Raw pressure fluctuations_ MED	<0.001	1.87	0.3	0.32	211.43	4.15
VeSBA_IQR	<0.001	1.00	0.25	0.26	216.32	9.04
Raw pressure fluctuations_ IQR	<0.001	1.94	0.26	0.28	216.39	9.11
VeSBA fluctuations_MED	<0.001	1.92	0.21	0.23	221.83	14.55
VeSBA_VAR	<0.001	1.67	0.16	0.17	228.02	20.74
VeSBA fluctuations_SUM	<0.001	1.85	0.16	0.17	228.14	20.86

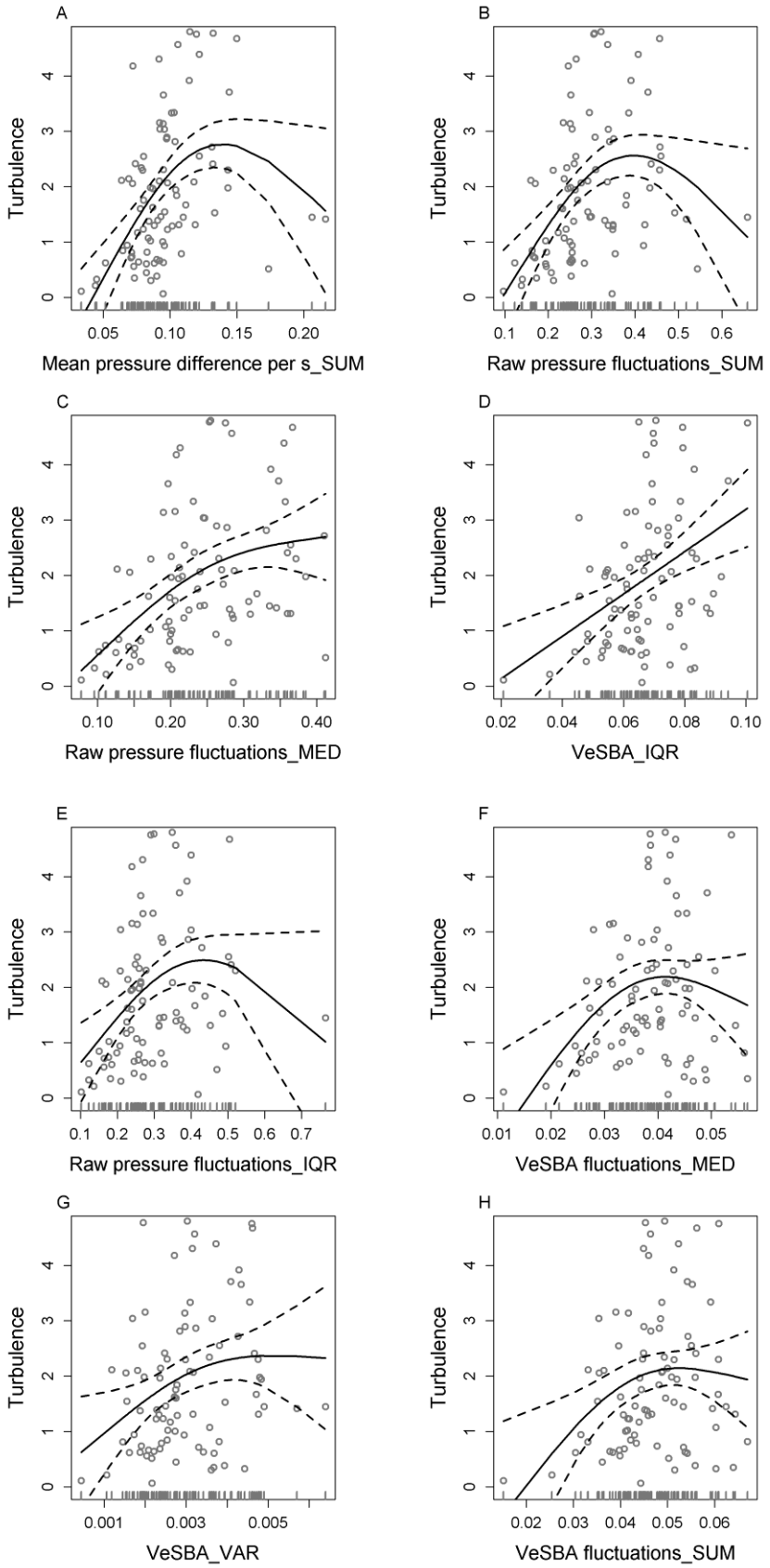
A
Turbulence
Mean pressure difference per s_SUM
B
Turbulence
Raw pressure fluctuations_SUM
C
Turbulence
Raw pressure fluctuations_MED
D
Turbulence
VeSBA_IQR
E
Turbulence
Raw pressure fluctuations_IQR
F
Turbulence
VeSBA fluctuations_MED
G
Turbulence
VeSBA_VAR
H
Turbulence
VeSBA fluctuations_SUM

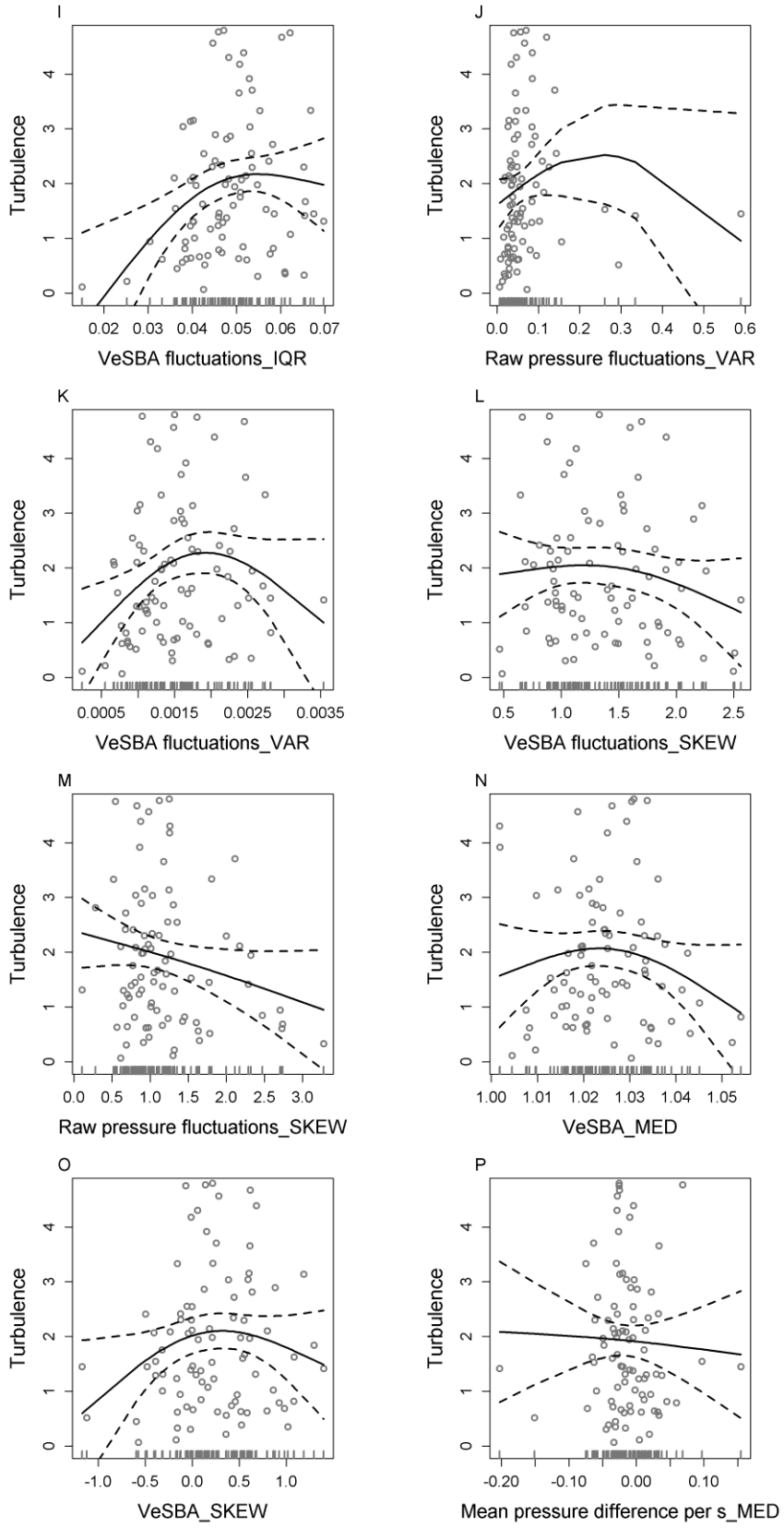

Figure S5. Ultralight-based proxies ranked from 3rd to 18th. The 16 models ranked below the second place are presented in rank order. Black solid curve indicates the predicted fit (dashed curves 95% confidence intervals) and grey points the raw observations.

Python scripts for estimating turbulence

```
#################### Script 1 ########################

import numpy as np
import scipy.signal as sig
import matplotlib.pyplot as plt
import matplotlib.lines as mlines
import re
import glob
import os
import csv
from powerspec import powerspec
dirs = sorted(glob.glob('Data/*'))
# Frequency of measurements
freq = 10
# Data cleaning filter window
win=7
# Data cleaning filter threshold
th=200
def readSonicCSV(file):
    uvw = np.loadtxt(file,usecols=(0,1,2),skiprows=1,delimiter=',')
    u = uvw[:,0]
    v = uvw[:,1]
    w = uvw[:,2]
    return u,v,w
def cleanSeries(x,w,th):
    xmed = sig.medfilt(x,w)
    ii = np.abs(xmed-x) > th
    x2 = np.copy(x)
    x2[ii] = xmed[ii]
    #x2[ii] = 0.0
    return x2
def calcPow(freq,S):
    y = np.log10(freq*S)
    x = np.log10(freq)
    i1 = np.min(np.nonzero(freq>0.05))
    i2 = np.max(np.nonzero(freq<1.0))
    istart = 0
    iend = 0
    c = 0
    cerr = 1e6
    for ist in np.arange(i1,i2-3):
        for ie in np.arange(ist+4,i2):
            ci = y[ist:ie+1]+2.0/3.0*x[ist:ie+1]
            ctmp = np.mean(ci)
            cerrtmp = np.sqrt(np.mean((ci-ctmp)**2))
            if (cerrtmp < cerr):
                cerr = cerrtmp
                c = ctmp
                istart = ist
                iend = ie
    se = cerr/np.sqrt(iend-istart)
    return c,istart,iend,cerr,se
tp = []
ts = []
tse1 = []
tse2 = []
tid = []
```

```
tke = []
col = []
mark = []
alpha = []
ids = []
lab = []
m = ['x','+','*','o']
for d in np.arange(len(dirs)):
    files = glob.glob('{}/*.csv'.format(dirs[d]))
    dirname = dirs[d]

lab.append('{}/{}/{}'.format(dirname[9:11],dirname[7:9],dirname[5:7]))
    with open ('{}/turb.dat'.format(dirs[d])) as tfile:
        tmp = tfile.readlines()
    turb = float(tmp[0])
    for f in np.arange(len(files)):
        fname = files[f]
        flightid = os.path.basename(os.path.splitext(fname)[0])
        ids.append(flightid)
        u, v, w = readSonicCSV(fname)
        n = len(u)
        up = u - np.mean(u)
        vp = v - np.mean(v)
        wp = w - np.mean(w)

        Uptmp = np.sqrt(up*up+vp*vp+wp*wp)
        Up = cleanSeries(Uptmp,win,th)
        TKE = 0.5*np.mean(Up**2)
        [S,f] = powerspec(Up,freq,True,8)
        c,istart,iend,cerr,se = calcPow(f,S)
        # Standard error x 1.96 gives a 95% confidence interval
        ci = 1.96*se
        plt.loglog(f,f*S,'g')
        plt.loglog([f[istart],f[iend]],np.power(10,-
2.0/3.0*np.log10([f[istart],f[iend]])+c),'k')
        plt.loglog([f[istart],f[iend]],np.power(10,-
2.0/3.0*np.log10([f[istart],f[iend]])+c-ci),'k:')
        plt.loglog([f[istart],f[iend]],np.power(10,-
2.0/3.0*np.log10([f[istart],f[iend]])+c+ci),'k:')
        plt.xlabel('f / s$^{-1}$')
        plt.ylabel('fS(f) / m$^2$ s$^{-1}$')
        plt.text(0.2,5000,'power = {:<5.3f}'.format(10**c))
        plt.text(0.2,3500,'95% CI = {:<5.3f} - {:<5.3f}'.format(10**(c-
ci),10**(c+ci)))
        plt.axis([10**-3,10**1,10**1.5,10**4])
        plt.savefig('spectra_{}.png'.format(flightid))
        plt.close()
        tp.append(turb)
        ts.append(10**c)
        # Calculate error bars - / + confidence interval.
        tse1.append(10**c*(1.0-10**(-ci)))
        tse2.append(10**c*(10**ci-1))
        tid.append(d)
        tke.append(TKE)
        col.append('C{}'.format(d%9))
        mark.append(m[d//9])
        if (cerr < 0.2):
            alpha.append(1.0)
        else:
            alpha.append(0.5)
```

```
marks = []
for d in np.arange(len(dirs)):
    mm =
mlines.Line2D([0],[0],c='C{}'.format(d%9),marker=m[d//9],label=lab[d])
    marks.append(mm)
for i in np.arange(len(tp)):

plt.errorbar(tp[i],ts[i],yerr=np.reshape([tse1[i],tse2[i]],(2,1)),c=col
[i],marker=mark[i],alpha=alpha[i])
plt.xlabel('Pilot turbulence rating')
plt.ylabel('Turbulence strength from sonic')
plt.legend(handles = marks,ncol=2,fontsize=6)
plt.savefig('turbulence.png')
plt.close()
for i in np.arange(len(tp)):
    plt.scatter(tp[i],tke[i],c=col[i],marker=mark[i],alpha=alpha[i])
plt.xlabel('Pilot turbulence rating')
plt.ylabel('TKE from sonic')
plt.legend(handles = marks,ncol=2,fontsize=6)
plt.savefig('tke.png')
plt.close()
for i in np.arange(len(tp)):

plt.errorbar(ts[i],tke[i],xerr=np.reshape([tse1[i],tse2[i]],(2,1)),c=co
l[i],marker=mark[i],alpha=alpha[i])
plt.xlabel('Turbulence strength from sonic')
plt.ylabel('TKE from sonic')
plt.legend(handles = marks,ncol=2,fontsize=6)
plt.savefig('turbulence_tke.png')
plt.close()
with open('turbulence.csv', 'w') as csvfile:
    fieldnames = ['flight','pilot','sonic','err1','err2','tke']
    writer = csv.DictWriter(csvfile,fieldnames=fieldnames)
    writer.writeheader()
    for i in np.arange(len(ids)):
        writer.writerow({'flight': ids[i], 'pilot': tp[i], 'sonic':
ts[i], 'err1': tse1[i], 'err2': tse2[i], 'tke': tke[i]})
```

#################### Script 2 ########################

```
# [S,f]=powerspec(x,sf,bin,Nbins)
#
# calculates the power spectral density (S) of x, defined such that
# the integral of S over frequency is the variance of x
#  sum(S)*df = variance, where df is the frequency interval
#         df = sf/N, where sf is sample freq, N length of series
# S has units of x^2 hz^-1
#
# INPUT
#  x   - vector of data values
#  sf  - sample frequency (hz)
#  bin - string, if ='bin' the power spectrum is smoothed by simple
averaging
#              into equal Nbins/decade log-width frequency bins (first
few points
#        are unaveraged, since df > bin width)
#  Nbins - number of bins per decade to use, defaults = 8
#
# OUTPUT
#  S   - power spectral density (units of x^2 hz^-1 = x^2 s)
#  f   - frequency series
import numpy as np
def powerspec(x,sf,bin = False,Nbins = 8):
    L = len(x)
    if L%2 == 1:
        # if length of x is odd, pad end with repeated value
        padded = True
        x=np.append(x, x[-1])
        nfft = L+1        # force even number of points in fft
    else:
        nfft = L          # force even number of points in fft
    df = float(sf)/nfft               # frequency interval
    f = np.arange(1,nfft/2)*df        # frequency series
    # get Fourier series
    Rxx = np.fft.fft(x,nfft)
    Sxx = Rxx*np.conj(Rxx)
    Sxx = Sxx/(nfft*sf)  # scale power spectra by timeseries length &
sample freq
    S = 2*Sxx[1 : nfft/2]  # fold over spectrum, don't include DC
component
    if bin:
        # define 1/8 decade logarithmically equal width frequency bin
limits, ff

logff=np.arange(np.floor(np.log10(np.min(f))),np.ceil(np.log10(np.max(f
)))),1/float(Nbins))
        ff=np.power(10,logff)
        # find the first bin which can contain at least 2 spectral
points
        minbin=np.min(np.where(df<(np.diff(ff)/2)))
        # find the last bin for which there is any data (to avoid
possibility of single
        # point average, ensure at least N points - say N=10)
        maxbin=np.max(np.where(ff<f[len(f)-10]))
        # first few points are not averaged
        i=f<=ff[minbin]
```

```
    binS=S[i]
    binf=f[i]
    # remaining points are averaged within frequency bins
    for n in np.arange(minbin,maxbin+1):
        i=np.logical_and(f>ff[n],f<=ff[n+1])
        binS=np.append(binS,np.mean(S[i]))
        # binf set to centre of bin
        binf=np.append(binf,np.mean(ff[n:n+2]))
    S=binS
    f=binf
return[np.real(S),f]
```

Chapter 3: Turbulence affects the flight kinematics of an obligate flapping flier.

Abstract

Turbulence is nearly ubiquitous in the natural environment, yet very little is known about how this impacts flapping fliers. I used a new proxy of freestream turbulence, based on small-scale fluctuations in altitude (pressure) measured onboard homing pigeons, to investigate how turbulence impacts their flight kinematics, flight effort and route choice. Similar to laboratory studies, birds increased the variability in their wingbeat frequency and amplitude in relation to turbulence; responses that are thought to increase flight stability. The effects of turbulence can also be reduced by increasing the mean wingbeat frequency. It was therefore surprising that pigeons in this study decreased their mean wingbeat frequency with increasing turbulence, but increased their wingbeat amplitude. The consequences for flight effort are unclear, as power varies as a cubic function of both variables. Overall, this provides the first evidence that freestream turbulence affects a range of flight kinematic variables in an obligate flapping flier in nature, and indicates that active responses to increase flight control might come without a significant energetic cost.

Introduction

The impact of atmospheric turbulence on the aviation industry is well known (Gultepe et al., 2019, Storer et al., 2019). Turbulence increases drag (Anderson, 2016), which can reduce lift production, leading to instability and abrupt changes in altitude. Pilots are therefore advised to adjust their flight route and/ or altitude to avoid turbulent regions in the atmosphere, aircraft damage and fuel waste (Kauffmann, 2002). However, detouring and flying at sub-optimal altitudes also comes at a significant cost (Kauffmann, 2002). Turbulence is also likely to have a significant impact on animal flight, forcing animals to adapt their kinematics to improve their flight stability and control, which in turn is likely to increase flight costs. Yet little is known about how animals adjust their kinematics to turbulence, and the consequences for power use and route choice.

In laboratory environments (e.g. Ortega et al 2013) and small natural habitat patches (Combes et al 2009, Crall et al 2016) insects have been shown to adjust their flight kinematics in relation to simulated turbulence. For instance, higher rolling instabilities have been reported for hawkmoths (*Manduca sexta*) flying in von Kármán vortex streets (Ortega-Jimenez et al., 2013). Wild orchid bees (*Euglossa imperialis*) extended their legs to enhance flight control in turbulent conditions, which increased the power output by up to 30% (Combes and Dudley, 2009). Turbulence also impacted flight costs in bumblebees (*Bombus impatiens*), which increased both their wingbeat frequency and amplitude (Crall et al., 2017).

Some similarities have been found in bird responses to turbulence. Ruby-throated hummingbirds (*Archilochus colubris*) flying in simulated turbulence in a wind tunnel made fine-scale adjustments of their body and tail, and increased stroke amplitude, in order to maintain a relatively stable position, at the expense of higher drag (Ravi et al., 2015). Anna's hummingbirds (*Calypte anna*) flying in von Kármán vortex streets also increased the variance in their wingbeat frequency and amplitude, and experienced an increase in metabolic costs of up to 25% as turbulence scale increased (Ortega-Jimenez et al., 2014).

Nevertheless, there are substantial differences between the laboratory and field in terms of the nature of the turbulence that animals encounter, and their ability to respond. Laboratory studies simulate turbulence by introducing structures such as cylinders into the flow, which generate discrete alternating vortices that are shed at predictable intervals. These von Kármán vortex streets are rare in nature compared to free-stream turbulence, which is characterized by rapid, complex and unpredictable disturbances in the flow across a wide range of spatial and temporal scales (Ravi et al., 2015). Hummingbirds altered their kinematics in relation to both

forms of turbulence in order to increase their flight stability, but their precise kinematic responses differed according to whether the turbulence was generated by a grid (intended to be closer to turbulence commonly found in nature) or a cylinder (Ravi et al., 2015).

Another important distinction between simulated and free-stream turbulence in natural environments is that the latter often includes strong upward components driven by thermal convection and the interaction between the wind and obstacles on the ground. Some animals, particularly soaring birds, have evolved strategies to exploit this rising air, detouring from a straight line path in order to gain altitude in, and glide between, successive updrafts (e.g. Murgatroyd et al., 2018, Pennycuick, 1972). Circling to gain altitude in thermal updrafts is not cost-effective for flapping fliers (Hedenström, 1993). Nonetheless, high resolution numerical simulations have revealed that European bee-eaters (*Merops apiaster*) switch from flapping to soaring/gliding flight when turbulence strength reaches a certain threshold, and in fact this decision is so crucial that they completely ignore wind support (Sapir et al., 2011). Anecdotal observations of other flapping fliers, such as pigeons, soaring over buildings in strong wind conditions also suggests that they are able to capitalize on the upward components of turbulence in some conditions. Therefore, turbulence may not always represent a cost for flapping fliers operating in the natural environment.

The demonstration in chapter 2 that fine-scale vertical displacements of flying pigeons can be used as a proxy for turbulence means that it is now possible to examine how birds respond to turbulence at fine-scales when flying in the natural environment. In this study we equipped solo-flying homing pigeons (*Columba livia Linnaeus*) with high-frequency data-loggers and released them in varying degrees of free-stream turbulence to establish how turbulence impacts their kinematics and behaviour. Homing pigeons are a model species in which to investigate the effects of turbulence on powered flight as they will return to their loft in a range of conditions, typically following a consistent route once they are familiar with the release location and terrain (Biro et al., 2004, Meade et al., 2005). However, in this study it became clear that pigeons took one of two distinct routes back to the loft, raising the possibility that route choice may also be influenced by changing aerial conditions. I therefore assessed responses to turbulence from the level of wingbeat kinematics, through to horizontal and vertical route choice. My specific objectives were to: 1) Quantify the extent to which pigeons varied their wingbeat kinematics (wingbeat frequency and amplitude) to increase their flight stability, (2) assess the consequences for power output, in terms of the mean wingbeat frequency and amplitude required to fly at a given airspeed, (3) evaluate how turbulence impacted the flight trajectory in terms of track tortuosity and route choice, with the

expectation that pigeons would fly at lower altitudes to reduce the level of turbulence they were exposed to. Taken together this should provide insight into the impact of turbulence on flapping fliers and the importance of this for kinematic and behavioural responses relative to other, well-studied aspects of the flight environment, namely wind.

Materials and methods

Data collection

Ten homing pigeons (*Columba livia Linnaeus*, with body mass 442 - 476 g) were equipped with a "Daily Diary" unit (DD, Wildbyte Technologies, Swansea University, UK) and a GPS logger (GiPSy 5, Technosmart Europe, Guidonia-Montecelio, Italy) integrated in a single 3D printed housing (Garde et al., 2021). Birds were released in an agricultural area near Radolfzell, Germany (see chapter 2) to fly solo back to their loft. Each bird was released >30 times prior to data collection in order to control for the effect of route familiarity on flight trajectories and kinematics (Taylor et al., 2017). During field trials, six birds were randomly selected for release on a given day, for a total of 23 days and 81 releases in two summers (July 2018, 2019, 48 flights) and one spring (April 2019, 33 flights). Each bird was released with an approximate gap of ten minutes from the previous bird to facilitate solo flight (see chapter 2), and releases took place in different hours across days to cover a wide range of turbulence levels (induced by thermal heating and/or wind strength/direction).

The DD units logged triaxial acceleration (at either 40 or 200 Hz, but all files recorded at 200 Hz were sub-sampled to 40 Hz for consistency) and barometric pressure (sampled at either 4 or 20 Hz depending on the acceleration frequency, but a final frequency of 4 Hz was used for all files). The GPS logger sampled at 1 Hz for all flights except for the flights in April 2019 (5 Hz), which were subsampled to 1 Hz. Wind speed and direction were recorded every 10 s using a Kestrel 5500 anemometer (Kestrel instruments, USA) positioned at a height of 5 m at the release site.

Data processing (i) the impact of turbulence on flight trajectory and route choice

The best turbulence proxy from chapter 2 was used to estimate variation in turbulence strength. This provided a qualitative estimate of turbulence, derived from the interquartile range of pressure fluctuations measured onboard pigeons within each 15-second segment of a pigeon's flight track. The 15-second window was selected based on trials and was considered large enough to capture the scale of large eddies at the mean flight altitude above ground birds flew (~ 80 m), also taking into account the mean flight ground speed of ~ 20 m s^{-1} and the total distance covered per segment.

The impact of turbulence on track properties was investigated at a number of levels including horizontal route choice, flight height (vertical route choice) and fine-scale track tortuosity. In addition, it became clear that pigeons performed multiple circles immediately after release as part of an orientation phase before either taking a route through the valley or over the hill (see chapter 2). I hypothesized that the circling phase may also serve to enable birds to sample the flight conditions, namely the turbulence and wind vector, which could in turn influence route choice. In order to investigate this, I removed the circling phase of each flight and quantified the number of circles and time spent circling using the GPS data. Flights were categorised according to their route, and I considered a flight to cross the hill when the total distance flown over the hill was at least 15% of the total distance covered. The final approach to the loft was also removed from all flight tracks, as this was often characterised by a short but highly tortuous section.

GPS data were used to estimate turning angle, which was taken as the difference in flight heading between consecutive GPS points. Turning angle was used as a measure of horizontal segment tortuosity instead of the straightness index (SI), as the relatively short segment length (mean = 280 m) restricted the inter-segment variation in SI. All three attributes were estimated using the move package version 4.0.0 (Kranstauber et al., 2020).

Flight height was estimated using the barometric pressure sensor data, which provided higher frequency measurements with smaller error compared to GPS derived altitude (Péron et al., 2020). Altitude above sea level (ASL) was estimated by smoothing the barometric pressure data over two seconds and using the pressure at sea level during each flight (estimated from the barometric pressure measured by the weather station at the release site), following Williams et al. (2015). Altitude ASL was used to estimate the vertical velocity (V_z, m s^{-1}), taken as the difference in altitude ASL (smoothed over two seconds) each second. Altitude ASL was also converted to altitude above ground (AGL), using the elevation of the terrain obtained from a 30 m digital surface model (DSM) (source: https://opendem.info/index.html).

Data processing (ii) the impact of turbulence on flight effort

Airspeed is a key determinant of flight costs. Airspeed, headwind component (HWC), and crosswind component (CRW) were estimated using the angle between the GPS heading/ ground speed vector and the wind speed vector (Garde, 2022), using the GPS and the wind data from the anemometer (Pennycuick, 2008). Wind measurements made by the anemometer were compared with those estimated using the ERA5 global reanalysis (hourly) (Copernicus

Climate Change Service) (Hersbach et al., 2018, Hersbach et al., 2020), to check that the weather station captured the prevailing wind conditions, rather than highly localised conditions e.g. due to the topography.

Wingbeat frequency and amplitude are thought to be the main kinematic variables that birds use to vary their mechanical power output in flight, and both were estimated using the triaxial acceleration data. Wingbeat frequency was estimated by counting the peaks in the dynamic heave signal within each second. The dynamic component was taken as difference between the raw and smoothed vertical acceleration values, where the smoothed values were derived using a 2 second window (Shepard et al., 2008). Wingbeat amplitude was estimated as the difference between the first peak and the lowest value of vertical acceleration within a wingbeat cycle (taken as the period between two consecutive peaks) (Krishnan et al., 2022 submitted to Royal Society Interface). Both wingbeat frequency and amplitude were averaged over two seconds to reduce the noise in the signal before further analysis.

Statistical analysis

I used generalised additive mixed effect models (GAMM) (GAM, package "mgcv" version: 1.8.31, Wood (2017)) to evaluate which flight characteristics were affected by changes in turbulence, in combination with other variables. First, I removed erroneous or incomplete data. This included all the segments of non-solo flights, all the segments of two flights for which wind data from the anemometer at the release site was missing, and finally segments with missing elevation data. I also excluded outliers in the distribution of turbulence to focus on the large proportion of the distribution, and the main effects, while avoiding fitting the model using the very small proportion of extreme values that was separated far from the overall distribution resulting in large uncertainty within the gap that was being created. This was accomplished by splitting the distribution of turbulence into five equal sized bins. I removed segments from the first or the last bin if that bin contained less than five segments, or in the case of the model of route choice, where each data point represented an entire flight, three flights. This process was repeated until all bins contained more than five segments or three flights (route choice model). Models that included outliers were also tested to assess whether this process changed the results substantially.

Prior to modelling, I assessed the distribution of each variable and square-root transformed the following variables, which had highly skewed distributions: the mean flight altitude, mean wingbeat frequency and amplitude, turbulence and the standard deviations of GPS turning angle, wingbeat frequency and amplitude, and airspeed.

The first model predicting the binomial response of route choice (valley/hill) included turbulence strength and headwind component of the first 15-second segment in the main bird track and the total circling duration of each orientation phase. The model predicting mean flight altitude per segment included turbulence strength and the headwind component. I anticipated that pigeons would fly lower to avoid high turbulence, similar to the response to headwinds (Liechti, 2006). The third model predicting the standard deviation of the turning angle included the same predictors. The fourth model, predicting mean airspeed also included the same predictors, with the addition of *Vz* (climb rate) and the mean flight altitude, to account for the influence of rapid ascents/ descents and changes in altitude on airspeed. The model of the standard deviation of airspeed included the same predictors.

I also used four models to assess the influence of turbulence on flight effort, taking the mean wingbeat frequency, the mean wingbeat amplitude and the standard deviations of wingbeat frequency and amplitude as the response variables and using the same predictors as the airspeed models.

In all models, basis dimension "k" was optimised using the option "select=TRUE" and flight ID was added as a random intercept except for the model of route choice where I used season ID. To account for temporal and spatial autocorrelation I used the time and the longitude and latitude of the mid-point of each 15-second segment nested in pigeon ID (flight ID for the model of standard deviation of airspeed) using the corARMA and corSpatial functions, nlme package version: 3.1.148, (Pinheiro et al., 2007). Model residuals were evaluated in two stages: i) outliers, uniformity, over/ under-dispersion and spatial/ temporal autocorrelation were assessed using the DHARMa package version: 0.4.4.0 (Hartig and Hartig, 2017), ii) residual plots were visually inspected in gam.check (with 100 simulations for each model). Models that failed the DHARMa test of uniformity (all but airspeed models) but displayed satisfactory plots for normality and homoscedasticity were selected for analysis, as the one-sample Kolmogorov-Smirnov test performed by DHARMa is highly sensitive to large sample sizes such as the one used in this study (n=1303), which might have resulted in smaller p-values (Uhm and Yi, 2021). All statistical analysis was conducted in RStudio version: 1.2.5 (RStudio Team, 2015) and the R programming language version: 3.6 (R Core Team, 2020).

Results

After excluding incomplete or erroneous data and filtering for outliers in the distribution of turbulence, 67 flights were used for the analysis of route choice, and 73 flights and 1303 segments were used to model the effect of turbulence on flight altitude, tortuosity, airspeed and effort. The exclusion of eight segments as extreme turbulence outliers (out of 1311) did not have any substantial effect on the results either on adj. R^2 and deviance explained or on the shape of the predicted relationships of any of the modelled predictors.

The decision of whether to fly over the hill or through the valley was not influenced by the headwind component or turbulence (Supplementary information Table S1). However, the probability of a bird flying over the hill increased with the time spent circling after the release (GAMM model of route choice, n= 67, adj. R^2 = 0.31, deviance explained = 36.5%, Supplementary information Table S1, Fig. S1).

Overall, turbulence had a significant impact on almost all the flight variables in the segment based models. These included the mean flight altitude above ground level, the tortuosity defined as the standard deviation of GPS turning angles, the mean wingbeat frequency and mean wingbeat amplitude estimated using the acceleration signal, their variability defined as the standard deviation, and finally the airspeed (bird's flight speed in relation to the wind vector) and its variability (standard deviation). Turbulence had the largest effect in the models of segment tortuosity and variation in airspeed, but the effect was less than that of flight altitude (above ground) and climb rate (the vertical displacement per second) in predicting wingbeat amplitude and wingbeat frequency (here turbulence was more significant than wind support) (Table. 1). Each of the model outputs is discussed in more detail below.

One multivariate model predicting mean flight altitude and tortuosity as the response variables and one multivariate model predicting mean wingbeat frequency, amplitude, airspeed and their standard deviations as the response variables were tested against the univariate models presented in table 1. The two multivariate models produced almost identical results as the univariate models. The significance level of the predictors (see supplementary information) and the shape of the predicted relationships were very similar in both approaches, but as processing and visualising the results of the univariate approach is simpler, the residuals tests of the univariate models performed better (i.e. QQ plots) and as

thorough model evaluation with Dharma is not supported with the multivariate model family, the univariate approach was selected for analysis.

Table 1. Summary of GAMM models and effects. The size and shape of its effect is standardised to represent the real modelled effect for comparison with other models and terms. The largest effect in each model is indicated in yellow.

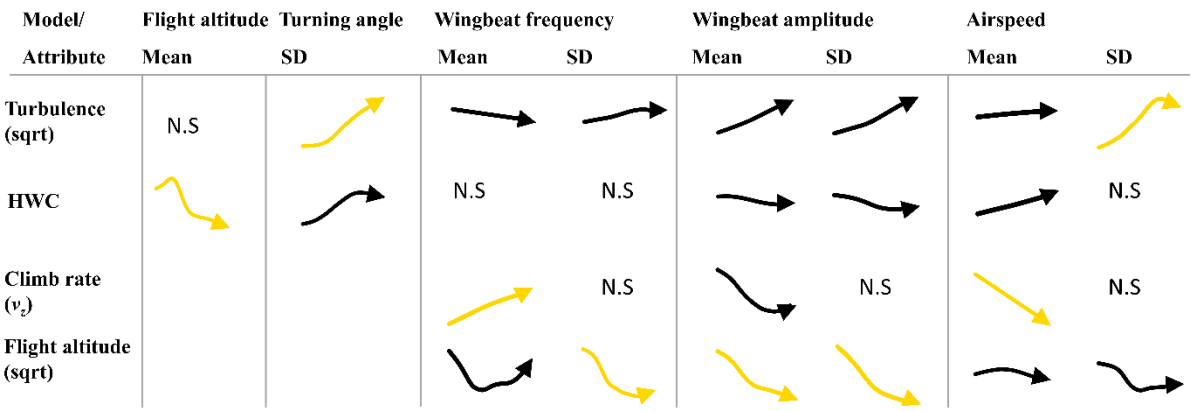

Flight altitude and path tortuosity

Flight height above ground did not vary with turbulence but it was affected by the headwind component, with birds flying lower with headwinds and at higher altitudes with tailwinds (n= 1303, adj. R^2 = 0.59, deviance explained = 61.3%, Supplementary information Table S2, Fig. S2). Turbulence did impact the horizontal path tortuosity, having the largest effect in the model, with segments becoming more tortuous with increasing turbulence strength and headwind component (n= 1303, adj. R^2 = 0.33, deviance explained = 36.3%, Supplementary information Table S3, Fig. S3).

Airspeed

Birds increased their airspeed with both headwind and turbulence level (Fig. 1A,B), although the effect size for turbulence was small (Table. 1, Supplementary information Table S4, n= 1303, adj. R^2 = 0.71, deviance explained = 72.3%). The most important determinant of airspeed was the climb rate with airspeed decreasing as birds climbed (Fig. 1C).

In contrast, turbulence was the most important determinant of airspeed variability (n= 1303, adj. R^2 = 0.37, deviance explained = 40%, Supplementary information Table S5) with the variability increasing with turbulence strength and with flight closer to the ground (Supplementary information Fig. S4).

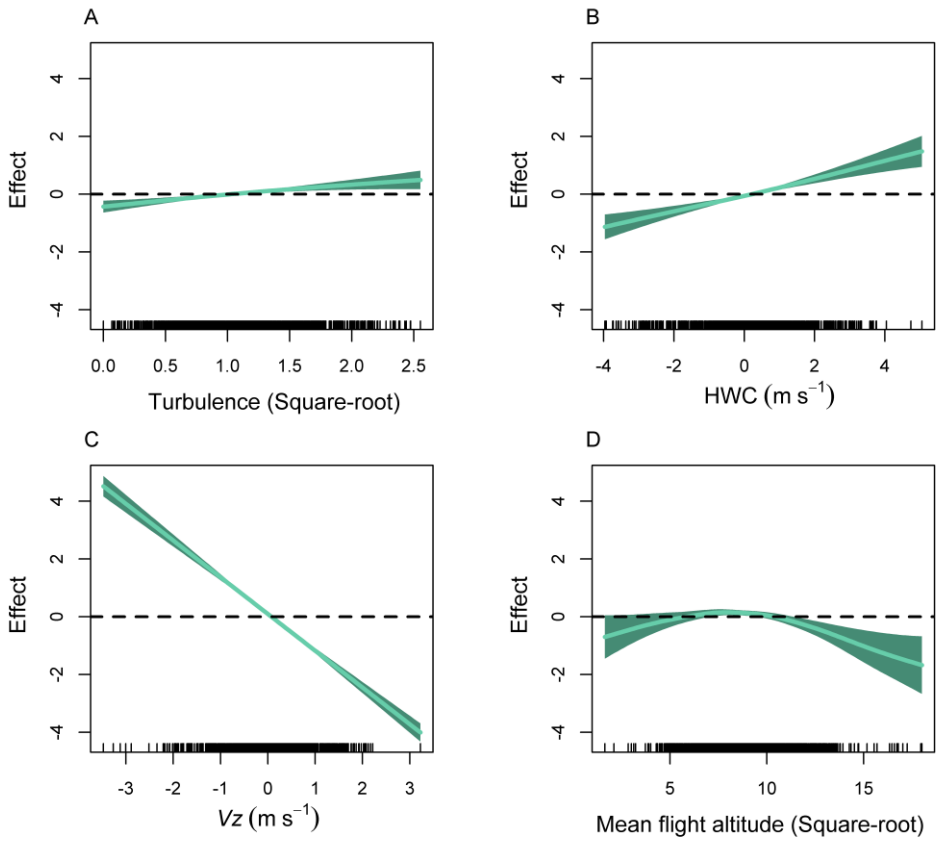

Figure 1. Model of mean airspeed per 15-second segment in relation to (A) turbulence, (B) headwind component, (C) vertical velocity and (D) mean flight altitude. Green shaded areas indicate the 95% confidence intervals.

Flight effort

Wingbeat frequency was highly variable overall (1.6 – 7.3 Hz) but tended to be lower in flights that continued through the valley compared to those that went over the hill (Fig. 2B), while wingbeat amplitude followed the opposite trend (Fig. 2C). In both cases, wingbeat frequency and amplitude appeared to be linked to the higher absolute flight height of tracks, with frequency being higher and amplitude being lower where pigeons climbed in anticipation of, and then over, the hill (Fig. 2A). There was no evidence that kinematics varied over time in the study period (Supplementary information Fig. S5).

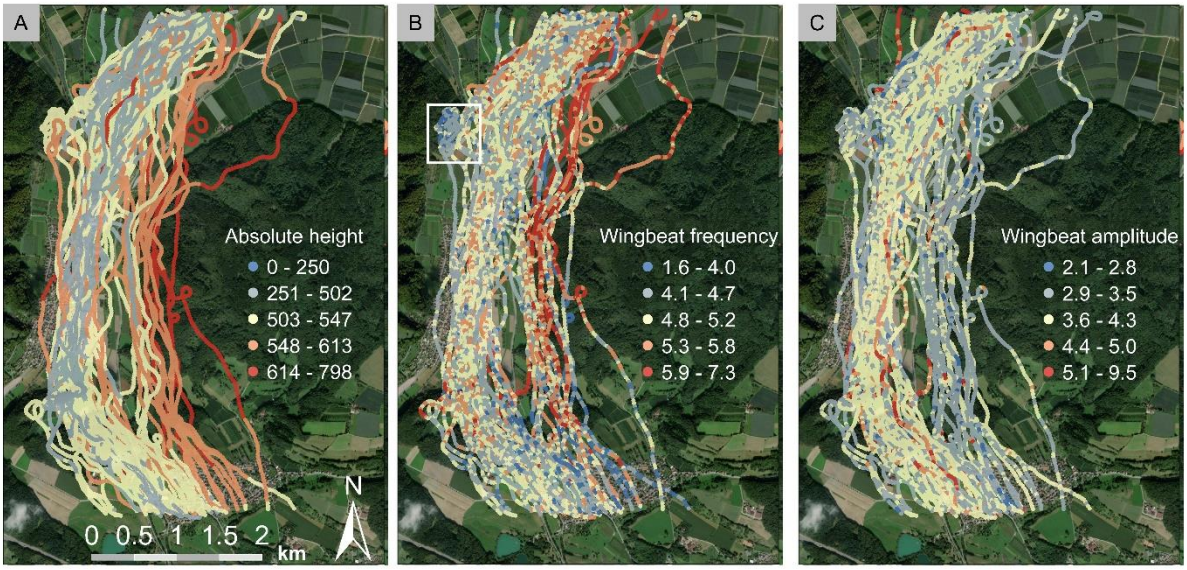

Figure 2. Flight tracks coloured according to (A) flight height (m ASL), (B) wingbeat frequency (Hz) and (C) amplitude (*g*). Birds flying over the hill (the wooded area to the right) increased their altitude ahead of the hill, and had a higher wingbeat frequency and lower amplitude. Aside from this tendency, wingbeat frequency and amplitude were variable along individual flight paths. Points represent the estimates in each second as measured by the Daily Diary. The white box in panel B highlights an area of high circling and low wingbeat frequency and amplitude.

Mean wingbeat frequency and amplitude followed the opposite trends with regard to turbulence (Fig. 3A,B). High turbulence was associated with lower wingbeat frequency and higher wingbeat amplitude. The same trend was also observed for the effect of climb rate, with higher wingbeat frequencies and lower amplitudes occurring as birds climbed (Fig. 3C,D). Wingbeat frequency and amplitude both tended to be higher at lower altitudes, with amplitude showing a steady reduction as height increased (Fig. 3E,F).

The standard deviation of wingbeat frequency and amplitude both increased with turbulence, more so for amplitude than for frequency (Supplementary information Fig. S6A, S7A). Both parameters decreased with flight height, which was the most important predictor (Supplementary information Table S7, S9 and Fig. S6B, S7C).

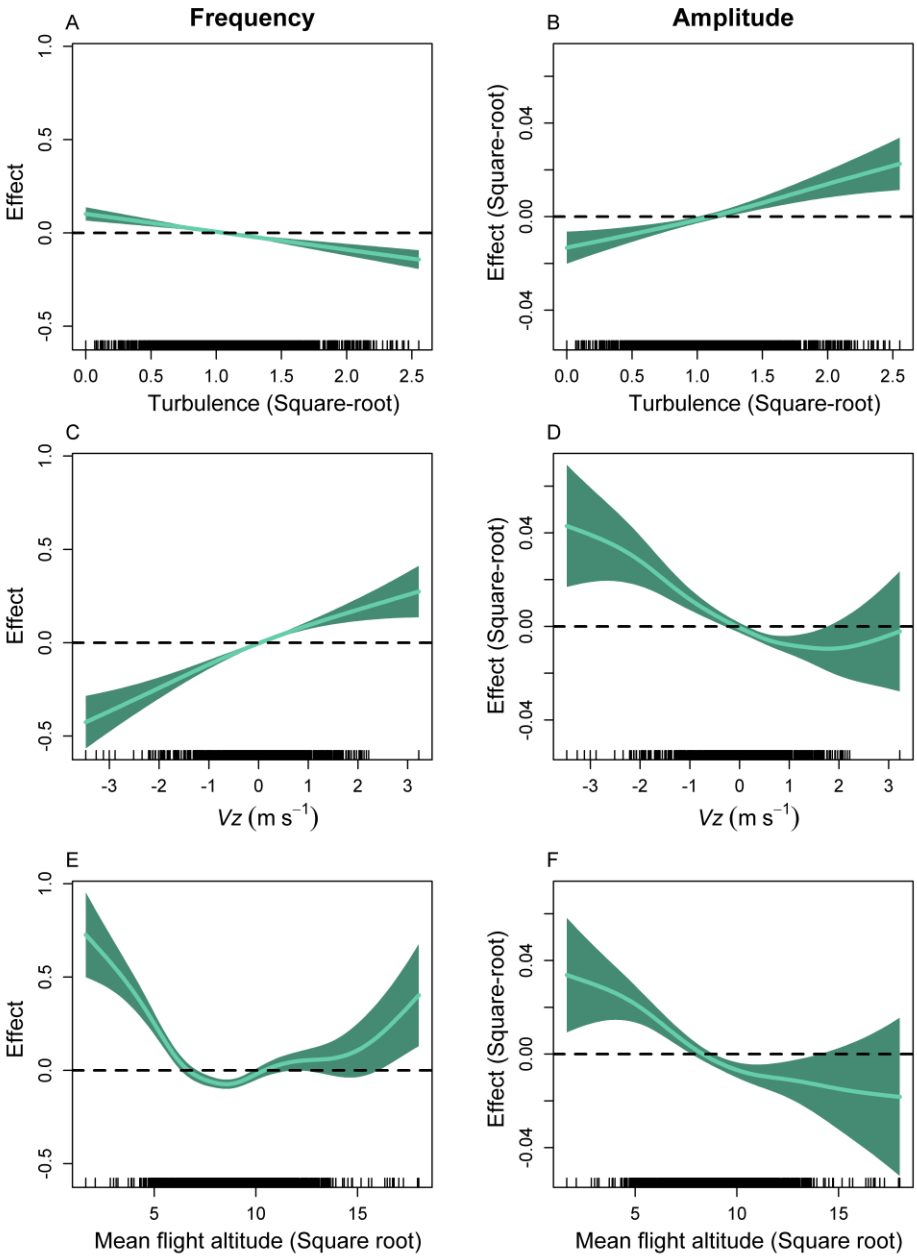

Figure 3. The most significant terms in the GAMM models of mean wingbeat frequency and amplitude. Turbulence had a negative effect on frequency (A) but a positive effect on amplitude (B), climb rate had a positive effect on frequency (C) and a negative on amplitude (D) whereas frequency decreased with altitude up to a certain level above which it increased (E) and amplitude decreased(E) (note the number of observations on the lowest and highest altitudes was small). Green shaded areas indicate the 95% confidence intervals.

Discussion

Information on the effects of freestream turbulence on flapping fliers is extremely limited (but see (Sapir et al., 2011). In this study I show that turbulence has a substantial impact on a wide range of flight parameters for an obligate flapping flier operating in the wild. Indeed, turbulence had a significant effect on all tested flight metrics, bar flight altitude. Nonetheless,

my results will likely underestimate the actual effect sizes of turbulence on flight kinematics because while I examined responses to free-stream turbulence at extremely fine-scales, compared to what has been possible to date (Bohrer et al., 2012, Sapir et al., 2011), I was still restricted to assessing the average response over flight segments of ~ 280 m (15 second intervals). This will have averaged out some of the variation in the kinematic response, as turbulent features may not have persisted across the entire length of each 15 second flight section.

I expected pigeons would make adjustments to their flight kinematics in order to maintain flight stability and that this would result in increased flight costs. One way that birds are thought to compensate for aerial perturbations is by varying their kinematics from one stroke to the next (Ravi et al., 2015), a strategy referred to as active flight control. My finding that wingbeat frequency and amplitude became more variable with increasing turbulence is therefore consistent with the idea that pigeons show instantaneous compensation for turbulence. Similar results were found in hummingbirds, which had more variable kinematics when flying both in freestream turbulence and in von Kármán vortex streets (Ortega-Jimenez et al., 2014, Ravi et al., 2015).

Flapping fliers can also reduce the effect of turbulence and increase passive stability by increasing their mean wingbeat frequency (Fisher et al., 2016, Hedrick et al., 2009, Ravi et al., 2015). It was therefore surprising that, in contrast to hummingbirds, pigeons in this study reduced their mean wingbeat frequency with increasing turbulence. The effect of turbulence on mean wingbeat frequency was lower than the effect of climb rate and flight height, as both the latter predicted a change in wingbeat frequency of ~0.75 Hz. Nonetheless, the predicted reduction of ~0.2 Hz in high turbulence is significant, and close to what is seen in the transition from cluster flocking to solo flight in other homing studies (Sankey and Portugal, 2019). Therefore, while pigeons did show kinematic compensation for turbulence through more variable wingbeat frequency and amplitude, they did not take additional steps to reduce the effect of turbulence by increasing their mean wingbeat frequency. In fact, pigeons only increased their wingbeat frequency during climbing flight and periods when headwinds necessitated an increase in airspeed (and also lower flight altitudes).

Much of our knowledge of how the physical environment affects flight effort has come from estimates of airspeed under changing conditions (Hedenström, 1993, Hedenström and Alerstam, 1995). There are well-established frameworks that predict how flying animals should modify their speed in relation to both climb rate and headwind component, and these

were the main parameters that influenced airspeed in my trials, in line with theoretical predictions (Hedenström et al., 2002, Hedenström, 2003, Berg and Biewener, 2008). In contrast, there is no quantitative framework predicting how flapping fliers should vary their speed in relation to turbulence. Broadly speaking, an increase in speed might be expected if turbulence represented an energetic cost, with the reverse being true if birds were extracting some energetic advantage from turbulence, akin to the behaviour of soaring birds (Hedenström, 1993). Previous work on insect flight performance has shown a significant decrease in airspeed with increasing turbulence scale (Ortega-Jimenez et al., 2013). Here I found a small increase in airspeed in relation to turbulence, but the response was too small to allow firm conclusions about potential benefits or cost from this alone. Turbulence was, however, the main driver of the variation in airspeed, and variable speeds are typically more costly than constant speeds due to the need for repeated accelerations (Pennycuick, 1968, Kramer and McLaughlin, 2001).

Overall, interpreting how freestream turbulence effects flight costs in these obligate flapping fliers is not straightforward. It was extremely surprising that pigeons reduced their wingbeat frequency in increasing turbulence, but this was accompanied by an increase in wingbeat amplitude, and it is unclear how these two contradictory trends play out in terms of the net power output. Nonetheless, two variables suggest that birds may experience lower flight costs in turbulent conditions. First, a reduction in wingbeat frequency was observed despite the slight increase in absolute airspeed and increased variation in airspeed, which would require greater acceleration power and has been linked to increased wingbeat frequency and amplitude (Usherwood et al., 2011). Second, the kinematic changes in increasing turbulence are most similar to those observed in descending flight. Indeed, the magnitude of the frequency and amplitude response for birds flying in high versus low turbulence was comparable to that between level flight and a descent rate of 2 m s^{-1} .

Is it possible that pigeons could be extracting energy from the turbulence? Exactly how this could be achieved is unclear, but possible mechanisms could include a reduction in the induced power requirements, if pigeons fly through turbulence with an upwards component, or the Katzmayr effect (Katzmayr, 1922), where an overall increase in lift could lead to an increase in thrust, although neither have been demonstrated in flapping fliers (Phillips, 1975). In some cases, segments included circling (with the duration of a single circle ranging from 10 to 27 seconds). Turning flight is costly (Usherwood et al., 2011), but there is at least one section in the data where birds had low wingbeat frequency and amplitude during turning

flight, raising the tantalising prospect that pigeons might have made fine scale adjustments to benefit from uplift.

Interestingly, pigeons in this study flew one of two broad routes back to the loft but turbulence did not predict route choice. This could be because turbulence did not differ much between the routes, despite the fact that objects on the ground like buildings and trees disturb the mean flow and lead to unsteady turbulent regimes (Stull, 1988). Alternatively, turbulence was neither too costly or beneficial to determine route choice. Finally, it could simply be because pigeons and other flapping fliers do not tend to alter their horizontal route in relation to flight conditions (Hedenström, 1993). In contrast, many small birds vary their flight height in relation to the head/ tailwind component, as also seen here (Liechti, 2006). Pigeons may therefore have been more likely to vary their flight height in relation to turbulence, however no relationship was observed. It could be that birds respond differently to the different categories of turbulence, as my turbulence proxy was positively correlated with both the magnitude of the wind and the thermal convection (Chapter 2). It would therefore be interesting to model their responses in relation to these specific terms.

Overall, this study demonstrates that pigeons increase their active flight stability in response to free-stream turbulence, as has been shown for hummingbirds flying in laboratory conditions (Ortega-Jimenez et al., 2014, Ravi et al., 2015). However, whilst this led to marked increases in metabolic rates for hummingbirds flying in relatively large vortex wakes (e.g. by 25% for flight in the wake of the large cylinder (Ortega-Jimenez et al., 2014)), it seems unlikely that pigeons in this study increased their flight power in strong turbulence. In fact, against the backdrop of the results from trials with hummingbirds, even the possibility that turbulence could be cost-neutral raises further questions about how birds achieve this whilst simultaneously increasing flight stability. This is likely to be of interest to engineers, as well as ecologists and biomechanics, given the challenges that near-ground turbulence presents for unmanned aerial vehicles (Abdulrahim et al., 2017, Joyo et al., 2013, Patel and Kroo, 2006).

References

Abdulrahim, M., Mohamed, A. & Watkins, S. Control strategies for flight in extreme turbulence. AIAA Guidance, Navigation, and Control Conference, 2017. 1909.

Anderson, J. D. 2016. *Fundamentals of Aerodynamics*, McGraw-Hill Education.

Berg, A. M. & Biewener, A. A. 2008. Kinematics and power requirements of ascending and descending flight in the pigeon (Columba livia). *Journal of Experimental Biology,* 211**,** 1120-1130.

Biro, D., Meade, J. & Guilford, T. 2004. Familiar route loyalty implies visual pilotage in the homing pigeon. *Proceedings of the National Academy of Sciences,* 101**,** 17440-17443.

Bohrer, G., Brandes, D., Mandel, J. T., Bildstein, K. L., Miller, T. A., Lanzone, M., Katzner, T., Maisonneuve, C. & Tremblay, J. A. 2012. Estimating updraft velocity components over large spatial scales: contrasting migration strategies of golden eagles and turkey vultures. *Ecology letters,* 15**,** 96-103.

Combes, S. A. & Dudley, R. 2009. Turbulence-driven instabilities limit insect flight performance. *Proceedings of the National Academy of Sciences,* 106**,** 9105-9108.

Crall, J., Chang, J., Oppenheimer, R. & Combes, S. 2017. Foraging in an unsteady world: bumblebee flight performance in field-realistic turbulence. *Interface focus,* 7**,** 20160086.

Fisher, A., Ravi, S., Watkins, S., Watmuff, J., Wang, C., Liu, H. & Petersen, P. 2016. The gust-mitigating potential of flapping wings. *Bioinspiration & biomimetics,* 11**,** 046010.

Garde, B. 2022. *Fine scale changes in flight effort revealed by animal borne loggers.* Ph.D Thesis, Swansea University.

Garde, B., Wilson, R. P., Lempidakis, E., Börger, L., Portugal, S. J., Hedenström, A., Dell'Omo, G., Quetting, M., Wikelski, M. & Shepard, E. L. 2021. Fine-scale changes in speed and altitude suggest protean movements in homing pigeon flights. *Royal Society open science,* 8**,** 210130.

Gultepe, I., Sharman, R., Williams, P. D., Zhou, B., Ellrod, G., Minnis, P., Trier, S., Griffin, S., Yum, S. & Gharabaghi, B. 2019. A review of high impact weather for aviation meteorology. *Pure and applied geophysics,* 176**,** 1869-1921.

Hartig, F. & Hartig, M. F. 2017. DHARMa: Residual Diagnostics for Hierarchical (Multi-Level Mixed) Regression Models. R package version 0.3.3.

Hedenström, A. 1993. Migration by soaring or flapping flight in birds: the relative importance of energy cost and speed. *Philosophical Transactions of the Royal Society of London. Series B: Biological Sciences,* 342**,** 353-361.

Hedenström, A. 2003. Twenty-three testable predictions about bird flight. *Avian migration.* Springer.

Hedenström, A. & Alerstam, T. 1995. Optimal flight speed of birds. *Philosophical Transactions of the Royal Society of London. Series B: Biological Sciences,* 348**,** 471-487.

Hedenström, A., Alerstam, T., Green, M. & Gudmundsson, G. A. 2002. Adaptive variation of airspeed in relation to wind, altitude and climb rate by migrating birds in the Arctic. *Behavioral Ecology and Sociobiology,* 52**,** 308-317.

Hedrick, T. L., Cheng, B. & Deng, X. 2009. Wingbeat time and the scaling of passive rotational damping in flapping flight. *Science,* 324**,** 252-255.

Hersbach, H., Bell, B., Berrisford, P., Biavati, G., Horányi, A., Muñoz Sabater, J., J, N., Peubey, C., Radu, R., Rozum, I., Schepers, D., Simmons, A., Soci, C., Dee, D. & Thépaut, J.-N. 2018. ERA5 hourly data on single levels from 1979 to present.

Hersbach, H., Bell, B., Berrisford, P., Hirahara, S., Horányi, A., Muñoz-Sabater, J., Nicolas, J., Peubey, C., Radu, R. & Schepers, D. 2020. The ERA5 global reanalysis. *Quarterly Journal of the Royal Meteorological Society,* 146**,** 1999-2049.

Joyo, M. K., Hazry, D., Ahmed, S. F., Tanveer, M. H., Warsi, F. A. & Hussain, A. Altitude and horizontal motion control of quadrotor UAV in the presence of air turbulence. 2013 IEEE Conference on Systems, Process & Control (ICSPC), 2013. IEEE, 16-20.

Katzmayr, R. 1922. Effect of periodic changes of angle of attack on behavior of airfoils.

Kauffmann, P. 2002. The business case for turbulence sensing systems in the US air transport sector. *Journal of Air Transport Management,* 8**,** 99-107.

Kramer, D. L. & McLaughlin, R. L. 2001. The behavioral ecology of intermittent locomotion. *American Zoologist,* 41**,** 137-153.

Kranstauber, B., Smolla, M. & Scharf, A. K. 2020. move: Visualizing and Analyzing Animal Track Data. R package version 4.0.0.

Krishnan, K., Garde , B., Bennison, A., Cole, N. C., Cole , E.-L., Darby , J., Elliott, K. H., Fell , A., Gómez-Laich , A., de Grissac, S., Jessopp, M., Lempidakis , E., Mizutani, Y., Prudor , A., Quetting, M., Quintana, F., Robotka , H., Roulin , A., Ryan, P. G., Schalcher , K., Schoombie , S., Tatayah, V., Tremblay, F., Weimerskirch , H., Whelan, S., Wikelski , M., Yoda, K., Hedenström, A. & Shepard , E. L. C. 2022. (in review). The role of wingbeat frequency and amplitude in flight power.: Royal Society Interface.

Liechti, F. 2006. Birds: blowin'by the wind? *Journal of Ornithology,* 147**,** 202-211.

Meade, J., Biro, D. & Guilford, T. 2005. Homing pigeons develop local route stereotypy. *Proceedings of the Royal Society B: Biological Sciences,* 272**,** 17-23.

Murgatroyd, M., Photopoulou, T., Underhill, L. G., Bouten, W. & Amar, A. 2018. Where eagles soar: Fine-resolution tracking reveals the spatiotemporal use of differential soaring modes in a large raptor. *Ecology and Evolution,* 8**,** 6788-6799.

Ortega-Jimenez, V. M., Greeter, J. S., Mittal, R. & Hedrick, T. L. 2013. Hawkmoth flight stability in turbulent vortex streets. *Journal of Experimental Biology,* 216**,** 4567-4579.

Ortega-Jimenez, V. M., Sapir, N., Wolf, M., Variano, E. A. & Dudley, R. 2014. Into turbulent air: size-dependent effects of von Kármán vortex streets on hummingbird flight kinematics and energetics. *Proceedings of the Royal Society B: Biological Sciences,* 281**,** 20140180.

Patel, C. & Kroo, I. Control law design for improving uav performance using wind turbulence. 44th AIAA Aerospace Sciences Meeting and Exhibit, 2006. 231.

Pennycuick, C. 1972. Soaring behaviour and performance of some East African birds, observed from a motor-glider. *Ibis,* 114**,** 178-218.

Pennycuick, C. J. 1968. Power requirements for horizontal flight in the pigeon Columba livia. *Journal of Experimental Biology,* 49**,** 527-555.

Pennycuick, C. J. 2008. *Modelling the flying bird*, Elsevier.

Péron, G., Calabrese, J. M., Duriez, O., Fleming, C. H., García-Jiménez, R., Johnston, A., Lambertucci, S. A., Safi, K. & Shepard, E. L. 2020. The challenges of estimating the distribution of flight heights from telemetry or altimetry data. *Animal Biotelemetry,* 8**,** 1-13.

Phillips, W. H. 1975. Propulsive effects due to flight through turbulence. *Journal of Aircraft,* 12**,** 624-626.

Pinheiro, J., Bates, D., DebRoy, S., Sarkar, D. & Team, R. C. 2007. Linear and nonlinear mixed effects models. *R package version,* 3**,** 1-89.

R Core Team 2020. R: A language and environment for statistical computing.

Ravi, S., Crall, J. D., McNeilly, L., Gagliardi, S. F., Biewener, A. A. & Combes, S. A. 2015. Hummingbird flight stability and control in freestream turbulent winds. *The Journal of Experimental Biology,* 218**,** 1444-1452.

RStudio Team 2015. RStudio: Integrated Development Environment for R. Boston, MA.

Sankey, D. W. & Portugal, S. J. 2019. When flocking is costly: reduced cluster-flock density over long-duration flight in pigeons. *The Science of Nature,* 106**,** 1-5.

Sapir, N., Horvitz, N., Wikelski, M., Avissar, R., Mahrer, Y. & Nathan, R. 2011. Migration by soaring or flapping: numerical atmospheric simulations reveal that turbulence

kinetic energy dictates bee-eater flight mode. *Proceedings of the Royal Society B: Biological Sciences,* 278**,** 3380-3386.

Shepard, E. L., Wilson, R. P., Halsey, L. G., Quintana, F., Laich, A. G., Gleiss, A. C., Liebsch, N., Myers, A. E. & Norman, B. 2008. Derivation of body motion via appropriate smoothing of acceleration data. *Aquatic Biology,* 4**,** 235-241.

Storer, L. N., Williams, P. D. & Gill, P. G. 2019. Aviation turbulence: dynamics, forecasting, and response to climate change. *Pure and Applied Geophysics,* 176**,** 2081-2095.

Stull, R. B. 1988. *An introduction to boundary layer meteorology,* Springer Science & Business Media.

Taylor, L. A., Portugal, S. J. & Biro, D. 2017. Homing pigeons (Columba livia) modulate wingbeat characteristics as a function of route familiarity. *Journal of Experimental Biology,* 220**,** 2908-2915.

Uhm, T. & Yi, S. 2021. A comparison of normality testing methods by empirical power and distribution of P-values. *Communications in Statistics-Simulation and Computation***,** 1-14.

Usherwood, J. R., Stavrou, M., Lowe, J. C., Roskilly, K. & Wilson, A. M. 2011. Flying in a flock comes at a cost in pigeons. *Nature,* 474**,** 494-497.

Williams, H. J., Shepard, E., Duriez, O. & Lambertucci, S. A. 2015. Can accelerometry be used to distinguish between flight types in soaring birds? *Animal Biotelemetry,* 3**,** 1-11.

Wood, S. N. 2017. *Generalized additive models: an introduction with R,* CRC press.

Chapter 3: Supplementary Information

Model of route choice

Table S1. GAMM model of route choice (n=67). From left to right: model terms, effective degrees of freedom, available degrees of freedom and p-value. Turbulence in this model is the predicted turbulence of the first 15-second segment in the pigeon tracks. Significance is indicated according to p-value: p< 0.001 (***), p< 0.01 (**), p< 0.005 (*).

Predictors	**Edf**	**Ref.df**	**p-value**
s (Turbulence)	1.727950307	9	0.176904
s (HWC)	6.298728407	9	0.276790
s (Total circling duration)	0.995698974	9	0.014472 *
s (Season, bs="re")	0.726570025	1	0.067356
Adjusted R^2	**0.31**		
Deviance explained	**36.5%**		

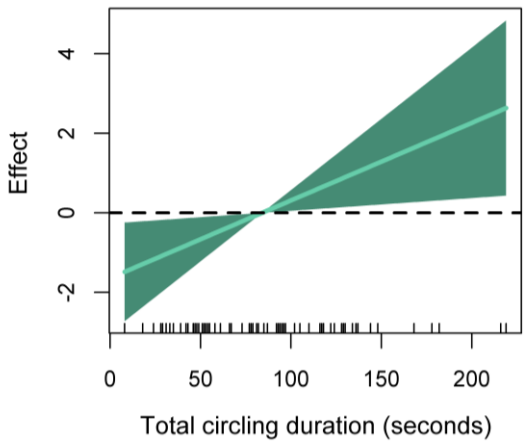

Figure S1. The effect of significant terms in the model of route choice. This included only the total time spent circling in seconds. Green shaded areas indicate the 95% confidence intervals.

Model of mean flight altitude

Table S2. GAMM model of mean flight altitude above ground per 15-second segment (n=1303). From left to right: model terms, effective degrees of freedom, available degrees of freedom and p-value. Significance is indicated according to p-value: p< 0.001 (***), p< 0.01 (**), p< 0.005 (*).

Predictors	**Edf**	**Ref.d**	**p-value**
s(sqrt(Turbulence))	0.00176595509	9	0.65059
s (HWC)	3.94200978691	9	1.4903e-09 ***
s (flight ID, bs="re")	68.73147418590	72	< 2.22e-16 ***
Adjusted R^2	**0.59**		
Deviance explained	**61.3%**		

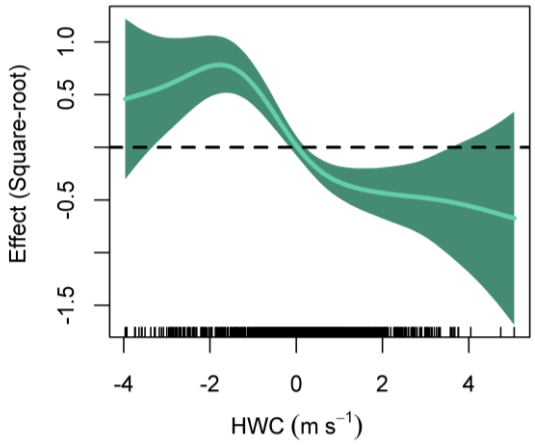

Figure S2. The effect of significant terms in the model of mean flight altitude per-second segment. This included only the headwind component. Green shaded areas indicate the 95% confidence intervals.

Model of horizontal path tortuosity

Table S3. GAMM model of the standard deviation of GPS turning angle per 15-second segment (n=1303). From left to right: model terms, effective degrees of freedom, available degrees of freedom and p-value. Significance is indicated according to p-value: p< 0.001 (***), p< 0.01 (**), p< 0.005 (*).

Predictors	**Edf**	**Ref.df**	**p-value**
s(sqrt(Turbulence))	2.34386010	9	6.6005e-07 ***
s (HWC)	1.71242279	9	0.00044722 ***
s (flight ID, bs="re")	62.59131939	72	< 2.22e-16 ***
Adjusted R^2	**0.33**		
Deviance explained	**36.3%**		

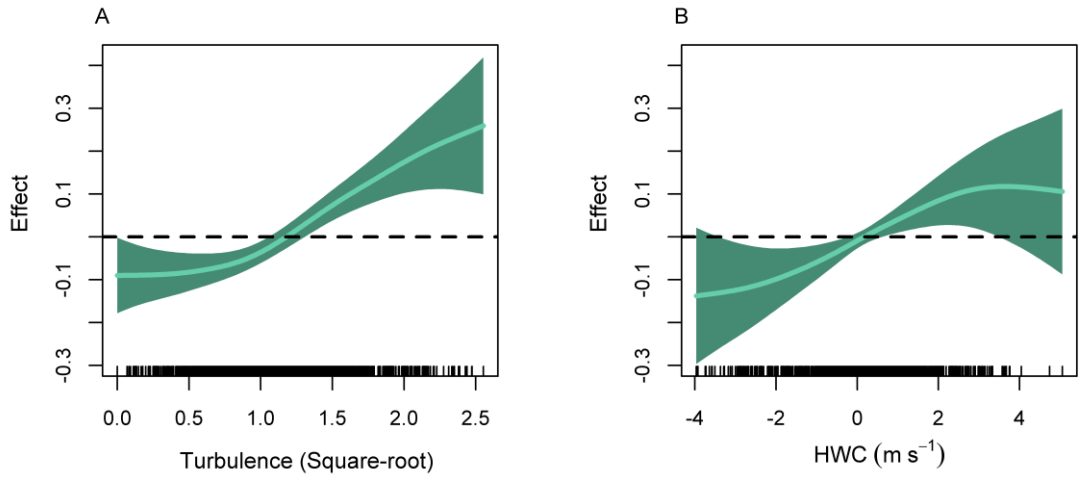

Figure S3. GAMM model of horizontal path tortuosity expressed as the square-root of the standard deviation of GPS turning angle, per 15-second segment. The effects of (A) turbulence and (B) headwind component indicate higher tortuosity with increasing turbulence (square-root) and headwind component (positive values). Green shaded areas indicate the 95% confidence intervals.

Model of mean airspeed

Table S4. GAMM model mean airspeed per 15-second segment (n=1303). From left to right: model terms, effective degrees of freedom, available degrees of freedom and p-value. Significance is indicated according to p-value: p< 0.001 (***), p< 0.01 (**), p< 0.005 (*).

Predictors	**Edf**	**Ref.df**	**p-value**
s(sqrt(Turbulence))	1.32251661	9	3.1703e-06 ***
s(HWC)	1.38962412	9	1.2889e-13 ***
s(*Vz*)	1.00113746	9	< 2.22e-16 ***
s(sqrt(flight altitude))	2.87999664	9	6.0239e-05 ***
s(flight ID, bs="re")	69.51683728	72	< 2.22e-16 ***
Adjusted R^2	**0.71**		
Deviance explained	**72.3%**		

Model of standard deviation of airspeed

Table S5. GAMM model of the square-root transformed standard deviation of airspeed per 15-second segment (n=1303). From left to right: model terms, effective degrees of freedom, available degrees of freedom and p-value. Significance is indicated according to p-value: p< 0.001 (***), p< 0.01 (**), p< 0.005 (*).

Predictors	**Edf**	**Ref.df**	**p-value**
s(sqrt(Turbulence))	4.01071821e+00	9	< 2.22e-16 ***
s(HWC)	1.90906150e-06	9	0.73725
s(*Vz*)	1.27862837e-06	9	0.45604
s(sqrt(flight altitude))	3.63748681e+	9	1.3722e-11 ***
s(flight ID, bs="re")	5.44663743e+01	72	< 2.22e-16 ***
Adjusted R^2	**0.37**		
Deviance explained	**40%**		

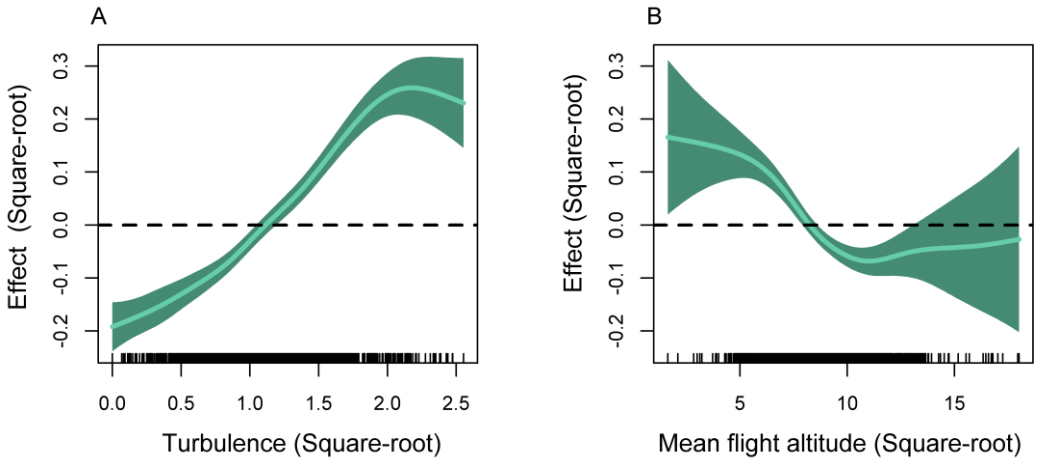

Figure S4. GAMM model of the square-root transformed standard deviation of airspeed, per 15-second segment. Only (A) turbulence and (B) flight altitude (square-roots) had a significant effect, indicating higher standard deviation with increasing turbulence and flight closer to the ground. Green shaded areas indicate the 95% confidence intervals.

Examination of the potential effect of track familiarity on mean wingbeat frequency.

Mean wingbeat frequency did not appear to vary according to the chronological order of flights, in any month of releases, and as birds became more familiar with the route to the loft (Fig. S5).

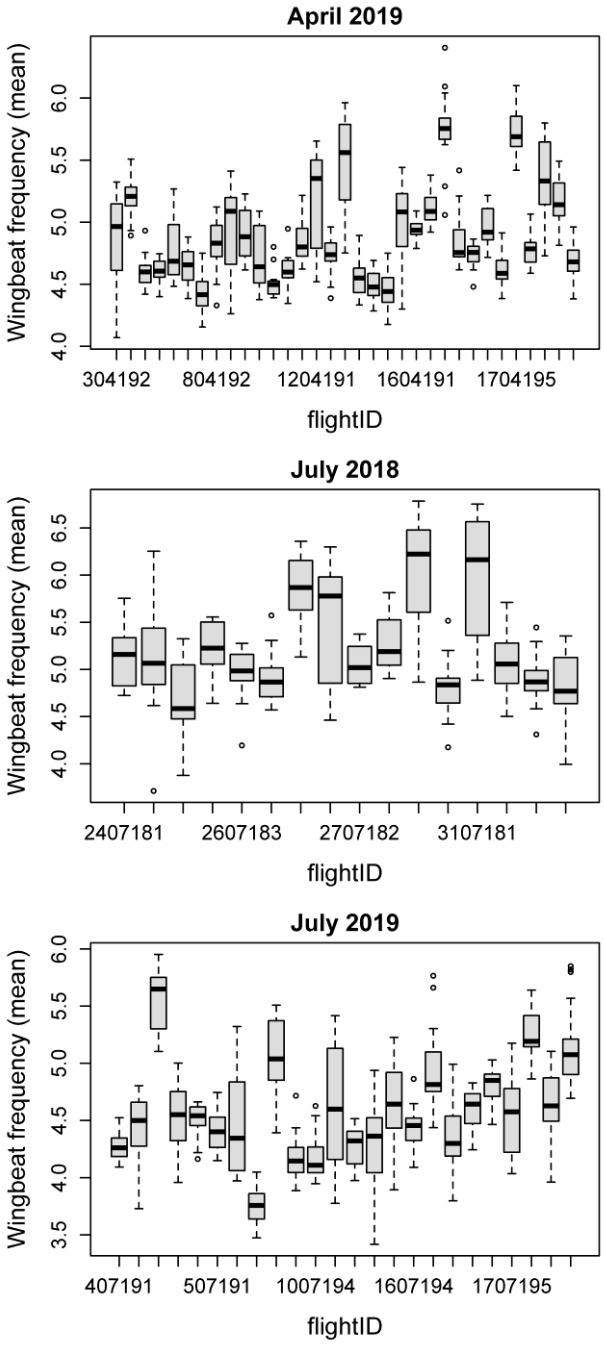

Figure S5. Mean wingbeat frequency per 15-second segment across flights grouped by month of releases (April 2019, and July 2018 and 2019). Flights are ordered chronologically.

Model of mean wingbeat frequency

Table S6. GAMM model of the square-root transformed mean wingbeat frequency per 15-second segment (n=1303). From left to right: model terms, effective degrees of freedom, available degrees of freedom and p-value. Significance is indicated according to p-value: p< 0.001 (***), p< 0.01 (**), p< 0.005 (*).

Predictors	**Edf**	**Ref.df**	**p-value**
s(sqrt(Turbulence))	0.970158873	9	7.4794e-09 ***
s(HWC)	1.823807567	9	0.20384
s(*Vz*)	1.824607503	9	< 2.22e-16 ***
s(sqrt(flight altitude))	5.456208366	9	8.8801e-15 ***
s(flight ID, bs="re")	70.425959681	72	< 2.22e-16 ***
Adjusted R^2	**0.75**		
Deviance explained	**76.2%**		

Model of standard deviation of wingbeat frequency

Table S7. GAMM model of the standard deviation of wingbeat frequency per 15-second segment (n=1303). From left to right: model terms, effective degrees of freedom, available degrees of freedom and p-value. Significance is indicated according to p-value: p< 0.001 (***), p< 0.01 (**), p< 0.005 (*).

Predictors	**Edf**	**Ref.df**	**p-value**
s(sqrt(Turbulence))	2.29202815047	9	8.9081e-06 ***
s(HWC)	1.06088859390	9	0.099284
s(*Vz*)	0.00125129761	9	0.375240
s(sqrt(flight altitude))	4.20571845021	9	< 2.22e-16 ***
s(flight ID, bs=”re”)	65.66305626969	72	< 2.22e-16 ***
Adjusted R^2	**0.43**		
Deviance explained	**46.5%**		

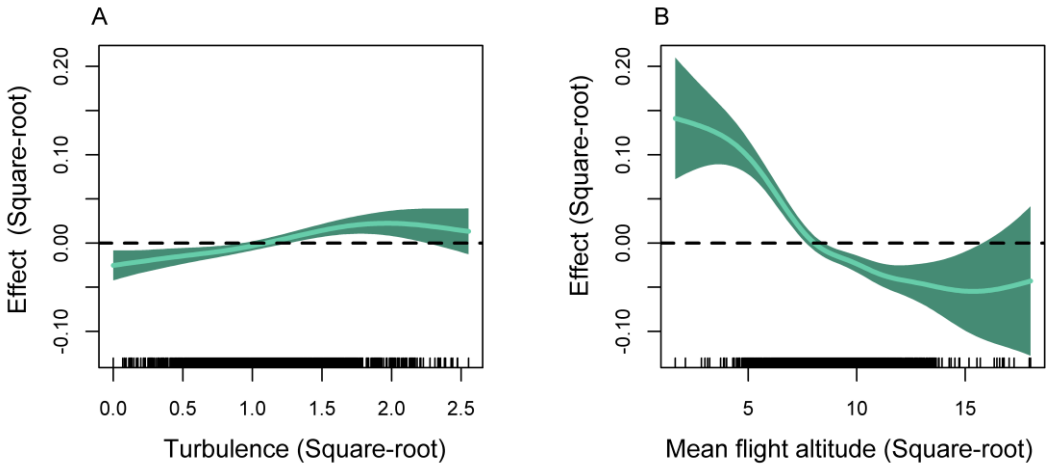

Figure S6. GAMM model of the square-root transformed standard deviation of wingbeat frequency, per 15-second segment. Only (A) turbulence and (B) flight altitude (square-roots) had a significant effect, indicating higher standard deviation with increasing turbulence and flight closer to the ground. Green shaded areas indicate the 95% confidence intervals.

Model of mean wingbeat amplitude

Table S8. GAMM model of the square-root transformed mean wingbeat amplitude per 15-second segment (n=1303). From left to right: model terms, effective degrees of freedom, available degrees of freedom and p-value. Significance is indicated according to p-value: p< 0.001 (***), p< 0.01 (**), p< 0.005 (*).

Predictors	**Edf**	**Ref.df**	**p-value**
s(sqrt(Turbulence))	1.45902470	9	1.0157e-06 ***
s(HWC)	1.01926656	9	0.044442 *
s(*Vz*)	2.59999913	9	4.8510e-05 ***
s(sqrt(flight altitude))	2.64663914	9	1.4750e-07 ***
s(flight ID, bs="re")	71.60274520	72	< 2.22e-16 ***
Adjusted R^2	**0.92**		
Deviance explained	**92.3%**		

Model of standard deviation of wingbeat amplitude

This is the only model for which the "inverse.gaussian" family was used.

Table S9. GAMM model of the square-root transformed standard deviation of wingbeat amplitude per 15-second segment (n=1303). From left to right: model terms, effective degrees of freedom, available degrees of freedom and p-value. Significance is indicated according to p-value: p< 0.001 (***), p< 0.01 (**), p< 0.005 (*).

Predictors	**Edf**	**Ref.df**	**p-value**
s(sqrt(Turbulence))	2.0186854703	9	3.5355e-06 ***
s(HWC)	1.4871729296	9	0.031627 *
s(*V*z)	0.0015476637	9	0.409552
s(sqrt(flight altitude))	2.3193779632	9	7.2188e-07 ***
s(flight ID, bs="re")	65.6233474596	72	< 2.22e-16 ***
Adjusted R^2	**0.37**		
Deviance explained	**42.5%**		

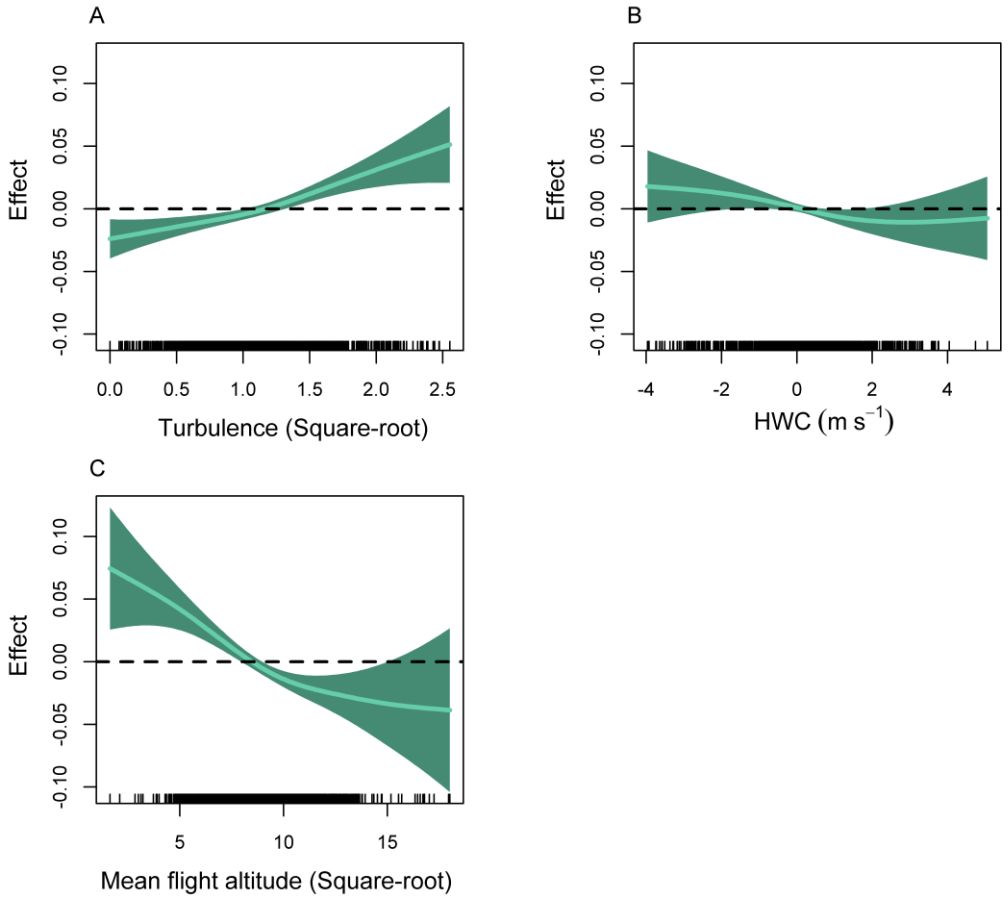

Figure S7. GAMM model of the square-root transformed standard deviation of wingbeat amplitude, per 15-second segment. Only (A) turbulence, (C) flight altitude (square-roots) and (B) headwind component had a significant effect, indicating higher standard deviation with increasing turbulence and flight closer to the ground. The effect of headwind component was relatively small indicating higher standard deviation of wingbeat amplitude with tailwind. Green shaded areas indicate the 95% confidence intervals.

Chapter 4: Pelagic seabirds reduce risk by flying into the eye of the storm.

The content of this chapter has been submitted in the "Proceedings of the National Academy of Sciences of the United States of America" (PNAS) as:

Lempidakis, E., Shepard, E.L.C , Ross, A.N., Matsumoto, S., Koyama, S., Takeuchi, I., and Yoda, K. Pelagic seabirds reduce risk by flying into the eye of the storm.

Abstract

Cyclones can cause mass mortality of seabirds, sometimes wrecking thousands of individuals. The few studies to track pelagic seabirds during cyclones show they tend to avoid the strongest winds. We tracked adult shearwaters in the Sea of Japan over 11 years and find that birds exposed to strong winds flew towards the eye of the storm, flying within ≤ 30 km of the eye and tracking it for up to 8 hours. This exposes shearwaters to some of the highest wind speeds near the eye wall (≤ 21 m s^{-1}), equivalent to those recorded for the largest albatrosses, but enables them to avoid strong onshore winds in the storm's wake. Extreme winds therefore become a threat when an inability to compensate for drift could lead to forced landings and collisions. Nonetheless, flying towards the eye could lead shearwaters closer to land in some scenarios, and flexibility in the birds' response, according to the storm identity and bird position, shows that adults take account of (i) the wind speed at their location, (ii) the trajectory of an approaching storm and (iii) the direction to the nearest landmass. This provides additional selective pressure for a map sense and explains why juvenile shearwaters, which navigate using a compass heading, are susceptible to being wrecked. Overall, this demonstrates that the ability to respond to storms is influenced by both flight and navigational capacities. This may become increasingly pertinent due to changes in extreme weather patterns.

Introduction

Cyclones can have devastating impacts, causing mass mortality of animals and disruption of entire ecosystems (Emanuel, 2005, Fiedler et al., 2013). The intensity of these extreme events (also called hurricanes and typhoons depending on their location) is predicted to increase with climate change (Seneviratne, 2021), while an increase in the frequency of the most intense storms is already being observed in regions prone to tropical cyclones (Kossin et al., 2020). Yet little is known about the capacity of organisms to respond to these systems, including the extent to which mobile animals can avoid them. Seabirds are particularly exposed to tropical cyclones because they develop over the ocean, and indeed, large numbers of seabirds can be wrecked after cyclones, numbering tens of thousands of individuals in the most extreme cases (Bailey and Davenport, 1972, Morley et al., 2016).

A handful of studies have managed to track pelagic seabirds in 1-2 tropical cyclones, showing that adults circumnavigate the most intense parts of these systems ((Hass et al., 2012, Weimerskirch and Prudor, 2019) but see (Catry et al., 2004, Thiebot et al., 2020)). This can lead to birds being displaced from their foraging area by up to 400 – 600 km (Weimerskirch and Prudor, 2019). Nonetheless, it is clear from widespread wrecks and inland strandings (Bugoni et al., 2007, Ryan et al., 1989, Hass et al., 2012), that avoidance is not always possible. Indeed, one great frigatebird (*Fregata minor*) that was tracked 250 km from a cyclone and encountered winds > 100 km h^{-1} appeared to have been killed (Weimerskirch and Prudor, 2019). It is therefore important to understand the conditions under which birds can, and cannot, avoid cyclones. Quantifying bird responses to extreme weather events remains challenging, as they are, by definition, infrequent. Cyclones are also variable in terms of their intensity, spatial extent, movement speed and trajectory. Understanding the behavioural rules that birds employ in an attempt to mitigate storm detriment therefore requires animals to be tracked during multiple, rare events.

We tracked 401 adult streaked shearwaters (*Calonectris leucomelas*) breeding on Awashima Island, Japan over 11-years. This region forms part of the Northwest Pacific cyclone belt, which is the world's most active cyclone basin and subject to large and extreme typhoons. Typhoon Hagibis in 2019, for example, was responsible for human fatalities in Japan and was estimated to cause $15 billion in terms of damage. Shearwaters breeding in this region should therefore represent a model system to understand how pelagic birds respond to extreme wind speeds. Furthermore, storm systems enter the Sea of Japan from the southeast and can influence the whole region, from Japan in the East, to Russia, North and

South Korea, in the North and West (Fig. 1A), restricting the opportunities for circumnavigation. We quantified the behavioural responses of shearwaters to 10 tropical cyclones and storms (Fig. 1, Table S1), specifically, using a combination of statistical and agent-based modelling to assess the flight direction in relation to (i) the eye of the typhoon/ storm and (ii) the nearest land. Overall, our aim was to provide novel insight into the capacity of seabirds to respond to the direct effects of extreme weather events.

Materials and Methods

Data collection

Streaked shearwaters breeding on Awashima Island (38° 27.102'N, 139° 14.363'E) were equipped with GPS loggers from 2008 to 2018, as described in (Koyama et al., 2021, Matsumoto et al., 2017, Yoda et al., 2021), providing movement data from 401 individuals. In summary, birds were instrumented with Gipsy 2 & 4 GPS loggers in 2010 - 2016 and AxyTrek loggers (Technosmart, Rome, Italy) in 2017 - 2018. Loggers were attached to the back of each bird with waterproof tape (Tesa, Hamburg, Germany) and cyanoacrylate glue. The logger and tape represented <5 % of bird body mass. Ethical permissions for tagging were granted by the Animal Experimental Committee of Nagoya University (GSES10–18). The experimental procedure was approved by the Ministry of the Environment Government of Japan.

GPS tracks were then selected for analysis according to whether they coincided with storm activity in the Sea of Japan. This resulted in 2,319 hours of observations from 75 individuals over 5 years (2010, 2014, 2015, 2017 and 2018), which were used for initial data exploration, where all birds were tracked during at least one storm. Flight was distinguished from drifting on the sea surface using a groundspeed threshold of 4.1 m s^{-1} following (Shiomi et al., 2012). We also applied a speed filter to remove positions that gave groundspeeds > 25 m s^{-1} to account for GPS location errors. This filtering threshold was identified using the cut-off point in groundspeed frequencies. Filters were applied to raw data, which were recorded at frequencies of 1 Hz to 1 minute depending on the year. This resulted in the removal of < 0.1 % of GPS locations for the storms Talim, Jebi and Cimaron, and < 5.2 % for the storms Kompasu and Goni (the five modelled storms). This did not result in any notable change in the distribution of step lengths between filtered and unfiltered data (Fig. S1), suggesting that we were not removing meaningful biological responses to high wind speed scenarios. In fact, the main determinant of the amount of data that was removed was the generation of GPS logger that was used, with older devices (e.g. those used during Kompasu and Goni)

apparently giving more frequent erroneous locations. Wind estimates were obtained from ERA5 global reanalysis models (Fig. 1A, Copernicus Climate Change Service (C3S) (Hersbach et al., 2018, Hersbach et al., 2020), for all bird locations. Global reanalyses combine real observations with forecast general circulation models to provide observation-constrained grids of the wind field that are capable of representing most tropical storms (Hodges et al., 2017). The two horizontal wind vectors (u, v) at 10 m from the surface were converted to horizontal wind speed and direction with a temporal resolution of one hour and a spatial resolution of 0.1°.

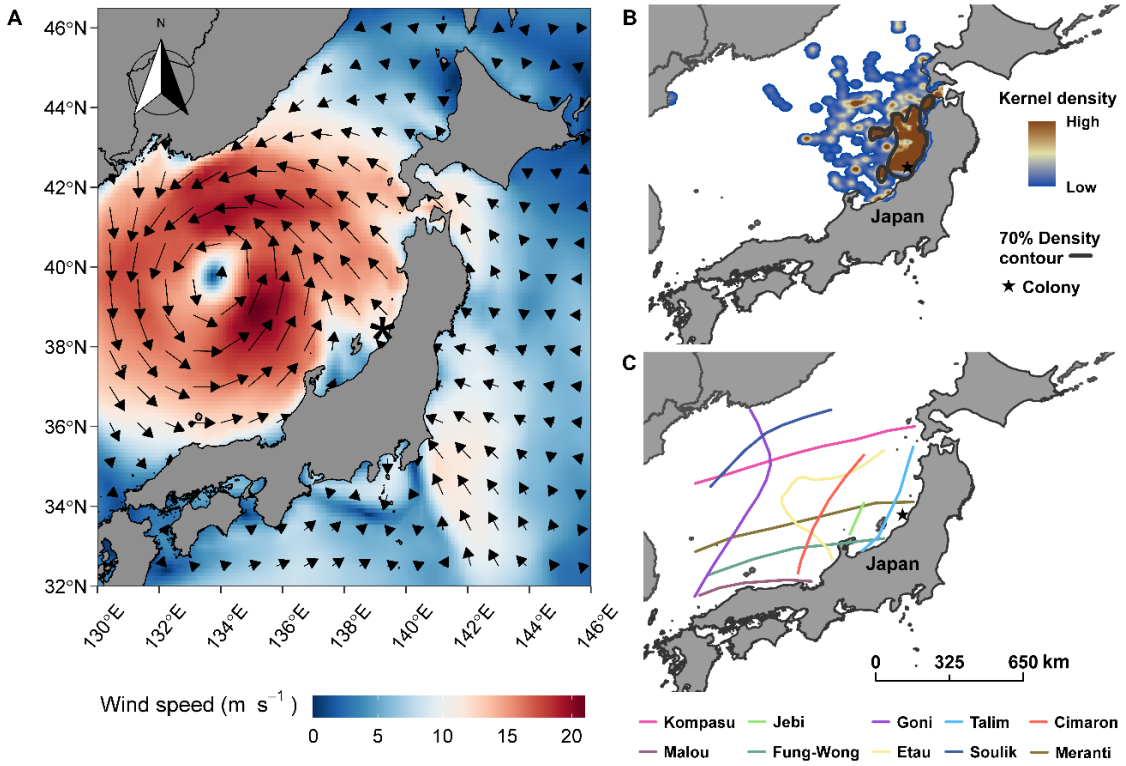

Figure 1. Distribution of streaked shearwaters and storms in the Sea of Japan. (A) The area affected during the passage of tropical cyclone Goni (26/08/2015 04:00:00 (UTC)). The black star indicates the location of the colony. The right panels show the 70% density contour of hourly interpolated GPS locations during the 10 storms (upper panel) and the tracks of storms that passed through the Sea of Japan when at least one tagged bird was at sea (lower panel). The five modelled typhoons/ storms are given in the first row of the legend.

Storm tracks were retrieved from the International Best Track Archive for Climate Stewardship (IBTrACS, http://ibtracs.unca.edu/index.php (Knapp et al., 2018, Knapp et al., 2010)), which provided the coordinates of the eyes of all major storms with a temporal resolution of six hours. Each storm track was interpolated to one hour temporal resolution to

match that of ERA5. Interpolations were run using the move package (version 4.0.0, (Kranstauber et al., 2020)) in R (version 4.0.1, (R Core Team, 2020)) and the great circle method. Storms were classified according to the maximum wind speed reported in IBTrACS for the periods where the storm passed through the Sea of Japan according to the Japan meteorological agency (JMA, https://www.jma.go.jp/jma/en/Activities/forecast.html#typh) (Table S1).

Statistical analysis

We used generalized additive mixed effect models (GAMMs, table S2) to assess how shearwaters responded to storms, as these models allow for complex, non-linear responses. Severe tropical storms and typhoons were selected for modelling because reanalyses tend to under-represent weaker tropical depressions/ storms, in terms of both intensity and spatial extent, with uncertainties increasing with decreasing strength (Hodges et al., 2017). This resulted in 690 hours of observation from 55 birds flying in five storms. All attributes relating to bird movement represent hourly averages of each term estimated using the raw GPS locations, in order to match the resolution of the bird movement paths to the ERA5 reanalysis data.

Our first model (model 1) assessed the direction that birds flew with respect to the eye of a storm, where the storm was that closest to each GPS location. The response variable was the flight direction that a bird flew in relation to the location of the storm eye in each hour of observations (IBTrACS interpolated resolution of eye locations) and based on the GPS heading. It ranged from 0^o to 180^o for flight straight towards the eye of the storm or straight away, respectively, with flight parallel to the eye indicated by values ~90^o. The global model included wind speed and wind direction at the birds locations within each hour of ERA5 (ERA5 temporal resolution) and bird position with respect to the storm eye (with 0^o indicating a bird was ahead of the storm and 180^o directly behind it). The model also included interactions between wind speed and direction to test whether the response varied by the combination of strong winds from different directions. We also tested the interaction between wind speed and bird position with respect to the storm to assess whether the response varied when a bird was ahead or behind a storm and simultaneously experienced strong or weak winds.. Storm ID was included as a random effect to account for effects associated with storms that might have not been described by the modelled predictors/ interactions. We then extended this model to test if proximity to land, the minimum distance between a bird's GPS location and the closest point on Honsu Island, improved the model fit. The same interactions

were included as for global model 1, with an additional interaction between wind speed and distance to land.

In a final model (model 2), we tested whether the flight direction with respect to land varied with wind speed and direction, with the expectation that birds would be less likely to fly towards land in strong winds. The response variable of this model was the flight direction that a bird flew in relation to its closest point on Honshu Island based on the GPS heading. It ranged from 0^o to 180^o for flight straight towards the closest point on land or straight away, respectively, with flight parallel to land indicated by values ~90^o.The global model was the same as the previous model.

The simultaneous bird response to both land and storm was assessed by comparing the predicted relationship of a predictor in the storm model with the same predictor in the land model. For example, we tested whether wind speed had a negative effect on the flight direction in relation to the storm eye, indicating a trend of flight towards, and a positive effect on flight direction in relation to land, indicating flight away.

Model selection was performed using the smoothing shrinkage method (Marra and Wood, 2011). First, simple predictors were added using the "s( )" smoothing and the penalised thin plate regression spline ("ts") as smooth basis (but "re" for random effects) to form the global model. Each pair of terms was then assessed for concurvity using the mgcv package (Wood, 2017). Less significant terms in pairs with "worst" case concurvity > 0.8 were removed from further analysis. Second, the smoothed effect of each predictor was evaluated and terms where the effect shrank to zero were removed. Evaluation and exclusion of zero effects was repeated by the addition of the interaction terms using the tensor product smoothing "ti ()" with a simultaneous assessment of whether the removal of an interaction from the model resulted in significant reduction in AIC (≤ 2). In the refined model that included all remaining single predictors and interactions, the smoothing basis was set to thin plate regression spline ("tp") for continuous predictors and cyclic cubic regression spline ("cc") for the circular wind direction. Finally, the base dimension (k) of each term was assessed using the gam.check function of mgcv (Wood, 2017) and increased appropriately where needed.

In each model, the number of GPS fixes averaged in each hour was used as a weight, normalized by the mean number of fixes in the modelled dataset. To account for temporal and spatial autocorrelation all models included the date/ hour and the hourly interpolated coordinates for each set of GPS coordinates within each hour, using the corARMA and

corSpatial functions from the nlme package, respectively (Pinheiro et al., 2017). The final models were evaluated for outliers, uniformity, over/ under-dispersion and spatial/ temporal autocorrelation using the DHARMa package (Hartig and Hartig, 2017), with the test of under-dispersion being significant for all models.

Agent based modelling

An agent-based model was developed to resolve (1) whether the response to the wind field resulted in birds flying towards the eye of the storm and (2) how often the predictions from model 1 resulted in birds being "wrecked" i.e. flying onto land. In both scenarios ten simulations of 400 agents were run, with agent starting points distributed randomly within the 70% kernel density contour of space use at-sea, determined across the five years of study (Fig. 1B). We used the output of model 1 (flight direction with respect to storm eye) to drive each agent's heading at any time step (one hour). The output from model 1 was converted from the predicted $0 – 180^{o}$ to $0 – 360^{o}$ using a binomial GAMM predicting whether the agent should fly right or left in relation to the storm. Agent flight speed was fixed as the mean hourly groundspeed of the observations collected during each storm (~ 8 - 9 m s^{-1}) or set to 9.3 m s^{-1} (~ 33 km h^{-1}) when the mean ground speed exceeded this threshold. As each cell in ERA5 covered an area of ~ 11 km^2, each agent was set to make three steps per hour (~11 km each to complete a movement of ~ 33 km), to guarantee that each cell was taken into account. Agents started moving when the distance between the storm eye and the agent was ≤ 500 km in order to capture the response to the storm. Movement was paused whenever this threshold was exceeded or the storm eye reached land. An agent was considered to reach the eye of a storm when its distance from the eye location was ≤ 30 km (the mean radius of 62 storm eyes as identified by (Kodama and Yamada, 2005). Results from this agent-based model were compared with two null models. A model of random movement and a model where agents moved to the exact direction as the direction where wind was blowing towards, at their locations. This is equivalent to a condition of full drift with a pure tailwind. We ran simulations for the five storms classified as severe tropical storms and typhoons (Table S3, movies S3 -S7).

Results

Isolating GPS tracks from the 75 shearwaters that were exposed to storms (Fig. 1B, C) showed that birds flew in all wind conditions, appearing no less likely to fly as wind speeds increased to typhoon strength (Fig. 2A, the maximum estimated wind speed in the Sea of Japan was 97 km h^{-1}/ 27 m s^{-1} (ERA5), Table S1). In all scenarios, birds flew with a strong

crosswind component, consistent with their dynamic soaring flight style (Fig. 2B) (Yonehara et al., 2016). In order to focus on the responses to the most extreme conditions, we then examined the movements of 55 shearwaters in the five strongest storms; three typhoons and two severe tropical storms Table S1), hereafter referred to as storms for simplicity.

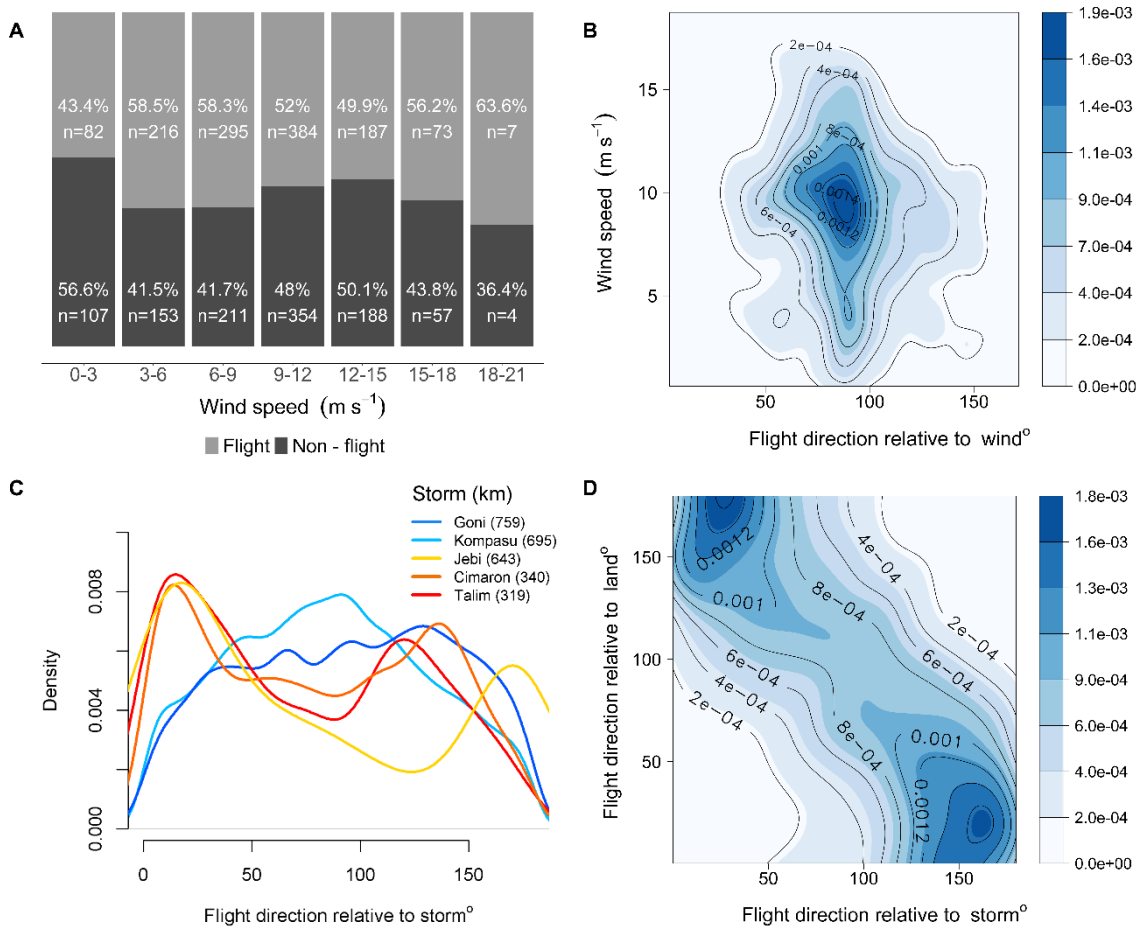

Figure 2. Bird behavior according to the wind field and land. (A) Hours of flight and non-flight behavior (n=2,318 h) according to wind strength when birds were at sea during the 10 storms. (B) Kernel density of hourly mean flight direction in relation to wind direction during the five strongest storms (n= 1618 h), highlighting the selection of crosswinds. (C) Flight direction in relation to the eye of the five strongest storms, derived from the raw GPS estimates, showing birds were more likely to respond to storms that passed closer to them. The colors indicate the distance between the eye and tracked birds (90% quantile of bird – storm distance) with distance decreasing from blue to red. (D) The normalized kernel density of hourly mean flight direction in relation to the closest point on land (n= 1618 h), in the five strongest storms, showing birds only flew towards the eye when this took them away from land.

Wind speed (estimated using ERA5 reanalysis data) was a good predictor of the birds' flight direction with respect to the storm eye, with birds flying away from the storm in speeds < 10 m s^{-1} and being attracted to the eye in strong winds (Table S2, Fig. S2A). This effect was larger in the most intense winds (Fig. S2A, Fig. 3). The bird's position relative to the storm's direction only influenced the response when birds were behind the storm. This was the result of individuals "chasing" the eye from behind with, for example, one bird chasing storm Talim for > 4 hours and two individuals chasing typhoon Cimaron for > 8 hours (Movies S1 and S2).

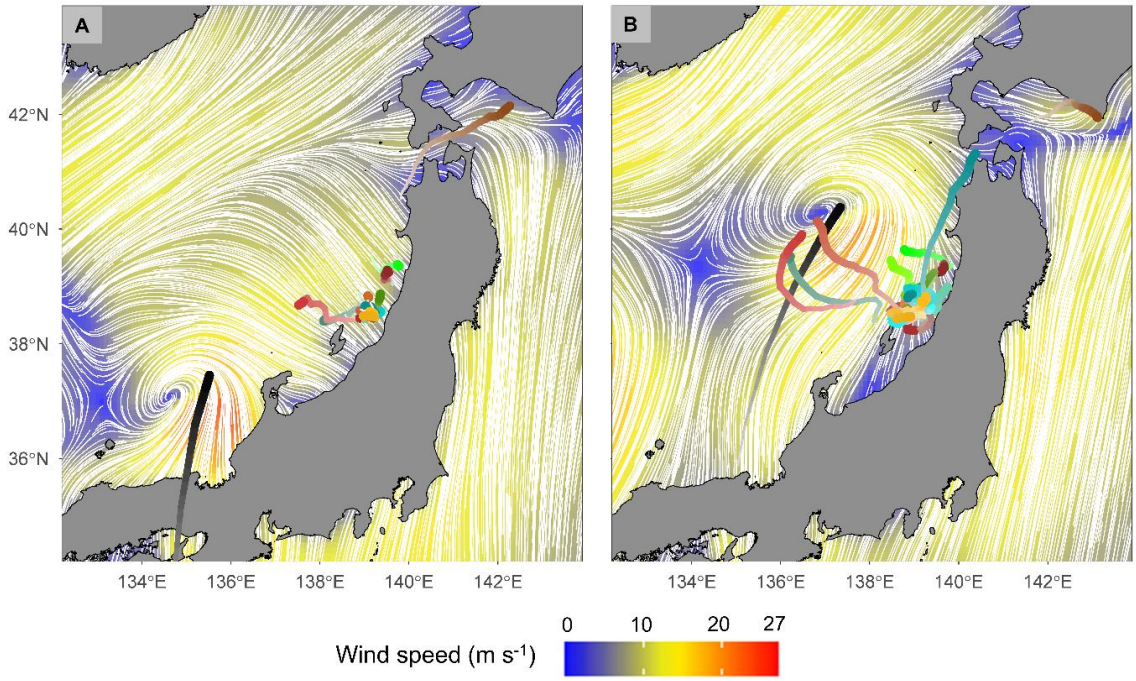

Figure 3. Bird responses to tropical cyclone Cimaron. (A) As Cimaron entered the Sea of Japan (black track), 32 birds were located within the 70% utilization area. (B) When the eye was at its closest to the birds, three birds had already flown towards and chased the eye (dark red and green), two more had initiated flight towards it (bright green) and the majority of birds located within a layer of weaker winds, remained sheltered near the shore. In the same hour another storm can be observed to the west.

Agent-based models confirmed that the birds' response to strong winds took them towards the eye of the storm. Agents that were programmed with the GAMM output of flight direction in relation to the storm eye and placed in a random grid in the core foraging area were exposed to the wind field of the five strongest storms. Of the agents that were capable of reaching the eye (based on distance, agent speed and simulation time), 30–66% came within 60 km came within 60 km of the central point of the storm, for all storms except Goni where no agents came this close, but few came within 30 km (apart from storm Talim, where this

figure reached 34%) (Table S3). Similar proximities were observed in the GPS data with four individuals coming within 30 km of the central point of a storm, and nine additional birds within 60 km (Movies S1 and S2).

Overall, agents showed a clear attraction to storms that came within 60 – 170 km of the core foraging area (typhoon Cimaron, storm Talim, typhoon Jebi, mean flight direction ≤ 70^{o}), but did not respond to storms that were further away (e.g. typhoon Goni, which was 330 km away at the closest point) (Table S3). This was likely driven by the dependence of flight direction on wind speed in the GAMM output.

When compared with the results from the null models of random movement and movement towards the direction that wind was blowing, the agent-based model programmed with the GAMM output behaved differently to a large extent especially in the case of typhoons Cimaron and Jebi and the severe tropical storm Talim (Table S3). The percentage of agents that sustained flight towards the eye was considerably lower in both the random and wind direction models, while the percentage of wrecked agents tended to be higher. Although a substantial percentage of agents reached within 30 km of the central point of the storm in the wind direction model of typhoon Jebi and storm Talim, as indicated by the percentage of agents that sustained flight towards the eye of the storm (≤ 70^{o}), these were cases where the eye moved to the agents locations rather than the agents moved towards the eye.

The GAMM also revealed that storm identity had a significant effect on flight direction, independent of wind speed (GAMM Table S2). This could be seen in the GPS tracks, which revealed that individuals positioned at the outer reaches of the usual foraging area when storm Talim entered the Sea of Japan circumnavigated the storm system by flying to the South and West (Movie S1).

Overall, the primary determinant of flight direction was the wind field, as adding distance to land to the GAMM of flight direction in relation to the storm did not improve the AIC or deviance explained. Nonetheless, the GAMM assessing flight direction with respect to land showed a positive and almost linear effect of wind strength on flight direction in relation to land, with shearwaters flying away from land as wind speeds increased (Table S2, Fig. S2B, Fig. 3). This response was also evident in the tracks of individuals sandwiched between storms and Honshu Island of Japan (Movies S1 and S2). While agents programmed without any knowledge of, or response to, the location of land rarely moved over land (Table S3), the simulated response to storm Komapsu resulted in ~ 86 % of the agents being “stranded” on land.

Discussion

We show that shearwaters flew towards the eye of multiple typhoons; a behaviour that was more likely as wind speed increased, with birds even moving towards the eye of the strongest typhoon in the study period (Fig. 3, Table S1). This strategy exposes birds to some of the strongest wind strengths, as speeds increase towards the eye wall and only decrease within the eye itself. Given that storm eyes have a diameter of 20-50 km (Kodama and Yamada, 2005), it is clear that the four birds that came within 30 km of the eye were operating in or close to the eye wall. These results are surprising given that almost all other seabirds tracked in relation to storms have avoided the strongest winds, either by remaining on or close to land in the case of pelicans, juvenile frigate birds and boobies (Wilkinson et al., 2019, Weimerskirch and Prudor, 2019), or by circumnavigating the storm system (Wilkinson et al., 2019, Weimerskirch and Prudor, 2019), in agreement with optimal navigation theory (McLaren et al., 2014).

Shearwaters differ from other species tracked in storms to date through their use of dynamic soaring flight, which enables them to extract energy from the vertical wind gradient (Spivey et al., 2014) and fly at low metabolic costs in strong winds (Davies et al., 2010, Furness and Bryant, 1996). But flight style cannot, in itself, explain this response to typhoons, because birds only flew towards the eye of the storm when this took them away from land and when they were experiencing strong winds (*cf.* Catry et al. (2004)). The context-dependency of this behaviour also means it is unlikely that birds moved towards the eye to exploit temporary increases in productivity (Nicoll et al., 2017). Furthermore, water mixing caused by storms is thought to reduce feeding opportunities for piscivorous predators (Secor et al., 2019).

Instead, our results suggest that birds fly towards the storm, and sometimes track its path, in order to avoid the strong onshore winds that occur in the wake of storms as they move north through our study area. This demonstrates that typhoon winds in themselves are not necessarily a risk for these, and other dynamic soaring seabirds, but they do present a danger when they could cause drift in unfavourable directions, such as towards land. Land may represent a range of threats for shearwaters, from the direct risk of collision and uncontrolled landings in extreme winds, as reported for procellariiformes during a 1984 storm in South Africa (Ryan et al., 1989), to the limited capacity to take-off once grounded and their susceptibility to predators, including crows and raptors (Yoda et al., 2017, Yoda et al., 2021). Indeed, adult shearwaters from our study population have never been tracked over land (Fig

S1B in Yoda et al. (2017)), although numerous fledgling mortalities are reported over land during migration, when inexperienced birds follow a compass bearing to their migration destination (Yoda et al., 2017).

The instances when shearwaters did circumnavigate a storm demonstrate that they have a flexible response to storm systems (*cf.* Thiebot et al. (2020)). Circumnavigation is unlikely to be feasible when birds are in their core foraging area close to Honshu Island, as storms approach from the southwest, sandwiching birds between the storm path and the land (Fig. 3, 4). Anticlockwise circumnavigation would require birds to sustain groundspeeds greater than the storm speed for hundreds of kilometres, as they fly north and west towards Russia and Korea, before exiting south of a storm. This seems untenable given that storms in our study reached translation speeds > 20 m s^{-1}. Clockwise circumnavigation from the core foraging area seems equally unlikely, as it would require birds to fly with strong headwinds that could also drift them towards Honshu (Fig. 4). The individuals that did circumnavigate a storm were northwest of the storm's path, where flying towards the eye would have taken them closer to land.

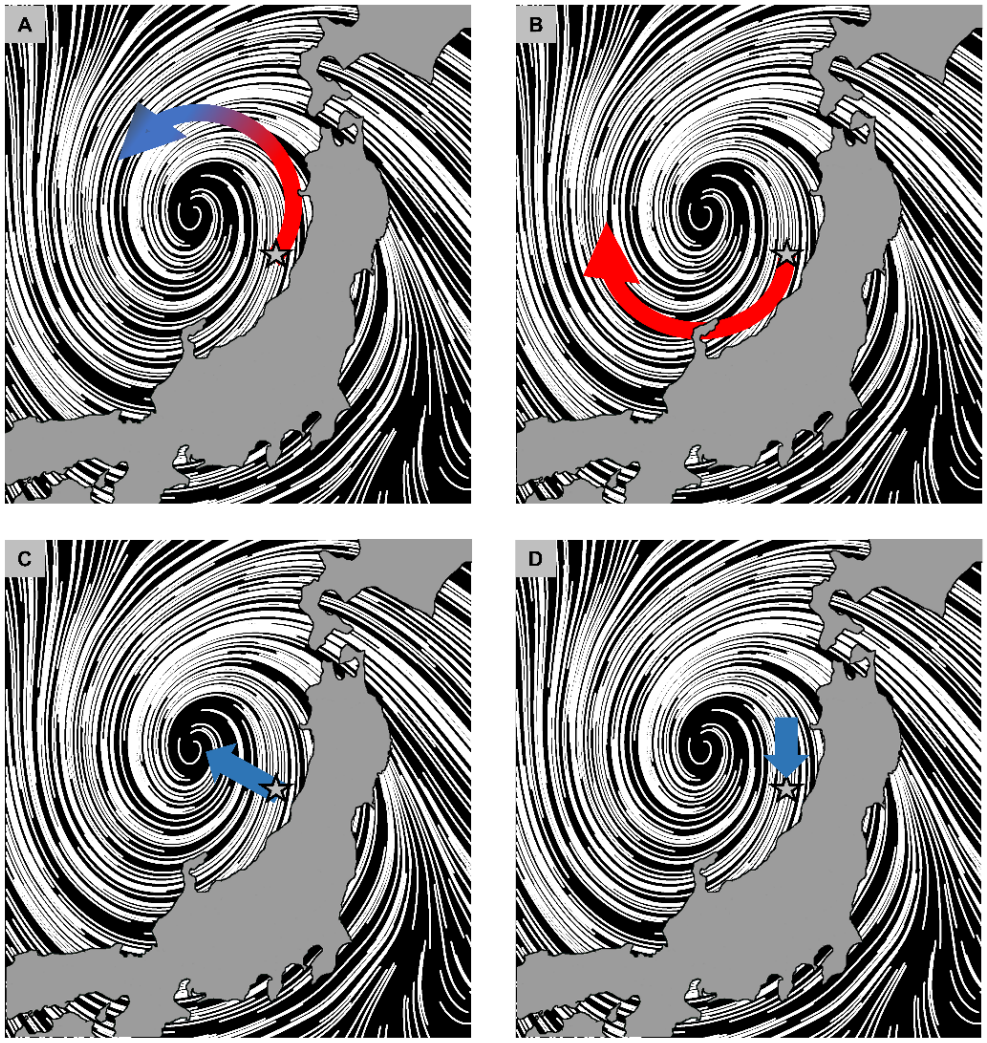

Figure 4. Theoretical responses to a hypothetical tropical cyclone travelling from south to north, for a bird located within the core utilization area near the Awashima colony. (A) Anticlockwise circumnavigation with wind support, a framework suggested by optimal navigation theory (McLaren et al., 2014) becomes a better option when the bird is positioned to the west of the eye (blue shade) when compensation for wind drift and avoiding land is less crucial. (B) Clockwise circumnavigation against onshore wind, an option necessitating airspeed higher than the strong headwinds to make progress and likely a high degree of compensation to avoid land. (C) Flight towards the eye of the storm with crosswind, an option that takes birds away from land and avoids the onshore wind region behind the eye. (D) Maintain position near shore for shelter, a choice that becomes plausible when winds at the bird's location are relatively weak.

The flexibility in the shearwater's strategy reveals that birds must be capable of estimating the wind speed at their location, the trajectory of an approaching storm, and the direction of the nearest landmass, whether that is Japan to the East, or China, Russia to the

West, all of which influence the most appropriate response. This supports earlier studies suggesting that adult birds have a map sense (Goto et al., 2017). Furthermore, the need to respond to regular typhoons provides an additional selective pressure for the development of such navigational capacities, which must incorporate an ability to locate and respond to moving weather systems, as well as land. Juveniles should be less well equipped to respond to storms, as fledgling shearwaters have been shown to use an innate compass bearing to migrate (Yoda et al., 2017). In support of this, young shearwaters (not tracked here) appear to be particularly susceptible to being wrecked after storms both within our study area and beyond (Kuroda, 1966, Oka and Maruyama, 1986, Syposz et al., 2018), although the exact cause of wrecking and/ or mortality is unclear.

The capacity of adult shearwaters to operate in typhoon winds, is notable for what it tells us about flight capacity, as well as navigational capacity. Birds are only able to compensate for wind drift (and hence resist being drifted onto land by strong onshore winds) when their airspeed exceeds the wind speed (Chapman et al., 2011). Streaked shearwaters are relatively small, weighing some 580 g, and typically fly with airspeeds up to ~ 14 m s^{-1} (Spear and Ainley, 1997), yet here we find that adults flew in winds up to 21 m s^{-1}. This is similar to the maximum predicted airspeed for wandering albatrosses (Richardson et al., 2018), which are heavier than streaked shearwaters by more than a factor of ten. The actual wind speeds experienced by shearwaters may have been even greater, as ERA5 tends to underestimate wind 10 m above the surface by 5 - 20 m s^{-1}, depending on the storm intensity and its stage of evolution (Malakar et al., 2020). Nonetheless, this will be tempered by the tendency to fly close to the water surface, which exposes shearwaters to lower wind speeds for most of the dynamic soaring cycle (Goto et al., 2017). For instance, wind speeds at a flight height of 5 m are predicted to drop from 21 to 18.5 m s^{-1} (Pennycuick, 1982). Variation of flight height in relation to increasing wind speed may therefore provide a way for procellariiformes to modulate their exposure to the strongest winds, while still extracting energy from them.

In general, airspeed and flight style (including flight height and reliance on flapping flight) should be key determinants of interspecific responses and vulnerability to typhoons. We predict that flying towards the storm eye is only likely to be an option for dynamic soaring birds, which do this because they can, with extreme winds only becoming costly or risky in particular scenarios, such as when they might be drifted onto land. More generally, flight speed, costs and flight height will determine the chances that birds can avoid or outrun

storms. The question is the extent to which these responses will be sufficient as typhoon intensity, as well as potentially size and duration, increase.

References

Bailey, E. P. & Davenport, G. H. 1972. Die-off of common murres on the Alaska Peninsula and Unimak Island. *The Condor,* 74**,** 215-219.

Bugoni, L., Sander, M. & Costa, E. S. 2007. Effects of the first southern Atlantic hurricane on Atlantic petrels (Pterodroma incerta). *The Wilson Journal of Ornithology,* 119**,** 725-729.

Catry, P., Phillips, R. A. & Croxall, J. P. 2004. Sustained fast travel by a gray-headed albatross (Thalassarche chrysostoma) riding an Antarctic storm. *The Auk,* 121**,** 1208-1213.

Chapman, J. W., Klaassen, R. H., Drake, V. A., Fossette, S., Hays, G. C., Metcalfe, J. D., Reynolds, A. M., Reynolds, D. R. & Alerstam, T. 2011. Animal orientation strategies for movement in flows. *Current Biology,* 21**,** R861-R870.

Davies, R. G., Irlich, U. M., Chown, S. L. & Gaston, K. J. 2010. Ambient, productive and wind energy, and ocean extent predict global species richness of procellariiform seabirds. *Global Ecology and Biogeography,* 19**,** 98-110.

Emanuel, K. 2005. Increasing destructiveness of tropical cyclones over the past 30 years. *Nature,* 436**,** 686-688.

Fiedler, P. C., Redfern, J. V., Van Noord, J., Hall, C., Pitman, R. L. & Ballance, L. T. 2013. Effects of a tropical cyclone on a pelagic ecosystem from the physical environment to top predators. *Marine Ecology Progress Series,* 484**,** 1-16.

Furness, R. W. & Bryant, D. M. 1996. Effect of wind on field metabolic rates of breeding northern fulmars. *Ecology,* 77**,** 1181-1188.

Goto, Y., Yoda, K. & Sato, K. 2017. Asymmetry hidden in birds' tracks reveals wind, heading, and orientation ability over the ocean. *Science advances,* 3**,** e1700097.

Hartig, F. & Hartig, M. F. 2017. DHARMa: Residual Diagnostics for Hierarchical (Multi-Level Mixed) Regression Models. R package version 0.3.3.

Hass, T., Hyman, J. & Semmens, B. 2012. Climate change, heightened hurricane activity, and extinction risk for an endangered tropical seabird, the black-capped petrel Pterodroma hasitata. *Marine Ecology Progress Series,* 454**,** 251-261.

Hersbach, H., Bell, B., Berrisford, P., Biavati, G., Horányi, A., Muñoz Sabater, J., J, N., Peubey, C., Radu, R., Rozum, I., Schepers, D., Simmons, A., Soci, C., Dee, D. & Thépaut, J.-N. 2018. ERA5 hourly data on single levels from 1979 to present.

Hersbach, H., Bell, B., Berrisford, P., Hirahara, S., Horányi, A., Muñoz-Sabater, J., Nicolas, J., Peubey, C., Radu, R. & Schepers, D. 2020. The ERA5 global reanalysis. *Quarterly Journal of the Royal Meteorological Society,* 146**,** 1999-2049.

Hodges, K., Cobb, A. & Vidale, P. L. 2017. How well are tropical cyclones represented in reanalysis datasets? *Journal of Climate,* 30**,** 5243-5264.

Knapp, K. R., Diamond, H. J., Kossin, J. P., Kruk, M. C. & Schreck, C. 2018. International best track archive for climate stewardship (IBTRACS) project, version 4. *NOAA National Centers for Environmental Information*.

Knapp, K. R., Kruk, M. C., Levinson, D. H., Diamond, H. J. & Neumann, C. J. 2010. The international best track archive for climate stewardship (IBTrACS) unifying tropical cyclone data. *Bulletin of the American Meteorological Society,* 91**,** 363-376.

Kodama, Y.-M. & Yamada, T. 2005. Detectability and configuration of tropical cyclone eyes over the western North Pacific in TRMM PR and IR observations. *Monthly weather review,* 133**,** 2213-2226.

Kossin, J. P., Knapp, K. R., Olander, T. L. & Velden, C. S. 2020. Global increase in major tropical cyclone exceedance probability over the past four decades. *Proceedings of the National Academy of Sciences,* 117**,** 11975-11980.

Koyama, S., Mizutani, Y. & Yoda, K. 2021. Exhausted with foraging: Foraging behavior is related to oxidative stress in chick-rearing seabirds. *Comparative Biochemistry and Physiology Part A: Molecular & Integrative Physiology*, 258**,** 110984.

Kranstauber, B., Smolla, M. & Scharf, A. K. 2020. move: Visualizing and Analyzing Animal Track Data. R package version 4.0.0.

Kuroda, N. 1966. A mass inland drift of Streaked Shearwaters over Kanto plain in November, 1965. *Journal of the Yamashina Institute for Ornithology,* 4**,** 388-396.

Malakar, P., Kesarkar, A., Bhate, J., Singh, V. & Deshamukhya, A. 2020. Comparison of reanalysis data sets to comprehend the evolution of tropical cyclones over North Indian Ocean. *Earth and Space Science,* 7**,** e2019EA000978.

Marra, G. & Wood, S. N. 2011. Practical variable selection for generalized additive models. *Computational Statistics & Data Analysis,* 55**,** 2372-2387.

Matsumoto, S., Yamamoto, T., Yamamoto, M., Zavalaga, C. B. & Yoda, K. 2017. Sex-related differences in the foraging movement of streaked shearwaters Calonectris leucomelas breeding on Awashima Island in the Sea of Japan. *Ornithological Science,* 16**,** 23-32.

McLaren, J. D., Shamoun-Baranes, J., Dokter, A. M., Klaassen, R. H. & Bouten, W. 2014. Optimal orientation in flows: providing a benchmark for animal movement strategies. *Journal of the Royal Society Interface,* 11**,** 20140588.

Morley, T. I., Fayet, A. L., Jessop, H., Veron, P., Veron, M., Clark, J. & Wood, M. J. 2016. The seabird wreck in the Bay of Biscay and South-Western Approaches in 2014: A review of reported mortality. *Seabird,* 29**,** 22-38.

Nicoll, M. A., Nevoux, M., Jones, C. G., Ratcliffe, N., Ruhomaun, K., Tatayah, V. & Norris, K. 2017. Contrasting effects of tropical cyclones on the annual survival of a pelagic seabird in the Indian Ocean. *Global Change Biology,* 23**,** 550-565.

Oka, N. & Maruyama, N. 1986. Mass mortality of short-tailed shearwaters along the Japanese coast. *Japanese Journal of Ornithology,* 34**,** 97-104.

Pennycuick, C. J. 1982. The flight of petrels and albatrosses (Procellariiformes), observed in South Georgia and its vicinity. *Philosophical Transactions of the Royal Society of London. B, Biological Sciences,* 300**,** 75-106.

Pinheiro, J., Bates, D., DebRoy, S., Sarkar, D., Heisterkamp, S., Van Willigen, B. & Maintainer, R. 2017. Package 'nlme'. *Linear and nonlinear mixed effects models, version,* 3.

Richardson, P. L., Wakefield, E. D. & Phillips, R. A. 2018. Flight speed and performance of the wandering albatross with respect to wind. *Movement ecology,* 6**,** 1-15.

Ryan, P., Avery, G., Rose, B., ROSS, G. B., Sinclair, J. & Vernon, C. 1989. The Southern Ocean seabird irruption to South African waters during winter 1984. *Marine Ornithology,* 17**,** 41-55.

Secor, D. H., Zhang, F., O'Brien, M. H. & Li, M. 2019. Ocean destratification and fish evacuation caused by a Mid-Atlantic tropical storm. *ICES Journal of Marine Science,* 76**,** 573-584.

Seneviratne, S. I., X. Zhang, M. Adnan, W. Badi, C. Dereczynski, A. Di Luca, S. Ghosh, I. Iskandar, J. Kossin, S. Lewis, F. Otto, I. Pinto, M. Satoh, S.M. Vicente-Serrano, M. Wehner, and B. Zhou 2021. Weather and Climate Extreme Events in a Changing Climate. *In:* MassonDelmotte, V., P. Zhai, A. Pirani, S.L. Connors, C. Péan, S. Berger, N. Caud, Y. Chen, L. Goldfarb, M.I. Gomis, M. Huang, K. Leitzell, E. Lonnoy, J.B.R. Matthews, T.K. Maycock, T. Waterfield, O. Yelekçi, R. Yu, and B. Zhou (ed.) *Climate Change 2021: The Physical Science Basis. Contribution of Working Group I to the Sixth Assessment Report of the Intergovernmental Panel on Climate Change.* Cambridge University Press. In Press.

Shiomi, K., Yoda, K., Katsumata, N. & Sato, K. 2012. Temporal tuning of homeward flights in seabirds. *Animal Behaviour,* 83**,** 355-359.

Spear, L. B. & Ainley, D. G. 1997. Flight speed of seabirds in relation to wind speed and direction. *Ibis,* 139**,** 234-251.

Spivey, R., Stansfield, S. & Bishop, C. 2014. Analysing the intermittent flapping flight of a Manx Shearwater, Puffinus puffinus, and its sporadic use of a wave-meandering wing-sailing flight strategy. *Progress in Oceanography,* 125**,** 62-73.

Syposz, M., Gonçalves, F., Carty, M., Hoppitt, W. & Manco, F. 2018. Factors influencing Manx Shearwater grounding on the west coast of Scotland. *Ibis,* 160**,** 846-854.

Team, R. C. 2020. R: A language and environment for statistical computing.

Thiebot, J.-B., Nakamura, N., Toguchi, Y., Tomita, N. & Ozaki, K. 2020. Migration of black-naped terns in contrasted cyclonic conditions. *Marine Biology,* 167**,** 1-12.

Weimerskirch, H. & Prudor, A. 2019. Cyclone avoidance behaviour by foraging seabirds. *Scientific reports,* 9**,** 1-9.

Wilkinson, B. P., Satgé, Y. G., Lamb, J. S. & Jodice, P. G. 2019. Tropical cyclones alter short-term activity patterns of a coastal seabird. *Movement ecology,* 7**,** 1-11.

Wood, S. N. 2017. *Generalized additive models: an introduction with R,* CRC press.

Yoda, K., Okumura, M., Suzuki, H., Matsumoto, S., Koyama, S. & Yamamoto, M. 2021. Annual variations in the migration routes and survival of pelagic seabirds over mountain ranges. *Ecology***,** e03297-e03297.

Yoda, K., Yamamoto, T., Suzuki, H., Matsumoto, S., Müller, M. & Yamamoto, M. 2017. Compass orientation drives naïve pelagic seabirds to cross mountain ranges. *Current Biology,* 27**,** R1152-R1153.

Yonehara, Y., Goto, Y., Yoda, K., Watanuki, Y., Young, L. C., Weimerskirch, H., Bost, C.-A. & Sato, K. 2016. Flight paths of seabirds soaring over the ocean surface enable measurement of fine-scale wind speed and direction. *Proceedings of the National Academy of Sciences,* 113**,** 9039-9044.

Chapter 4: Supplementary Information

Estimation of flight directions relative to storm and land

In order to identify whether birds were attracted to or avoided the storms, we estimated the flight direction with respect to the eye of the storm using equations 1 and 2:

$$FDS = FD - SA + 360 \quad \{for\ FD < SA\}c \quad (1)$$

$$FDS = FD - SA \quad \{for\ FD >= SA\} \quad (2)$$

where FDS is the flight direction with respect to the eye ($0 – 360^o$) which was converted to the range of $0 – 180^o$, with 0^o and 180^o indicating flight straight towards and away respectively, FD is the GPS derived flight heading ($0 – 360^o$) and SA is the storm angle ($0 – 360^o$), which is the direction a bird would have to travel to fly straight to the eye of the storm.

To assess whether shearwaters show a distinct response depending on whether the storm is heading towards or away from the bird, we calculated the bird position with respect to the storm direction of travel using equations 3 and 4:

$$BP = SAP - SD + 360 \quad \{for\ SAP < SD\} \quad (3)$$

$$BP = SAP - SD \quad \{for\ SAP >= SD\} \quad (4)$$

where BP is the bird position with respect to the eye ($0 – 360°$) which was converted to the range of $0 – 180°$ with $0°$ indicating that the bird was located in-front of a storm and $180°$ exactly behind, SAP is the opposite direction from SA and SD is the direction to which a storm is travelling ($0 – 360°$).

To assess whether shearwaters fly away from land to reduce the risk of being wrecked, we estimated the minimum distance to land in ArcMap 10.5.1 (ESRI, Redlands, California) and the flight direction with respect to the closest point on land at each bird location, using the equations 5 to 8:

$$FDL = | FD - LD | \quad \{\text{for } LD \leq 180 \text{ and for } FD \leq 180\} \quad (5)$$

$$FDL = FD + 360 - LD \quad \{\text{for } LD > 180 \text{ and for } FD \leq 180\} \quad (6)$$

$$FDL = LD + 360 - FD \quad \{\text{for } LD \leq 180 \text{ and for } FD > 180\} \quad (7)$$

$$FDL = | (360 - FD) - (360\text{-}LD) | \quad \{\text{for } LD > 180 \text{ and for } FD > 180\} \quad (8)$$

where FDL is the flight direction with respect to the closest location on land (0 – 360°) which was converted to the range of 0 – 180°, with 0° and 180° indicating flight straight towards land and away respectively and LD is the direction that a bird would have to fly to travel straight to that location (0 – 360°).

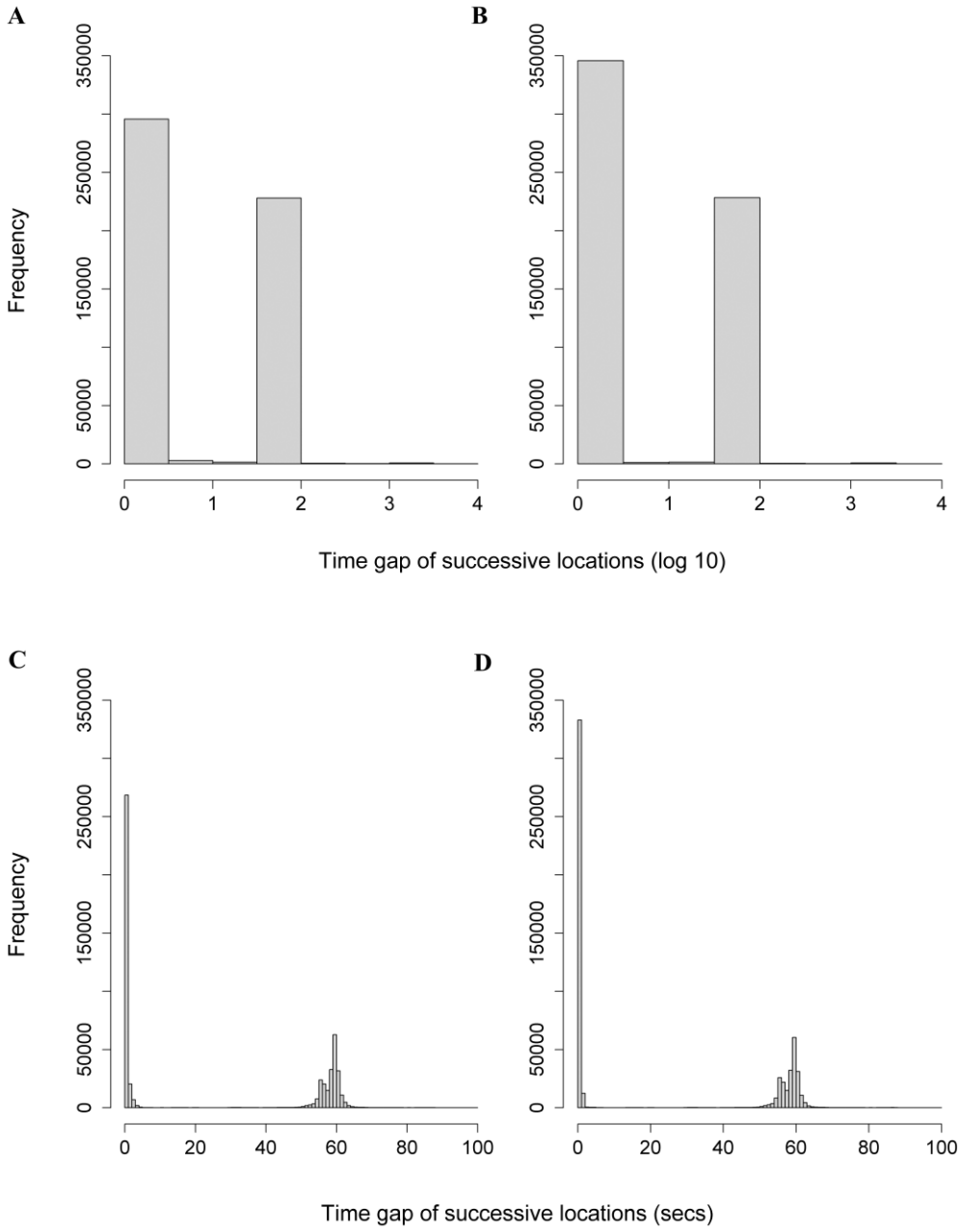

Figure S1. Frequency of time gaps between successive GPS locations in log 10 (A, B) and in seconds (C, D). Frequencies are given for the GPS dataset filtered by using a 25 m s-1 ground speed filter (A, C) and for the un-filtered dataset (B, D).

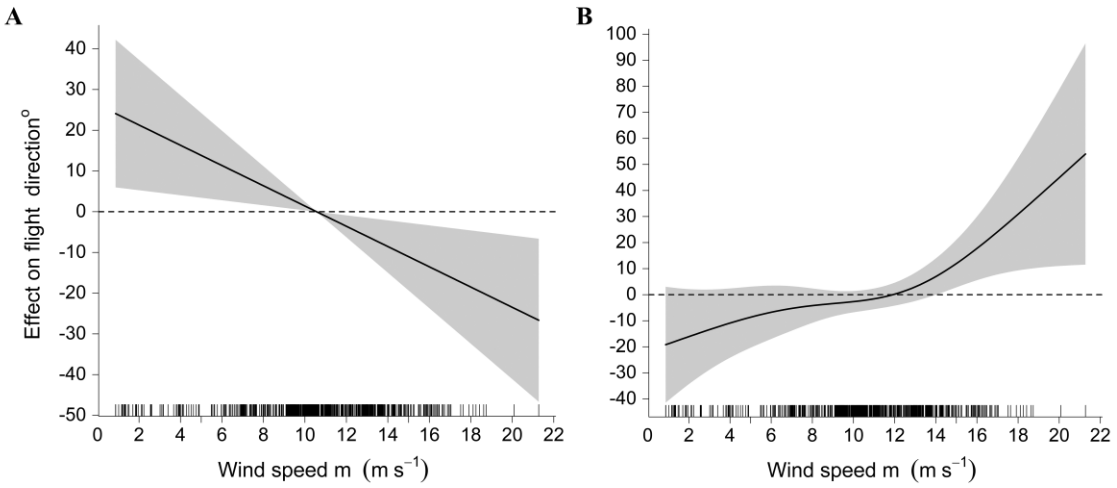

Figure S2. Partial effect (contribution) of wind speed to the overall predictions of GAMM models of flight direction in relation to (A) storm and (B) land. Negative values indicate attraction and positive values avoidance

.

Table S1. Tropical storms were categorized using the maximum wind speed within the Sea of Japan, provided by IBTrACS, and using the Japan Meteorological Agency (JMA) international classification. Maximum wind speed estimates within the Sea of Japan are given for both IBTrACS and ERA5, for the period that a storm travelled within the study area.

Storm	Period	Max hourly wind speed (IBTrACS, m s^{-1})	Max hourly wind speed (ERA5, m s^{-1})	Classification (JMA)
Kompasu	02-03/09/2010	25.7	16.0	Severe tropical storm
Malou	07-08/09/2010	18.0	17.2	Tropical storm
Meranti	12/09/2010	14.9	21.6	Tropical depression
Fung-Wong	24-25/09/2014	15.9	13.4	Tropical depression
Goni	25-26/08/2015	33.4	24.4	Typhoon
Etau	09-11/09/2015	19.5	20.7	Tropical storm
Talim	17-18/09/2017	26.7	22.5	Severe tropical storm
Cimaron	23-24/08/2018	32.9	27.1	Typhoon
Soulik	24-25/08/2018	23.1	21.0	Tropical storm
Jebi	04/09/2018	41.1	24.5	Typhoon

Table S2. Generalized additive models predicting flight direction relative to the storm track (model 1) and distance to land (model 2). From left to right: model terms indicating the base dimension (k) when this differed from the default value, effective degrees of freedom (edf) and p-values.

	Term	**Edf**	**P-value**
Model 1: Flight direction relative to storm Link: gaussian LogLik: -3727.715 (df= 42.99)	ti(Bird position, k=37)	16.0	< 0.001 ***
	ti(wind speed)	1.0	< 0.01 **
	ti(wind direction, wind speed)	7.5	< 0.001 ***
	ti(Bird position, wind speed)	8.1	< 0.001 ***
	s(Storm ID)	2.5	< 0.001 ***
Model 2: Flight direction relative to land Link: gaussian LogLik: -3759.483 (df= 24.28)	ti (bird- land distance)	1.7	n.s
	ti(wind speed)	2.5	< 0.005 *
	ti(wind direction)	1.7	< 0.005 *
	ti(wind direction, wind speed)	5.9	< 0.001 ***
	ti(Bird position, wind speed)	2.9	< 0.005 *
	ti(bird – land distance, wind speed)	3.4	<0.05 *
	s(Storm ID)	2.9	< 0.001 ***
	AIC	**Adj. R^2**	**Dev. explained**
Model 1	7541.4	0.22	26.6 %
Model 2	7568.7	0.18	21.4 %

Table S3. Results of ten agent-based simulations operating in five major storms. From left to right: storm name, mean wind speed at agent locations, percentage of agents flown, percentage and number of agents wrecked from the number of agents flown, percentage and number of agents flown with mean flight direction in relation to a storm ≤ 70^{o}, percentage and number of agents reaching ≤ 30 and ≤ 60 km of the eye, from the agents capable of reaching the eye that were not wrecked. Overall, agents showed an attraction to storms that came within 60 – 170 km of the core foraging area but did not respond to storms that were further away. Results are also given for a null model of random movement and a null model where agents moved at the exact same direction as wind was blowing towards.

Storm	**Mean wind speed (m s-1)**	**Flown %**	**Wrecked % (agents)**	**Towards storm % (agents)**	**Reached eye ≤ 30 km % (agents)**	**Reached eye ≤ 60 km % (agents)**
Kompasu	6.8	100	91.4 (3654)	0.1 (5)	17.5 (60)	55.2(158)
Wind dir.	7.7	-	47.5 (1902)	3.5 (141)	0 (0)	7.9 (166)
random	9.0	-	34.8 (1393)	5.4 (217)	0.9 (11)	1.9 (41)
Goni	13.3	81.2	0.3 (9)	0 (0)	0.0 (0)	0 (0)
Wind dir.	15.5	-	0 (0)	6.0 (200)	29.2 (787)	29.2 (787)
Random	12.7	-	1.5 (47)	9.1 (285)	0 (0)	0 (0)
Talim	14.4	100	18.2 (727)	55.9 (2235)	33.9 (1093)	57.8 (1231)
Wind dir.	14.5	-	30.9 (1239)	7.7 (309)	0 (0)	2.5 (35)
Random	13.2	-	25.3 (1015)	9.5 (383)	37.2 (1088)	71.6 (1328)
Cimaron	11.5	100	3.3 (135)	39.7 (1586)	2.7 (62)	27.6 (866)
Wind dir.	9.8	-	0.05 (2)	8.1 (325)	9.0 (347)	14.7 (541)
Random	9.8	-	29.3 (1175)	6.9 (275)	2.5 (37)	5.7 (120)
Jebi	15.1	100	1.2 (48)	61.9 (2475)	0.2 (1)	43.6 (397)
Wind dir.	14.9	-	0.1 (5)	21.9 (876)	44.8 (133)	51.9 (330)
Random	15.0	-	10.3 (413)	21.3 (851)	0 (0)	13.2 (65)

Movie legends

Movie S1.

GPS tracks of streaked shearwaters during the passage of severe tropical storm Talim (black track) in 2017, animated over the wind field estimated by ERA5 reanalysis, wind speed (m s^{-1}).

Movie S2.

GPS tracks of streaked shearwaters during the passage of typhoon Cimaron, tropical storm Soulik and typhoon Jebi (black tracks in order of appearance) in 2018, animated over the wind field estimated by ERA5 reanalysis, wind speed (m s^{-1}).

Movie S3.

The tracks of 100 agents, programmed with the output of GAMM model 1, moving in the wind field in the Sea of Japan during the passage of severe tropical storm Kompasu (black track) in 2010.

Movie S4.

The tracks of 100 agents, programmed with the output of GAMM model 1, moving in the wind field in the Sea of Japan during the passage of typhoon Goni (black track) in 2015.

Movie S5.

The tracks of 100 agents, programmed with the output of GAMM model 1, moving in the wind field in the Sea of Japan during the passage of severe tropical storm Talim (black track) in 2017.

Movie S6.

The tracks of 100 agents, programmed with the output of GAMM model 1, moving in the wind field in the Sea of Japan during the passage of typhoon Cimaron (black track) in 2018.

Movie S7.

The tracks of 100 agents, programmed with the output of GAMM model 1, moving in the wind field in the Sea of Japan during the passage of typhoon Jebi (black track) in 2018.

Chapter 5: Airflow modelling predicts seabird breeding habitat across islands.

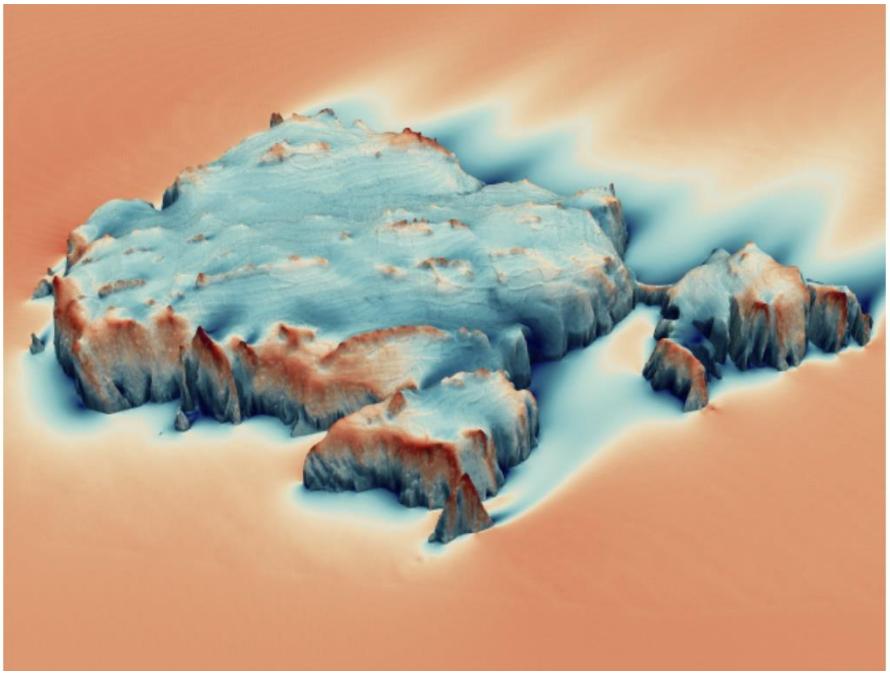

The content of this chapter has been published in the journal "Ecography" as:

Lempidakis, E., Ross, A.N., Börger, L. and Shepard, E.L., 2022. Airflow modelling predicts seabird breeding habitat across islands. *Ecography*, *2022*(1).

Abstract

Wind is fundamentally related to shelter and flight performance: two factors that are critical for birds at their nest sites. Despite this, airflows have never been fully integrated into models of breeding habitat selection, even for well-studied seabirds. Here we use computational fluid dynamics to provide the first assessment of whether flow characteristics (including wind speed and turbulence) predict the distribution of seabird colonies, taking common guillemots (*Uria aalge*) breeding on Skomer island as our study system. This demonstrates that occupancy is driven by the need to shelter from both wind and rain/ wave action, rather than airflow characteristics alone. Models of airflows and cliff orientation both performed well in predicting high quality habitat in our study site, identifying 80% of colonies and 93% of avoided sites, as well as 73% of the largest colonies on a neighbouring island. This suggests generality in the mechanisms driving breeding distributions, and provides an approach for identifying habitat for seabird reintroductions considering current and projected wind speeds and directions.

Introduction

Reproductive success is closely linked to the physical characteristics of breeding sites in many taxa (Birkhead et al., 1985, Harris et al., 1997). In colonial animals, breeding sites can represent the nexus of reproductive activity for tens of thousands of individuals (Buckley and Buckley, 1980). There is therefore a clear need to establish what drives colony location in order to identify the availability of breeding habitat, and predict how areas differ in quality, now and in the future (Frid and Dill, 2002, Parmesan and Yohe, 2003, Jetz et al., 2007, Sorte and III, 2007, Dunlop, 2009, Chambers et al., 2011, Rushing et al., 2020).

Over 95% of seabirds are colonial breeders (Rolland et al., 1998). Seabirds are also more at risk than other comparable groups of birds, with widespread decline in populations due to commercial fisheries, pollution, habitat change and the introduction of invasive predators (Croxall et al., 2012). In some cases this has led to entire breeding colonies being lost (Jones et al., 2008, Brooke et al., 2018). Thus, conservation practitioners need to know where to focus restoration efforts e.g. by decoy deployment and acoustic attraction to re-seed breeding activity (Jones and Kress, 2012). This is crucial given that there will always be a fitness cost associated with breeding in sub-optimal habitat (Brown, 1969). However, while a wide range of studies have analysed breeding site characteristics in seabirds (Buckley and Buckley, 1980, Birkhead et al., 1985, Harris et al., 1997, Keslinka et al., 2019) and compared them with available habitat (Clark et al., 1983), we are unaware of any that have successfully applied predictions from one site to another (*cf.* Aarts et al., 2008). Achieving such generality and transferability is paramount for conservation success, as well as being of fundamental ecological interest.

The tendency of seabirds to breed on offshore islands and/ or coastal cliffs has been attributed to the need to reduce exposure to terrestrial predators and be close to feeding areas (Buckley and Buckley, 1980, Cody, 1969). Nonetheless, for cliff nesting species, it is clear that not all cliffs are equal, as colonies tend to be clumped, with great swathes of cliff habitat left empty (Harris et al., 1997). Indeed, cliffs should vary in their accessibility to terrestrial predators (primarily through variation in slope angle), as well as the availability of suitable breeding ledges, with species varying in their need for different ledge characteristics according to their body size and nest building habit (Birkhead et al., 1985, Squibb and Hunt Jr, 1983).

There are also compelling reasons why airflows should affect breeding habitat preferences, particularly for groups such as seabirds, which are exposed to strong flows.

Wind can affect the risk of eggs/ birds being displaced from the nest (Hamer et al., 2001), as well as influencing exposure to rain (particularly in cliff nesting species) and heat stress (through evaporative heat loss, (Oswald and Arnold, 2012)), both of which can cause mortality (Hamer et al., 2001). Wind also has a strong influence on flight capacity. In common guillemots (*Uria aalge*) and razorbills (*Alca torda*), 60% of attempts to land at their cliff nests were found to fail in a strong breeze, which may have consequences for the ability to provision chicks as well as adult energy budgets (Shepard et al., 2019). This raises the possibility that site selection might be influenced by the ability to land. Indeed, frigatebirds (*Fregata magnificens*) nest in relatively wind-still areas, despite the potential benefits of wind in aiding heat loss for this tropical species. This most likely reflects the difficulties that frigatebirds experience in flying close to the nest in high winds (Diamond, 2002). While a reduction in wind speed would be beneficial for their flight capacity, other factors may also influence landing ability, including turbulence, as this requires compensatory manoeuvring (*cf.* Cheney et al., 2020, Ravi et al., 2015). Up- or downdrafts may also be relevant, for instance, downdrafts could even facilitate landing in fast-flying birds such as guillemots, by reducing their groundspeed as they ascend to their cliff nesting sites.

Despite the potential importance of wind, there is a notable lack of information on the precise wind flow characteristics associated with colony presence and absence (though see (Burger and Lesser, 1978), which reflects the difficulties of making measurements over complex, often steep terrain. Here we use an opensource model based on computational fluid dynamics (CFD) to estimate a range of airflow characteristics that relate to shelter (including the magnitude of the wind and the horizontal component), and variables that could specifically impact landing ability (the vertical wind component, wind gusts (short peaks in wind speed) and turbulence (rapid unsteadiness in wind speed and direction) (Shepard et al., 2019). We then assess whether wind components can predict the presence and absence of common guillemots (*Uria aalge*) breeding on Skomer island, UK. Our specific objectives were to: (i) assess whether airflows associated with the prevailing wind direction predict site selection (patterns of presence and absence), and habitat quality (colony density), and then, (ii) test our model of habitat selection by predicting colony presence and absence on a neighbouring island. This test is considerably stronger than standard cross-validation, but rarely performed (Aarts et al., 2008). Finally, (iii) we run airflow simulations to quantify the wind conditions that breeding guillemots are exposed to with changes in wind direction. Overall, our approach should provide insight into the conditions birds select and avoid in the prevailing wind, and why, and the "penalty" they suffer in terms of the adverse conditions

they are exposed to if the wind direction changes, either over the short-term, or as part of larger scale climatic shifts (Young et al., 2011, Young and Ribal, 2019).

Materials and Methods

The first step in our study was to predict the distribution of guillemot colonies on Skomer Island (51° 44.271'N, 5° 17.668'W), and apply this model to predict colony occurrence on the neighbouring island of Skokholm. The distribution of guillemots on Skomer was taken from the 2015 guillemot breeding bird survey (Stubbings et al., 2015). This provides counts of breeding birds within 71 adjoining horizontal sections, with individual survey sections being delineated by topographical features. In order to assign slope angles and wind parameters to each section, the survey was digitized in ArcMap 10.5.1 (ESRI, Redlands, California), and horizontal section boundaries were mapped onto a digital elevation model (DEM) (50 cm resolution retrieved from Lle Geo-Portal http://lle.gov.wales).

Each section was then defined vertically with a minimum height of 10 m ASL to account for variation in tide height (maximum tide height ~ 5 m on the day the DEM was produced), maximum wave height (taken to be 3 m), and the minimum distance above water that birds tend to nest, taken as 2 metres (Harris et al., 1997). The maximum height of each section was taken as 15 m from the top of the cliff, which was the mean upper limit of nests for three major colonies (Cole et al., 2019).

A similar approach was taken to digitize the distribution of guillemots breeding on Skokholm Island using the 2018 breeding bird survey (Brown and Eagle, 2018) (Supporting information Fig. S2A). However, because the elevation of Skokholm's cliffs is much lower, the minimum distance from the top of the cliffs, was set at 7 m (this was arrived at in consultation with the island wardens). The small proportion of occupied cliffs that did not satisfy this threshold was not mapped (~ 9% of the coastline at 7 m height). In cases where estimated bird numbers were given in relation to a single point on the map, we used a minimum section length of 30 m of coastline, unless ascribing this width to adjacent colonies would have resulted in unoccupied sections of < 30 m, in which case we assigned a section of 30-50 m in length. This approach resulted in 91 sections, with 35 being colonised (Supporting information Fig. S2B).

Modelling of wind conditions

Wind conditions were modelled using the computational fluid dynamics (CFD) package OpenFOAM (openfoam.org version 5.x). OpenFOAM is widely used for modelling

atmospheric boundary layer flows (e.g. in the wind energy industry) and has been extensively validated over a similarly steep island (Bechmann et al., 2011).

The initial coarse model domain was 5300 x 5000 x 1000 m, with a horizontal resolution of 20 m and a vertical resolution of 10 m. The bottom boundary represented the surface of the island which was taken from a DEM of Skomer with 2 m resolution (Lle Geo-Portal http://lle.gov.wales). After establishing the initial mesh, the tool snappyHexMesh in OpenFOAM was used to incorporate the DEM, refining initial mesh cells close to the surface up to 3 times and performing standard mesh quality tests and corrections (https://cfd.direct/openfoam/user-guide/v6-snappyhexmesh/). This resulted in a finer resolution close to surface of 2.5 m in the horizontal and 1.25 m in the vertical. Simulations were completed when convergence was achieved using a steady-state incompressible solver with a k-ε turbulence closure scheme (using standard settings).

Simulations of the wind over Skomer and Skokholm were run for the prevailing SW direction (see Supporting information Fig. S3, Table S1 for summary wind data) assuming that birds would be most likely to select breeding habitat in relation to these conditions. Wind simulations were also run for NW, NE and SE winds around Skomer in order to assess the penalty that birds face when the wind direction changes. The initial wind speed was set to 10 m s^{-1} at 20 m height. The following airflow characteristics were extracted from the model output at 2 m normal to the ground surface (this height was selected to estimate the airflow conditions that birds would be exposed to close to their breeding cliffs): The two horizontal and vertical wind components (U_0, U_1 and U_2 respectively), mean wind speed (MeanU), turbulent kinetic energy (TKE, a measure of the absolute wind unsteadiness), dynamic pressure (P, given relative to the background hydrostatic pressure set in the simulations), kinematic viscosity (Nut) of the air medium and turbulence dissipation rate (ε). These outputs were further used to estimate horizontal wind speed; wind gusts and turbulence intensity (TI, the ratio of turbulence to wind speed, indicating the importance of wind variability with respect to the mean flow strength).

Each of the four OpenFOAM simulations (i.e. for NW, NE, SE and SW wind directions) resulted in 76,908 data points across all cliff sections. Each airflow variable was then reduced to the following summary statistics within each 3d section area; median, interquartile range (IQR) and skewness. Median statistics were used to identify the strength of each wind parameter within a section. The IQR values identify the variability or gradient of

each wind parameter within a section. High skewness statistics for horizontal wind speed (skewed right) correspond to shelter.

Statistical analysis

The complete set of 27 airflow variables was tested for collinearity by producing a correlation hierarchy table for each initial wind condition. Highly correlated terms (Pearson correlation coefficient ≥ 0.7) were removed from the analysis, making sure that statistics from at least one airflow parameter representing either exposure, wind strength or turbulence were maintained, leading to the inclusion of 15 wind parameters. The mean slope angle per section was added to the total set, together with the logarithmic area of each section (as an offset) and parameters were standardized using the MuMin package (Barton and Barton, 2015) version 1.43.17.

We considered that it would be stretching the data to model the density or number of breeding birds as a continuous variable, particularly as the extent of each section did not correspond with the beginning or end of occupied/ unoccupied areas. We therefore ran separate models, with colony presence defined as (i) the presence of any breeding birds, (ii) the 10 largest ($n \geq 592$ individuals) or (iii) the 11 densest colonies (density ≥ 0.835 m^{-1}) (thresholds were selected by visually identifying clear breakpoints; however, we also conducted a sensitivity analysis to evaluate the robustness of our results to the choice of 'largest colonies"). For the latter two categories, areas with breeding birds that did not fall into either the largest or densest categories were excluded from the modelling. This allowed us to test what distinguishes the highest quality habitat from the lowest quality habitat (assuming these correspond to the largest/ densest areas, and areas with a complete lack of breeding birds, respectively). The excluded areas represented 23.5% and 27.7% of all breeding birds for the largest and densest classifications and resulted in trained datasets of 43 and 44 sections for the largest and densest datasets.

A two-step approach was used to build the global model and identify the final, best-fitting models. First, to reduce the large number of covariates (as compared to the number of data points), a random forest classifier was fitted, using the package randomForest (Liaw and Wiener, 2002) version 4.6.14. The 10 most important terms were then included to build the global logistic regression model. This variable set was further simplified using the dredge function (MuMin package (Barton and Barton, 2015), to perform stepwise Bayesian information criterion (BIC) selection, penalising for model size to highlight the terms with the strongest effects. In the case of the models for largest and densest colonies in a NW wind, the

number of terms in dredge had to be gradually reduced to eight and seven respectively, to prevent fitting models with probabilities of zero and one. The simplest model among the top models with a difference in BIC ≤ 2 was selected as the best final model. This was compared to a model of mean slope and orientation, where sections were defined as either windward or leeward with respect to the prevailing SW wind. The same method of model selection was used to identify the top simplest model across the combinations of these two parameters. In order to interpret the output of the orientation model we also estimated the total mean solar radiation (W h m^2) during the breeding season in 2015 using ArcMap 10.7 (assuming generally clear sky).

The final models were assessed for spatial autocorrelation using the DHARMa package (Hartig 2020) version 0.3.3 and for goodness of fit using the McFadden (McFadden, 1973) pseudo R^2. Values between 0.2 – 0.4 were considered as very satisfactory (Naugle et al. 1999). Model performance was also evaluated in terms of overall accuracy (OA); true skill statistic (TSS), sensitivity and specificity (Allouche et al., 2006, Börger and Nudds, 2014). The effect size of each predictor included in the final model was determined by computing the odds ratio.

The previous steps were repeated for all four initial wind directions, with three logistic regression models of colony presence/absence implemented per direction, in order to identify links between wind and slope that were robust to different colony definitions.

Finally, to predict the distribution of the largest colonies on Skokholm (eleven colonies with n≥ 146 individuals), we applied the model of the 10 largest colonies on Skomer, using conditions experienced in the prevailing SW wind, and converting the predicted odds into presence/absence by selecting the cut-off value which maximises the true skill statistic (Allouche et al., 2006, Börger and Nudds, 2014).

All statistical analyses were conducted in in R (Team, 2020) version 3.6.3 and RStudio (Team, 2015) version 1.1.463.

Results

Predicting colony distribution on Skomer island

Wilcoxon rank sum tests for all colony classifications revealed statistically different slope angles between colonies and non-colonies on Skomer Island (taking presence as any positive count, W = 611724994, p < 2.2e-16;as the largest colonies, W = 199340779, p < 2.2e-16; or the densest, W = 71820756, p < 2.2e-16). Unoccupied sections were generally less steep than

occupied sections (median slope angles 45º and 51º respectively) and the densest and largest colonies were associated with the steepest cliffs (median= 68.5º, Supporting information Fig. S4B). Slope angle varied with cliff orientation, with mean slope angle being lowest for cliffs with S and SE orientations. Cliffs facing SW have relatively high mean slope angles (Supporting information Fig. S4A). Despite this, most occupied sections were orientated away from the prevailing SW wind (Fig. 1).

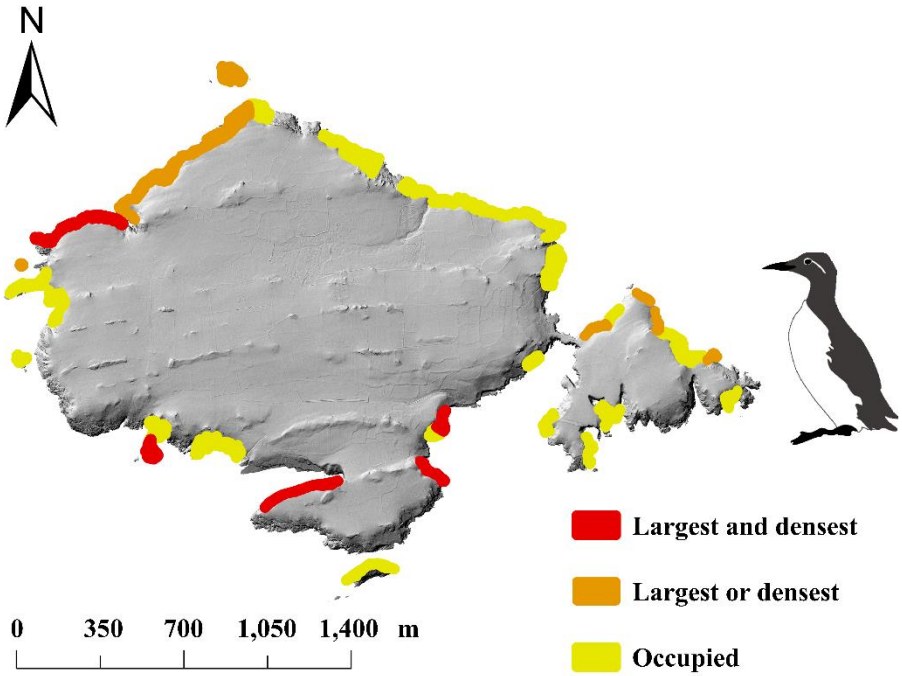

Figure 1. The guillemot survey sections on the cliffs of Skomer and the distribution of breeding guillemots. Areas classified as both densest and largest are indicated in red (n = 7 sections). Areas that were identified as either among the largest (n = 3) or densest (n = 4) are indicated in orange respectively. Residual occupied areas are indicated in yellow.

Colony presence and absence on Skomer was predicted well by wind variables and slope angle, with the simplest top model correctly identifying 80% of the colonies and 93% of avoided sites for the prevailing SW wind, where presence was taken as the 10 largest colonies (see Table 1 for the full list of model outputs). While mean slope angle was included in two of three models for SW, NW and NE wind directions, airflow parameters always had a higher effect size (Supporting information Table S2). A sensitivity analysis confirmed the variables in the final models were largely consistent, irrespective of whether colony presence was taken as the 11, 12, 13, 14 or 15 largest colonies (Supporting information Tables S3 – S5).

A narrow set of airflow parameters was identified as significant in predicting colony presence across wind directions and there was broad agreement between the airflow characteristics identified for any wind direction, irrespective of the way colonies were classified (Table 1). Pressure statistics were included in all SW models, with colonies having a lower median pressure and pressure gradient (Table 1). These variables are both linked to lower exposure (Fig. 2, Supporting information Fig. S5), a relationship that was confirmed by a simple model predicting presence according to whether sections had a windward or leeward orientation in relation to the prevailing SW wind and slope angle. This model of orientation and slope angle performed similarly to the model with pressure and slope for the largest colonies (Supporting information Table S6). Given the importance of exposure in determining colony presence, it was surprising that no wind speed parameters were included in the simplest top models for SW winds.

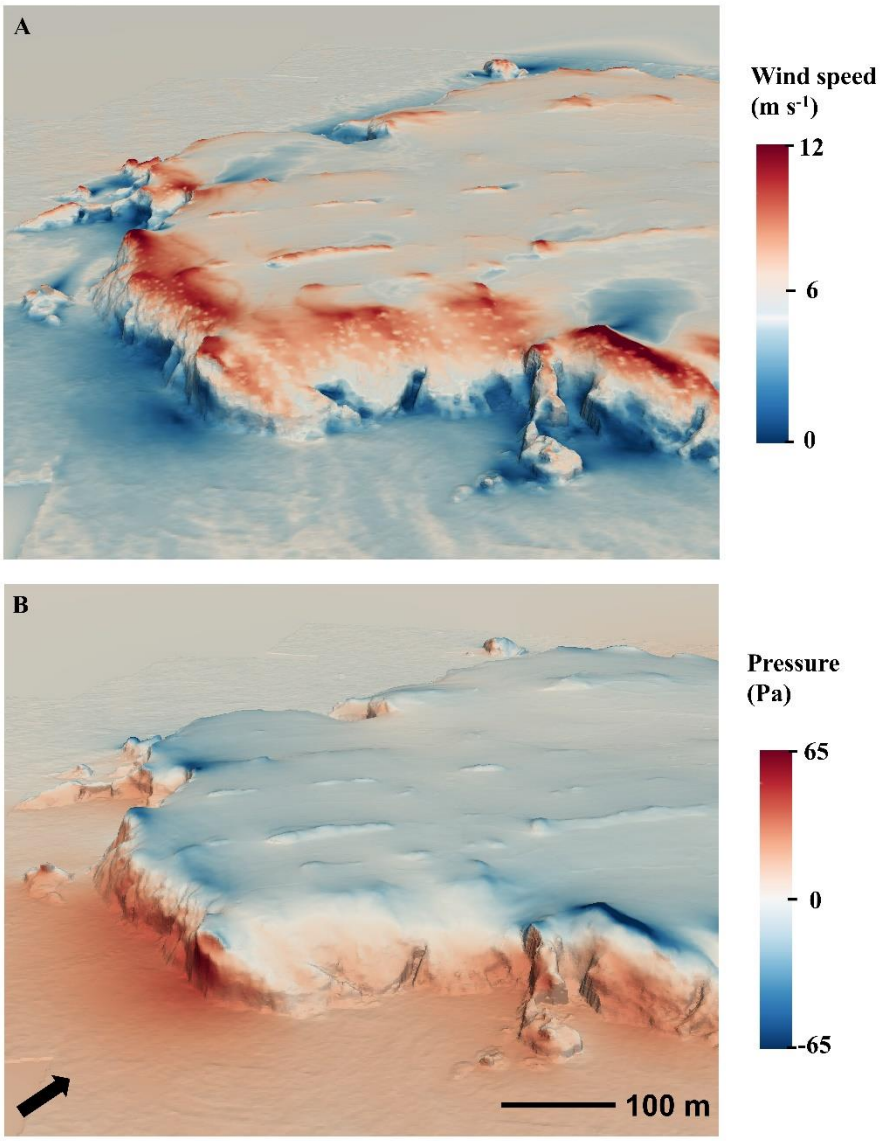

Figure 2. The OpenFoam model output of A) wind speed and B) pressure, over a windward cliff ("Skomer head") with SW wind (denoted with a black arrow). In the lower parts of the cliffs, the wind is blocked, resulting in high pressure regions where flow is decelerated. Closer to the top (55 - 60 m ASL), the flow is accelerated, generating areas of low pressure. This results in highly variable pressure values on windward cliffs. On leeward cliffs, flow separation occurs, viscous forces take over, and areas of consistently low pressure are generated that are not associated with high wind speeds.

Colonies were associated with higher turbulence compared to unoccupied sites, particularly in NW and NE winds (Table 1). In NE winds, colonies experienced both higher wind speeds (Fig. 3) (positive horizontal median, for any bird presence and negative horizontal skewness for the largest/ densest colonies) and higher turbulence (here TKE

estimates in the largest/ densest colonies). In fact, airflow models of colony location performed well across all modelled wind directions except for SE winds, indicating that colonies are characterised by particular sets of flow characteristics in most scenarios. For SE winds only one colony classification yielded a reasonable model fit (McFadden[41] $R^2 \geq 0.2$, table 1) and here colony presence was predicted by slope angle alone (Table 1).

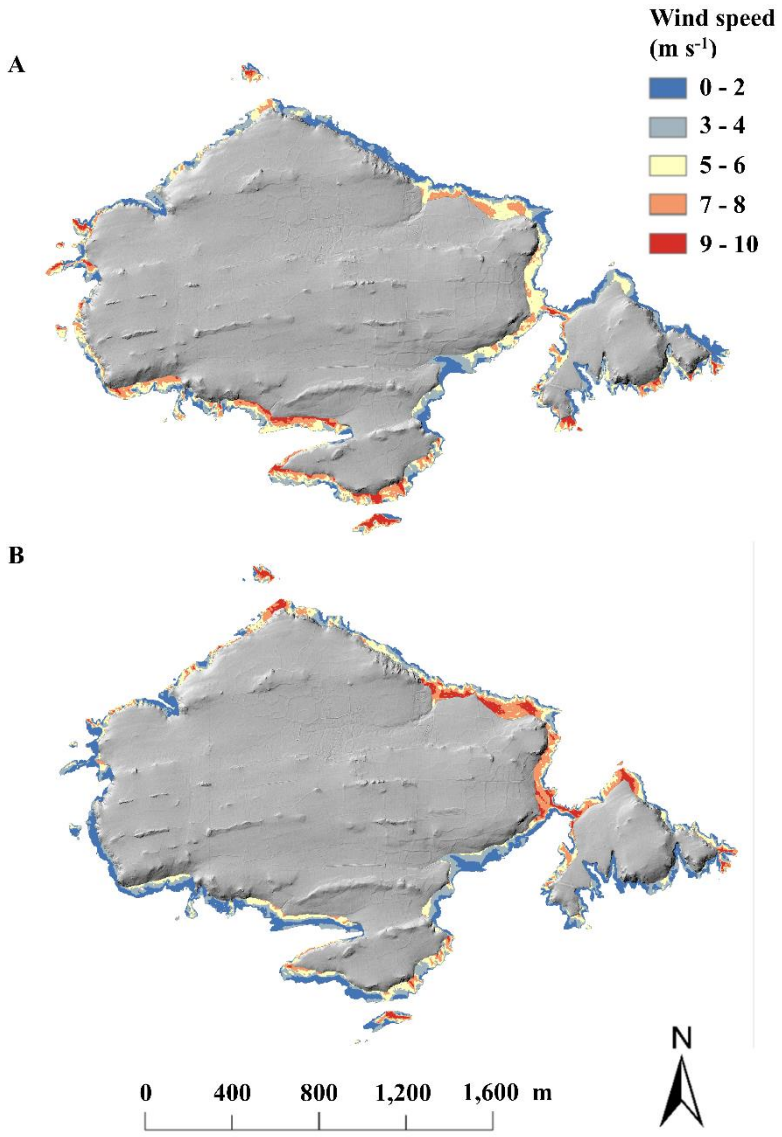

Figure 3. Modelled horizontal wind speeds on the cliffs of Skomer. Modelled wind speeds under A) a SW and B) a NE wind direction. Mean wind speeds were reduced on leeward cliffs, increased on windward cliffs and reached their highest estimates at the crests, as expected. Winds were modelled 2 m normal to the surface and the mapped area was constrained by the 4 m and 40 m elevation contours.

Across the different colony classifications, the pseudo R^2 was lowest in models of any occupancy (SW 0.28; NW 0.24, SE 0.12, NE 0.38) compared to those predicting the 10 largest colonies (SW 0.59; NW 0.58, SE 0.32, NE 0.74) or the 11 densest (SW 0.17; NW 0.40, SE 0.15, NE 0.67) (Table 1, Table S6). The overall accuracy and true skill statistics followed the same general trend, being highest for the 10 largest colonies (Table 1, Table S6). The sensitivity tended to be somewhat lower than specificity for any presence (sensitivity: SW 0.63; NW 1.00, SE 0.21, NE 0.60 and specificity: SW 0.69; NW 0.21, SE 0.96, NE 0.84), but increased for the largest and densest colonies indicating a better ability to predict true presence compared to true absence in these cases.

Table 1. The outputs of logistic regression models predicting colony presence for four different initial wind directions. Three summary statistics were modelled for each section and wind property: "skewness" (Skew); "median" (Med) and "interquartile range" (IQR). In addition, three colony classifications were tested, where colony presence was taken as i) any positive count, ii) the 10 largest colonies and iii) the 11 densest colonies. Shelter from higher wind speeds is associated with low pressure (PMed) and reduced pressure range (PIQR). Exposure to higher wind speeds is highlighted by negative and decreased skewness in horizontal wind speed. Higher turbulence is indicated by increased TKE median and low TKE skewness. TI terms follow the same pattern. Significance is indicated according to p-value: $p< 0.001$ (***), $p< 0.01$ (**), $p< 0.005$ (*), and model predictors are listed in order of descending effect size (Supporting information Table S2).

	SW				NW				SE				NE			
Colony definition	**Term**	**P-value / Significance**		**Est.**	**Term**	**P-value / Significance**		**Est.**	**Term**	**P-value / Significance**		**Est.**	**Term**	**P-value / Significance**		**Est.**
Any count	PMedian	< 0.001	***	-2.27	TISkew	< 0.01	**	-1.94	TKEIQR	< 0.05	*	-1.36	TKESkew	< 0.001	***	-4.39
	TISkew	< 0.05	*	-1.54	TKESkew	< 0.01	**	-2.27	MeanSlope	< 0.01	**	+1.88	MeanSlope	< 0.001	***	+2.80
	MeanSlope	< 0.05	*	+1.49									HorizontalMedian	< 0.01	**	+2.12
10 Largest	PIQR	< 0.05	*	-6.23	TKESkew	< 0.01	**	-5.96	MeanSlope	< 0.001	***	+3.59	TKEIQR	< 0.01	**	+7.75
	HorizontalIQR	< 0.01	**	+5.65	MeanSlope	< 0.01	**	+2.56					HorizontalSkew	< 0.05	*	-7.26
	MeanSlope	< 0.001	***	+4.08									MeanSlope	< 0.01	**	+4.53
11 Densest	PMedian	< 0.05	*	-2.50	TKESkew	< 0.05	*	-4.10	MeanSlope	< 0.05	*	+1.95	TKEMedian	< 0.01	**	+8.27
					MeanSlope	< 0.05	*	+1.92					U_2Median	< 0.01	**	-4.23
													HorizontalSkew	< 0.05	*	-3.34
McFadden pseudo R^2 – OA/ TSS/ Sensitivity/ Specificity																
Any count	0.28 – 0.66/ 0.32/ 0.63/ 0.69				0.24 – 0.63/ 0.21/ 1.00/ 0.21				0.12 – 0.56/ 0.18/ 0.21/ 0.96				0.38 – 0.71/ 0.45/ 0.60/ 0.84			
10 Largest	0.59 – 0.90/ 0.73/ 0.80/ 0.93				0.58 – 0.86/ 0.81/ 1.00/ 0.81				0.32 – 0.86/ 0.60/ 0.70/ 0.90				0.74 – 0.97/ 0.90/ 0.90/ 1.00			
11 Densest	0.17 – 0.65/ 0.48/ 0.90/ 0.57				0.40 – 0.84/ 0.78/ 1.00/ 0.78				0.15 – 0.72/ 0.51/ 0.81/ 0.69				0.67 – 0.88/ 0.84/ 1.00/ 0.84			

Predicting colony distribution on Skokholm

The model predicting the largest colonies on Skomer for SW winds also performed well when applied to the island of Skokholm (Fig. 4), correctly predicting the distribution of ~ 73% of the largest colonies (eight out of eleven), and ~ 63% of unoccupied cliff sections (35 out of 56), which corresponds to ~ 80% of the total unoccupied area (60,863 m^2 of 76,259 m^2). Model performance, although lower than the models on Skomer, was satisfactory with an overall accuracy of 0.64 and TSS of 0.35. The model predicting the largest guillemot colonies on Skomer according to orientation and slope performed better than the airflow model when applied to Skokholm, correctly predicting all the largest colonies, and ~ 71% (40 of the 56) unoccupied sections, with an overall accuracy of 0.76 and TSS of 0.71.

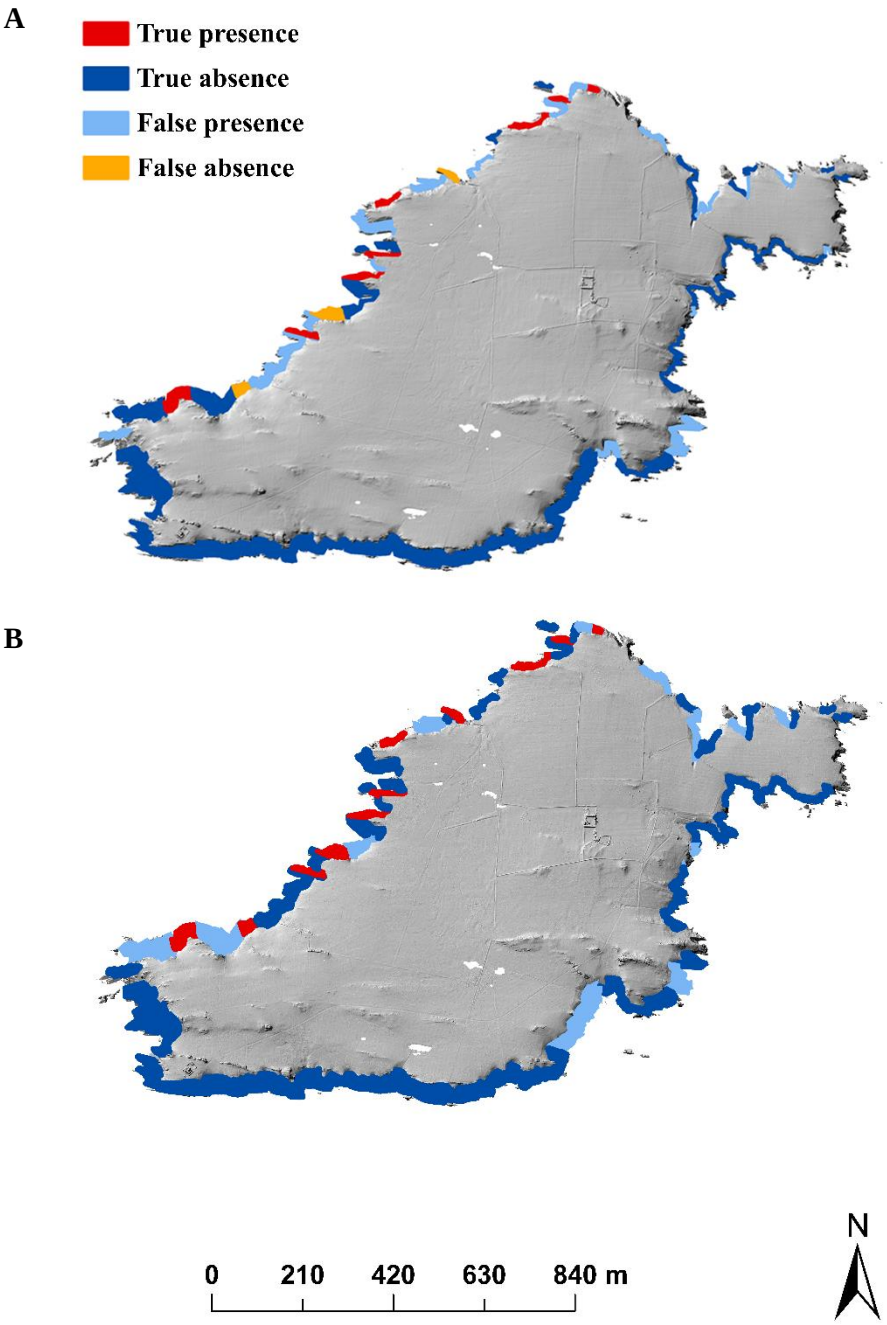

Figure 4. Predicted distribution of guillemot colonies on Skokholm. A) distribution predicted using the model of the largest colonies on Skomer and the wind field on Skokholm as predicted under the prevailing SW wind and B) distribution predicted using the mean cliff slope and orientation in relation to the SW wind.

Discussion

Wind regimes are changing, in terms of the mean strength, and the frequency of extreme weather events (Young et al., 2011, Young and Ribal, 2019). Yet most research on how wind affects seabirds has focused on their at-sea behaviour (though see (Weimerskirch et al., 2012, Schrimpf and Lynch, 2020). We modelled the airflows around our study site to test the role of different wind characteristics in breeding habitat selection, and showed that a simple model of airflows and slope angle performed very well for common guillemots, even when applied to the separate island of Skokholm. Both this approach and a model of cliff orientation showed that birds select sheltered, leeward sites. Indeed, a model of orientation and slope performed better in predicting the distribution of breeding birds on Skokholm. Nonetheless, the orientation model cannot tell us what birds are sheltering from. We demonstrate how airflow modelling can provide mechanistic insight into the factors driving habitat selection, as well as quantify the airflow conditions that birds are exposed to in different wind directions.

While colony presence on Skomer was predicted by low exposure to the prevailing SW wind, surprisingly, it was not predicted by low wind speed. Instead, areas of low pressure and low pressure variability were powerful predictors of cliff occupancy, both of which are characteristic of sheltered areas. Birds are less likely to be responding to the pressure values directly, than the exposure that they are correlated with, because the absolute difference in pressure values between occupied and unoccupied sites is equivalent to the changes experienced over the diurnal cycle.

The absence of wind speed from models of guillemot distributions can be explained by "orographic blocking", a process whereby windward cliffs can block the oncoming flow, with the blocking effect increasing with cliff height and slope. This produces low wind speeds over large parts of windward cliffs, bar the top where flow is accelerated (Fig 2, Supporting information Fig. S5). Low wind speeds therefore occur in both leeward and windward sites. The fact that birds avoid the latter, even though they tend to occur on suitably steep slopes, suggests that shelter from rain (Cheney et al., 2020), and/ or wave action during storms, is at least as important as low wind speed in determining site use (the former is much more frequent in the breeding season, (Newell et al., 2015)). Therefore, while the ability to fly, and specifically to land, at the nesting site may affect habitat selection, it is also influenced by the need to shelter young from rain, as well as storm surges. Nevertheless, flight capacity may be most important for species such as large albatrosses, which require relatively high winds to take-off and

therefore may be constrained to nest in exposed areas, despite the intuitive benefits of shelter for chicks across species in temperate or cold climates.

Heat stress is an important determinant of chick survival in some systems (Oswald et al., 2008), but it seems unlikely to be the primary driver of habitat selection here, as while occupied cliffs tend to experience lower solar radiation than unoccupied sites, three of the largest and four of the densest colonies on Skomer still experience high degrees of insolation (Supporting information Fig. S6).

The fact that our models performed better in correctly predicting the largest/ densest colonies, compared to the presence of any breeding birds, suggests that they work best in predicting high quality habitat. Previous studies have shown that breeding success increases with the density of breeding pairs (Birkhead, 1977, Harris et al., 1997). Areas that can support larger numbers are therefore of higher quality. Such areas have previously been described in terms of the number of walls, slope and width of the ledge where the egg was incubated, and distance from the top of the cliff (Birkhead et al., 1985, Harris et al., 1997). The ability to predict high quality breeding habitat without such fine-scale topographical information is advantageous, as it allows habitat quality to be predicted in remote and inaccessible sites. Our models perform extremely well even with limited topographical information, but the addition of ledge width and length could potentially improve them further. However, acquisition of such information would require extensive surveys of entire islands, occupied and unoccupied areas (DSMs do not allow the identification of ledges with confidence). Our models confirm the value of steep slopes to guillemots, which offer the possibility of breeding in high densities with better protection from predators (Birkhead et al., 2018), as well as easier access to the sea when chicks jump from their nests (Berger, 2008, Gilchrist and Gaston, 1997). Nonetheless, steep cliffs with a south-westerly orientation are avoided, even though they are widely available.

Our model may be more accurate than the frequency of false positives suggests, as cliffs that are currently unoccupied may still offer suitable habitat that only becomes used when existing sites reach full capacity. Indeed, photographs of the breeding cliffs on Skomer from the 1930s provide evidence that numbers were much higher historically (Harris, 1991), and whole island counts undertaken since 1963 demonstrate that numbers have been increasing since then (Meade et al., 2013). Sites identified as “false positives”, therefore represent potentially high quality habitat that could be suitable for re-establishing breeding colonies in systems where breeding activity occurs in a fraction of the former range. Similarly, our method could be used to

model the specific wind strengths that areas are exposed to in storm conditions in systems where that can affect breeding success (Newell et al., 2015). Finally, in cases where populations are increasing, our approach could be extended to see whether airflow characteristics can predict colony growth rates, or areas most likely to be expanded into.

While guillemots preferentially breed in areas that are not exposed to the prevailing wind, they cannot shelter from all wind directions. Winds diametrically opposed to the prevailing direction (here NE winds) will be problematic for any species seeking sheltered sites. The penalty of exposure to NE winds for the 10 largest colonies on Skomer was a ~10% increase in mean wind speed compared to the same at-sea wind speeds from the SW. How this might impact birds will vary with the magnitude of the wind when it comes from a different direction. Nonetheless, our results highlight that colonies experience increased exposure from changes in wind direction, independent of wind speed. Increases in wind speed, as already observed in the North Atlantic and other areas (Young et al., 2011, Young and Ribal, 2019), should therefore be most detrimental at the nest when accompanied by a change in wind direction (Weimerskirch et al., 2012).

Most studies on the potential effects of climate change on wind have mainly focused on changes in storm frequency and intensity and in mean wind strength (Young et al., 2011, Young and Ribal, 2019), while changes in wind direction have received far less attention (but see Beniston et al., 2007, Moemken et al., 2018). As the distribution of breeding colonies in this study depends on the wind direction with the highest storm frequency changes in wind direction (Beniston et al., 2007, Blennow and Olofsson, 2008), whether these result to a new most frequent storm direction or to a more evenly spread directional distribution, could consequently increase the vulnerability of colonies to storms surges. This could potentially lead to a need for distributional shifts, as the suitability of cliffs that are now selected or avoided could change, with unknown pressure on interspecies competition However, in this study it is hard to assess whether the most frequent wind direction or the prevailing wind direction is more important as these coincide on Skomer and Skokholm.

A further challenge potentially facing birds on Skomer in NE and NW winds is increased turbulence. The absolute levels of turbulence that birds experience in SW winds are low because the wind speeds themselves are low. However, in NE winds of the same magnitude, birds experience both stronger winds and increased turbulence. Disturbed wind fields are known to have a critical impact on the safety of aircraft landings, but almost nothing is known about how

turbulence affects landing in birds (*cf.* Chang et al., 2016). Nonetheless, it seems likely that this will only make landing more difficult, resulting in more aborted attempts and higher associated costs, particularly in species such as guillemots with low manoeuvrability (Shepard et al., 2019).

Overall therefore, our results show that CFD can be used to predict occupancy directly, or combined with other approaches, such as the use of orientation, or wind fetch (Schrimpf and Lynch, 2020), to provide insight into the mechanisms underpinning habitat selection. The approach we have developed in this study is therefore likely to be applicable to a range of seabirds, in terms of assessing drivers of habitat selection and the trade-offs that some animals face. Indeed, CFD is particularly well-suited to modelling habitat selection in seabirds, as marine and coastal environments experience some of the most extreme wind conditions (Wiley and Wunderle, 1993), and wind fields also tend to be more uniform ahead of islands. Although CFD models tend to be computationally expensive, they are widely used, with many open access platforms available and can be run on personal computers (depending on the area size and resolution). Our approach can therefore easily be replicated with even basic knowledge of GIS and remote sensing, in combination with broadly available survey data. A key future challenge will be to test this approach over larger areas. Combining airflow modelling with data on breeding success in a range of conditions (*cf.* Cleeland et al., 2020), will also provide new mechanistic insight into the basis for habitat selection and how global change may impact birds at their nesting sites.

References

Aarts, G., MacKenzie, M., McConnell, B., Fedak, M. & Matthiopoulos, J. 2008. Estimating space-use and habitat preference from wildlife telemetry data. *Ecography,* 31**,** 140-160.

Allouche, O., Tsoar, A. & Kadmon, R. 2006. Assessing the accuracy of species distribution models: prevalence, kappa and the true skill statistic (TSS). *Journal of applied ecology,* 43**,** 1223-1232.

Barton, K. & Barton, M. K. 2015. Package 'MuMIn'. *Version,* 1**,** 18.

Bechmann, A., Sørensen, N. N., Berg, J., Mann, J. & Réthoré, P.-E. 2011. The Bolund experiment, part II: blind comparison of microscale flow models. *Boundary-Layer Meteorology,* 141**,** 245.

Beniston, M., Stephenson, D. B., Christensen, O. B., Ferro, C. A., Frei, C., Goyette, S., Halsnaes, K., Holt, T., Jylhä, K. & Koffi, B. 2007. Future extreme events in European climate: an exploration of regional climate model projections. *Climatic change,* 81**,** 71-95.

Berger, U. 2008. Tissue distribution of perfluorinated surfactants in common guillemot (Uria aalge) from the Baltic Sea. *Environmental science & technology,* 42**,** 5879-5884.

Birkhead, T., Greene, E., Biggins, J. & Nettleship, D. 1985. Breeding site characteristics and breeding success in Thick-billed Murres. *Canadian Journal of Zoology,* 63**,** 1880-1884.

Birkhead, T. R. 1977. The effect of habitat and density on breeding success in the common guillemot (Uria aalge). *The Journal of Animal Ecology***,** 751-764.

Birkhead, T. R., Thompson, J. E. & Montgomerie, R. 2018. The pyriform egg of the Common Murre (Uria aalge) is more stable on sloping surfaces. *The Auk: Ornithological Advances,* 135**,** 1020-1032.

Blennow, K. & Olofsson, E. 2008. The probability of wind damage in forestry under a changed wind climate. *Climatic Change,* 87**,** 347-360.

Börger, L. & Nudds, T. D. 2014. Fire, humans, and climate: modeling distribution dynamics of boreal forest waterbirds. *Ecological Applications,* 24**,** 121-141.

Brooke, M. d. L., Bonnaud, E., Dilley, B., Flint, E., Holmes, N., Jones, H., Provost, P., Rocamora, G., Ryan, P. & Surman, C. 2018. Seabird population changes following mammal eradications on islands. *Animal Conservation,* 21**,** 3-12.

Brown, J. L. 1969. Territorial behavior and population regulation in birds: a review and re-evaluation. *The Wilson Bulletin***,** 293-329.

Brown, R. & Eagle, G. 2018. Skokholm Seabird Report 2018.

Buckley, F. G. & Buckley, P. A. 1980. Habitat selection and marine birds. *Behavior of marine animals.* Springer.

Burger, J. & Lesser, F. 1978. Selection of colony sites and nest sites by common terns *Sterna Hirundo* in ocean county, New Jersey. *Ibis,* 120**,** 433-449.

Chambers, L. E., Devney, C. A., Congdon, B. C., Dunlop, N., Woehler, E. J. & Dann, P. 2011. Observed and predicted effects of climate on Australian seabirds. *Emu-Austral Ornithology,* 111**,** 235-251.

Chang, J. J., Crall, J. D. & Combes, S. A. 2016. Wind alters landing dynamics in bumblebees. *Journal of Experimental Biology,* 219**,** 2819-2822.

Cheney, J. A., Stevenson, J. P., Durston, N. E., Song, J., Usherwood, J. R., Bomphrey, R. J. & Windsor, S. P. 2020. Bird wings act as a suspension system that rejects gusts. *Proceedings of the Royal Society B,* 287**,** 20201748.

Clark, L., Ricklefs, R. E. & Schreiber, R. 1983. Nest-site selection by the Red-tailed Tropicbird. *The Auk,* 100**,** 953-959.

Cleeland, J. B., Pardo, D., Raymond, B., Terauds, A., Alderman, R., McMahon, C. R., Phillips, R. A., Lea, M.-A. & Hindell, M. A. 2020. Introduced species and extreme weather as key drivers of reproductive output in three sympatric albatrosses. *Scientific reports,* 10**,** 1-11.

Cody, M. 1969. Ecological Adaptations for Breeding in Birds. Davi Lack. Methuen, London, 1968 (U. S. distributor, Barnes and Noble, New York). xii + 409 pp., illus. $15. *Science,* 163**,** 1185-1187.

Cole, E.-L., Waggitt, J. J., Hedenstrom, A., Piano, M., Holton, M. D., BÖRGER, L. & Shepard, E. L. 2019. The Ornithodolite as a tool to quantify animal space use and habitat selection: a case study with birds diving in tidal waters. *Integrative zoology,* 14**,** 4-16.

Croxall, J. P., Butchart, S. H., Lascelles, B., Stattersfield, A. J., Sullivan, B., Symes, A. & Taylor, P. 2012. Seabird conservation status, threats and priority actions: a global assessment. *Bird Conservation International,* 22**,** 1-34.

Diamond, A. W. S. E. A. 2002. Magnificent Frigatebird (Fregata magnificens), version 2.0. *In:* Gill, A. F. P. a. F. B. (ed.) *The Birds of North America.* Ithaca, NY, USA: Cornell Lab of Ornithology.

Dunlop, J. 2009. The population dynamics of tropical seabirds establishing frontier colonies on islands off south-western Australia. *Marine Ornithology,* 37**,** 99-105.

Frid, A. & Dill, L. 2002. Human-caused disturbance stimuli as a form of predation risk. *Conservation Ecology,* 6.

Ganske, A., Tinz, B., Rosenhagen, G. & Heinrich, H. 2016. Interannual and multidecadal changes of wind speed and directions over the North Sea from climate model results. *Meteorologische Zeitschrift,* 25**,** 463-478.

Gilchrist, H. G. & Gaston, A. J. 1997. Factors affecting the success of colony departure by thick-billed murre chicks. *The Condor,* 99**,** 345-352.

Hamer, K. C., Schreiber, E. & Burger, J. 2001. Breeding biology, life histories, and life history-environment interactions in seabirds. *Biology of marine birds***,** 217-261.

Harris, M., Wanless, S., Barton, T. & Elston, D. 1997. Nest site characteristics, duration of use and breeding success in the Guillemot Uria aalge. *Ibis,* 139**,** 468-476.

Harris, M. P. 1991. Population changes in British common murres and Atlantic puffins, 1969-88.

Jetz, W., Wilcove, D. S. & Dobson, A. P. 2007. Projected impacts of climate and land-use change on the global diversity of birds. *PLoS Biol,* 5**,** e157.

Jones, H. P. & Kress, S. W. 2012. A review of the world's active seabird restoration projects. *The Journal of Wildlife Management,* 76**,** 2-9.

Jones, H. P., Tershy, B. R., Zavaleta, E. S., Croll, D. A., Keitt, B. S., Finkelstein, M. E. & Howald, G. R. 2008. Severity of the effects of invasive rats on seabirds: a global review. *Conservation Biology,* 22**,** 16-26.

Keslinka, L. K., Wojczulanis-Jakubas, K., Jakubas, D. & Neubauer, G. 2019. Determinants of the little auk (Alle alle) breeding colony location and size in W and NW coast of Spitsbergen. *PloS one,* 14**,** e0212668.

Liaw, A. & Wiener, M. 2002. Classification and regression by randomForest. *R news,* 2**,** 18-22.

McFadden, D. 1973. Conditional logit analysis of qualitative choice behavior.

Meade, J., Hatchwell, B. J., Blanchard, J. L. & Birkhead, T. R. 2013. The population increase of common guillemots Uria aalge on Skomer Island is explained by intrinsic demographic properties. *Journal of avian biology,* 44**,** 055-061.

Newell, M., Wanless, S., Harris, M. P. & Daunt, F. 2015. Effects of an extreme weather event on seabird breeding success at a North Sea colony. *Marine Ecology Progress Series,* 532**,** 257-268.

Oswald, S. A. & Arnold, J. M. 2012. Direct impacts of climatic warming on heat stress in endothermic species: seabirds as bioindicators of changing thermoregulatory constraints. *Integrative Zoology,* 7**,** 121-136.

Oswald, S. A., Bearhop, S., Furness, R. W., Huntley, B. & Hamer, K. C. 2008. Heat stress in a high-latitude seabird: effects of temperature and food supply on bathing and nest attendance of great skuas Catharacta skua. *Journal of Avian Biology,* 39**,** 163-169.

Parmesan, C. & Yohe, G. 2003. A globally coherent fingerprint of climate change impacts across natural systems. *Nature,* 421**,** 37-42.

Ravi, S., Crall, J. D., McNeilly, L., Gagliardi, S. F., Biewener, A. A. & Combes, S. A. 2015. Hummingbird flight stability and control in freestream turbulent winds. *Journal of Experimental Biology,* 218**,** 1444-1452.

Rolland, C., Danchin, E. & Fraipont, M. d. 1998. The evolution of coloniality in birds in relation to food, habitat, predation, and life-history traits: a comparative analysis. *The American Naturalist,* 151**,** 514-529.

Rushing, C. S., Royle, J. A., Ziolkowski, D. J. & Pardieck, K. L. 2020. Migratory behavior and winter geography drive differential range shifts of eastern birds in response to recent climate change. *Proceedings of the National Academy of Sciences,* 117**,** 12897-12903.

Schrimpf, M. & Lynch, H. 2020. The role of wind fetch in structuring Antarctic seabird breeding occupancy. *Ibis*.

Shepard, E., Cole, E.-L., Neate, A., Lempidakis, E. & Ross, A. 2019. Wind prevents cliff-breeding birds from accessing nests through loss of flight control. *eLife,* 8**,** e43842.

Sorte, F. A. L. & III, F. R. T. 2007. Poleward shifts in winter ranges of North American birds. *Ecology,* 88**,** 1803-1812.

Squibb, R. C. & Hunt Jr, G. L. 1983. A Comparsion of Nesting-Ledges Used by Seabirds on St. George Island. *Ecology,* 64**,** 727-734.

Stubbings, E., Büche, B., Riera, E. M., Green, R. & Wood, M. J. 2015. Seabird monitoring on Skomer Island in 2015. *Seabird monitoring on Skomer Island in 2015*.

Team, R. 2015. RStudio: Integrated Development Environment for R. Boston, MA.

Team, R. C. 2020. R: A language and environment for statistical computing.

Weimerskirch, H., Louzao, M., de Grissac, S. & Delord, K. 2012. Changes in wind pattern alter albatross distribution and life-history traits. *science,* 335**,** 211-214.

Wiley, J. W. & Wunderle, J. M. 1993. The effects of hurricanes on birds, with special reference to Caribbean islands. *Bird Conservation International,* 3**,** 319-349.

Young, I., Zieger, S. & Babanin, A. V. 2011. Global trends in wind speed and wave height. *Science,* 332**,** 451-455.

Young, I. R. & Ribal, A. 2019. Multiplatform evaluation of global trends in wind speed and wave height. *Science,* 364**,** 548-552.

Chapter 5: Supplementary Information

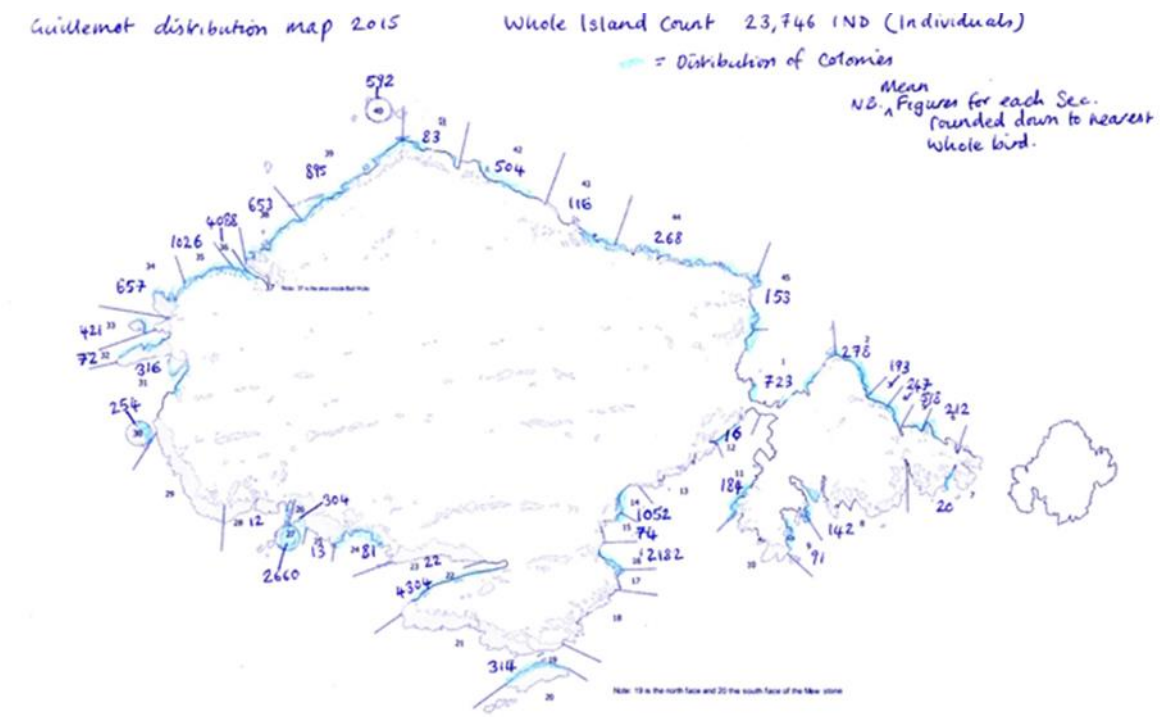

Figure S1. The guillemot survey map reproduced from the 2015 Guillemot survey data on Skomer. The 45 sections presented, were sub- divided into a total of 71 sections, with the blue shades indicating the horizontal areas that the birds are located.

A

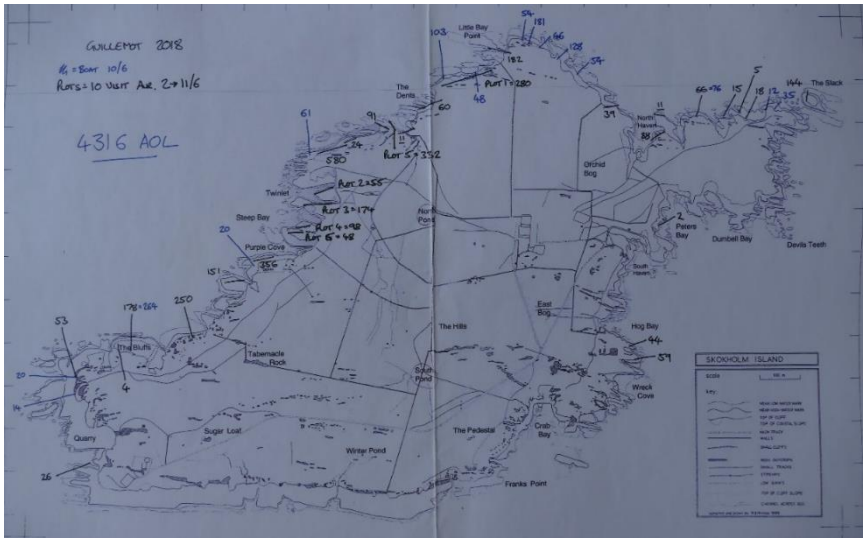

B

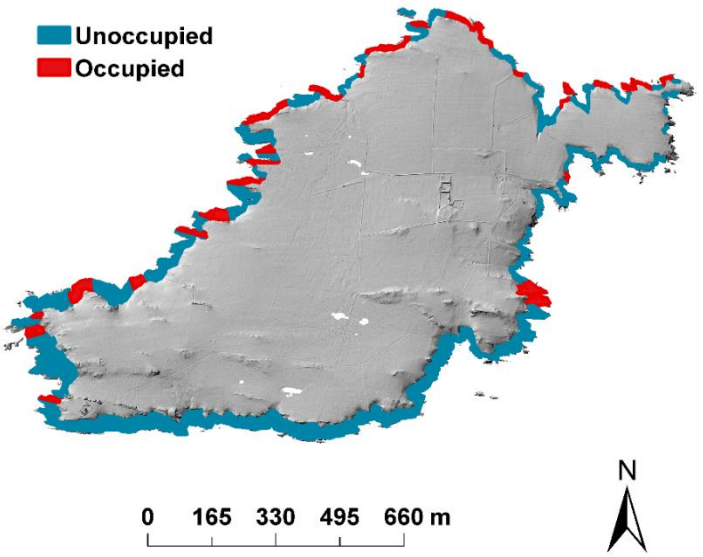

Figure S2. A) The guillemot survey map reproduced from the 2018 Guillemot survey data on Skokholm and B) the resulting digitised sections with blue indicating unoccupied and red occupied cliffs.

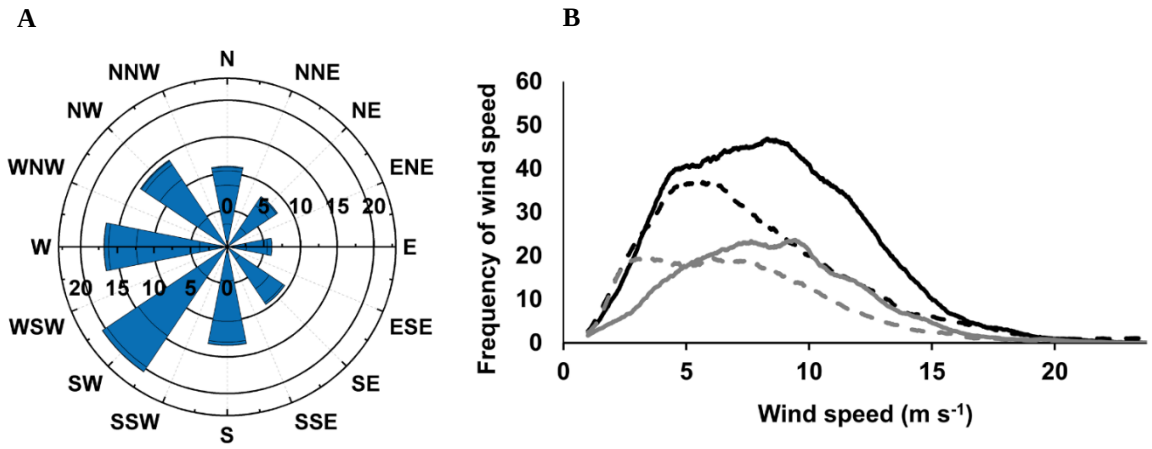

Figure S3. Wind speeds and directions during auk breeding seasons for 2007 to 2017. A) Overall frequency of wind directions on Skomer (2007-2017) , B) The frequency of average wind speed, given per 100 observations across the four different wind directions that were modelled: SW with solid black, NW with dashed black, SE with solid grey and NE with dashed grey, lines.

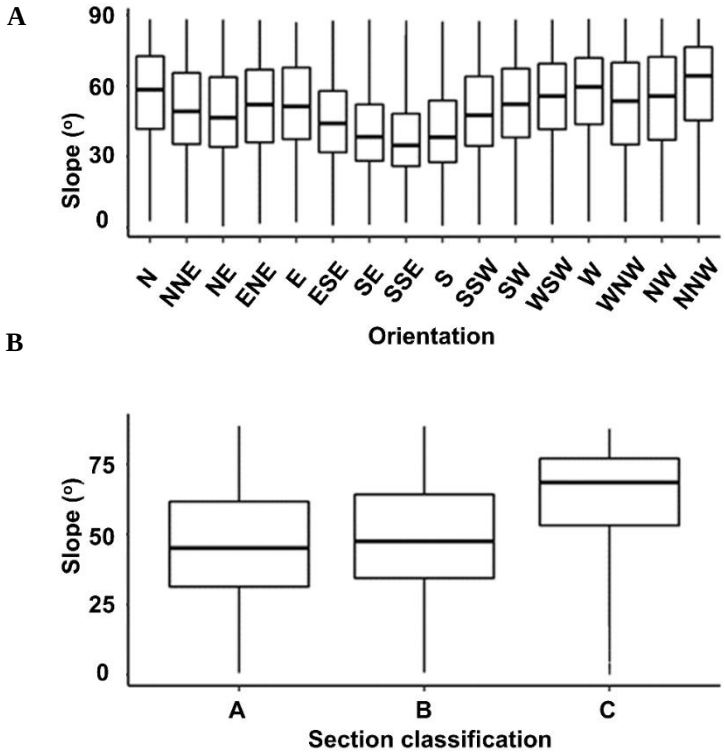

Figure S4. Slope angles selected by breeding birds in relation to those available on Skomer. A) Mean slope angle (°) according to cliff orientation (number of points per orientation bin; 2911-8718). B) Slope angle for (A) unoccupied sections (n=33, median= ~45.1°), (B) occupied but not classified as either largest or densest sections (n=31, median= ~47.5°) and (C) sections classified as both largest and densest (n=7, median= 68.5°).

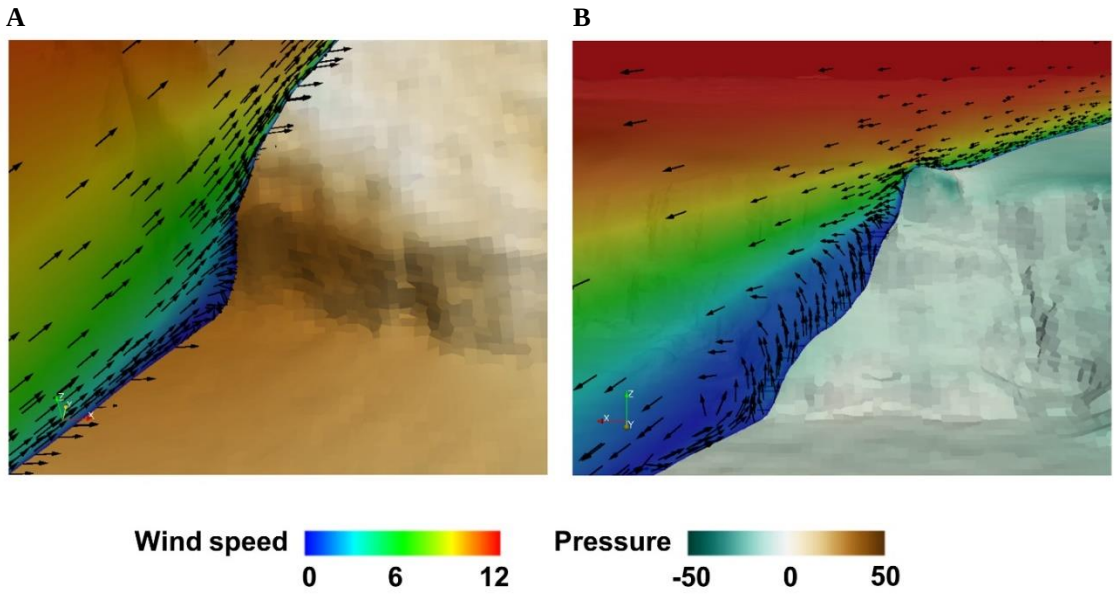

Figure S5. Wind speed and pressure over A) a windward cliff and B) a leeward cliff on Skomer, in a SW wind. In each case the cliff face is the section to the right, which is represented in 3 dimensions and coloured according to the gauge pressure (that is, relative to the initial condition set in OpenFoam) distribution 2 m normal to the surface. The associated 2-dimensional vertical profile of mean wind speed is indicated in colour to the left of the cliff. Arrows indicate the mean flow vectors. Together, these illustrate how the flow onto a windward cliff result in high pressure, and low pressure develops in sheltered leeward sites.

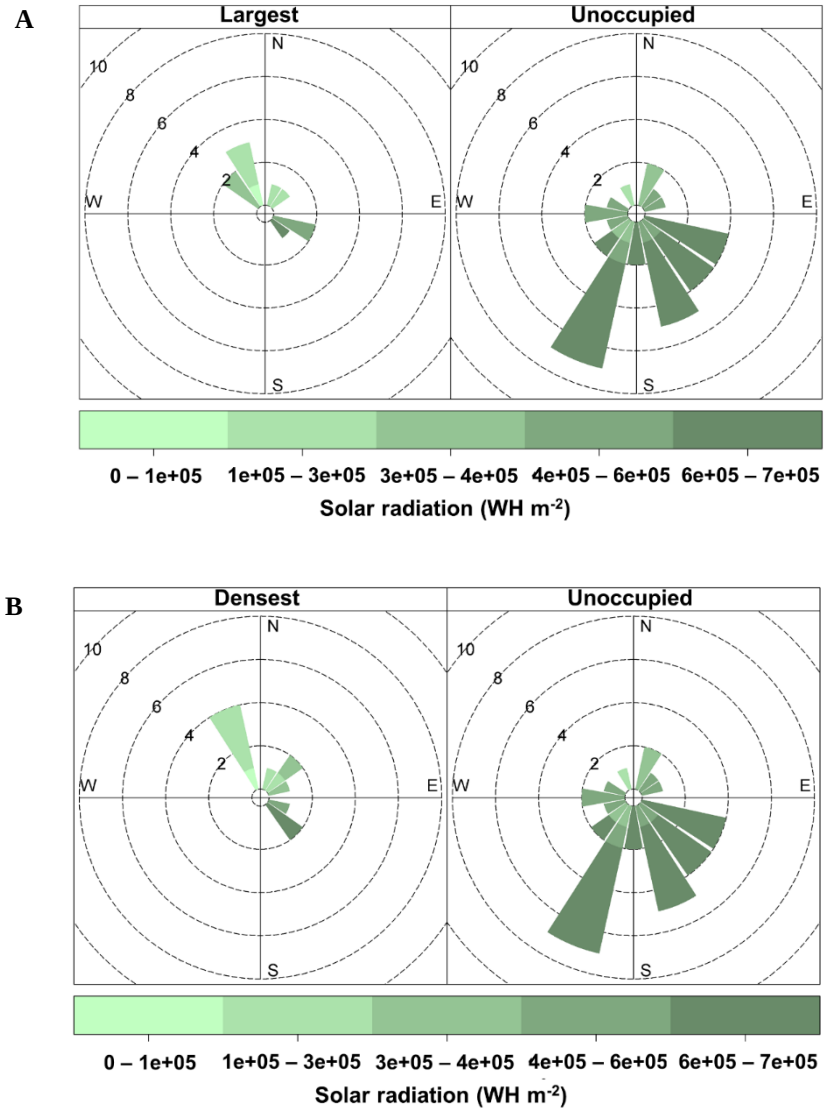

Figure S6. Total mean solar radiation during the breeding season in 2015 (Watt hours sq. m) on Skomer, according to whether cliff sections were home to the A) largest colonies, B) densest colonies or unoccupied. Grid circles represent number of cliffs/ colonies, with radiation intensity indicated by the colour scale.

Table S1. Wind data for the months of March to August 2007-2017, representing the guillemot breeding season. Data are from the weather station at Wooltack point on the mainland (51° 42.581'N 5° 3.786'W), ~1 km from Skomer Island.

Direction	Count	Wind speeds <15 m s^{-1}	Wind speeds ≥15 m s^{-1}	% near gale winds within each group	% near gale winds from total obs	% near gale winds from total storms	Group direction % from total wind obs
SW	46096	44356	1740	3.77	0.77	20.36	20.52
W	37800	36365	1435	3.8	0.64	16.79	16.83
NW	32052	30308	1744	5.44	0.78	20.4	14.27
S	30223	29210	1013	3.35	0.45	11.85	13.46
N	24877	23490	1387	5.58	0.62	16.23	11.08
SE	21253	20538	715	3.36	0.32	8.37	9.46
NE	18573	18105	468	2.52	0.21	5.48	8.27
E	13746	13701	45	0.33	0.02	0.53	6.12

Table S2. Effect sizes for the Skomer habitat selection model, expressed as odds ratios. Odds ratios > 1 were estimated for predictors with a positive coefficient, odds ratios <1 were estimated for predictors with a negative coefficient, and odds ratios close to 1 were the result of predictors with a relatively small effect on the probability of a section being classified as a colony. Model predictors are listed in order of descending effect size.

	SW		**NW**		**SE**		**NE**	
Colony definition	**Term**	**Odds ratio**	**Term**	**Odds ratio**	**Term**	**Odds ratio**	**Term**	**Odds ratio**
Any count	PMedian TISkew MeanSlope	1.0e-01 2.1e-01 4.5e+00	TISkew TKESkew	1.4e-01 1.0e-01	TKEIQR MeanSlope	2.5e-01 6.6e+00	TKESkew MeanSlope HorizontalMedian	1.2e-02 1.7e+01 8.3e+00
Largest	PIQR HorizontalIQR MeanSlope	2.0e-03 2.9e+02 5.9e+01	TKESkew MeanSlope	2.6e-03 1.3e+01	MeanSlope	3.6e+01	TKEIQR HorizontalSkew MeanSlope	2.3e+03 7.0e-04 9.3e+01
Densest	PMedian	8.1e-02	TKESkew MeanSlope	1.6e-02 6.9e+00	MeanSlope	7.1e+00	TKEMedian U_2Median HorizontalSkew	3.9e+03 1.4e-02 3.5e-02

Sensitivity analysis

Table S3. The sensitivity analysis of the top simplest model terms for different thresholds of number of birds and number of largest colonies, with the prevailing SW wind. Significance is indicated with p-values: p< 0.001 (***), p< 0.01 (**), p< 0.005 (*).

Largest colonies / Number of birds threshold	**Top simplest model - terms**	**McFadden pseudo R^2 – OA/ TSS/ Sensitivity/ Specificity**
10/592	PIQR (*), HorizontalIQR (**), MeanSlope (***)	0.59 – 0.90/ 0.73/ 0.80/ 0.93
11/518	PIQR (*), HorizontalIQR (**), MeanSlope (***)	0.57 – 0.81/ 0.75/ 1.00/ 0.75
12/504	PIQR (*), HorizontalIQR (*), MeanSlope (***)	0.54 – 0.80/ 0.72/ 1.00/ 0.72
13/421	PIQR (n.s.), MeanSlope (*), PMedian (**), U_2IQR (**)	0.55 – 0.84/ 0.74/ 0.92/ 0.81
14/316	PIQR (*), MeanSlope (*), PMedian (**), U_2IQR (**)	0.52 – 0.82/ 0.67/ 0.85/ 0.81
15/314	PIQR (*), HorizontalIQR (n.s.), MeanSlope (**), PMedian (**), U_2IQR (**), U_2Skew (*)	0.64 – 0.93/ 0.87/ 0.93/ 0.93

Table S4. The sensitivity analysis of the top simplest model terms for different thresholds of number of birds and number of largest colonies, with NW wind. Significance is indicated with p-values: p< 0.001 (***), p< 0.01 (**), p< 0.005 (*).

Largest colonies / Number of birds threshold	**Top simplest model - terms**	**McFadden pseudo R^2 – OA/ TSS/ Sensitivity/ Specificity**
10/592	TKESkew (**), MeanSlope (**)	0.58 – 0.86/ 0.81/ 1.00/ 0.81
11/518	TKESkew (**), MeanSlope (**)	0.59 – 0.86/ 0.81/ 1.00/ 0.81
12/504	TKESkew (**), MeanSlope (**)	0.55 – 0.84/ 0.78/ 1.00/ 0.78
13/421	TKESkew (***), MeanSlope (*)	0.55 – 0.82/ 0.75/ 1.00/ 0.75
14/316	TKESkew (***), MeanSlope (**)	0.50 – 0.80/ 0.68/ 0.92/ 0.75
15/314	TKESkew (***), MeanSlope (**)	0.50 – 0.77/ 0.66/ 1.00/ 0.66

Table S5. The sensitivity analysis of the top simplest model terms for different thresholds of number of birds and number of largest colonies, with NE wind. Significance is indicated according to p-value: p< 0.001 (***), p< 0.01 (**), p< 0.005 (*).

Largest colonies / Number of birds threshold	**Top simplest model - terms**	**McFadden pseudo R^2 – OA/ TSS/ Sensitivity/ Specificity**
10/592	TKEIQR (**), HorizontalSkew (*), MeanSlope (**)	0.74 – 0.97/ 0.90/ 0.90/ 1.00
11/518	TKEIQR (**), HorizontalSkew (*), MeanSlope (**)	0.76 – 0.97/ 0.90/ 0.90/ 1.00
12/504	TKEIQR (**), HorizontalSkew (*), MeanSlope (**)	0.74 – 0.95/ 0.88/ 0.91/ 0.96
13/421	HorizontalSkew (*), TKEMedian (***), U_2Median (***)	0.67 – 0.80/ 0.72/ 1.00/ 0.72
14/316	HorizontalMedian (**), TKESkew (**), MeanSlope (***)	0.57 – 0.80/ 0.68/ 0.92/ 0.75
15/314	HorizontalMedian (**), TKESkew (**), MeanSlope (***)	0.59 – 0.89/ 0.70/ 0.73/ 0.96

Model of cliff orientation and slope angle

For the implementation of the mean cliff orientation and slope angle models, the same model selection was performed as for the airflow models, as described in the main text.

Table S6. Logistic regression models of leeward/ windward cliff orientation with respect to the prevailing SW wind on Skomer.

Colony definition	**Orientation model:** **McFadden pseudo R^2 – OA/ TSS/ Sensitivity/ Specificity**
Any count	Aspect + MeanSlope 0.17 – 0.63/ 0.30/ 0.42/ 0.87
10 largest	Aspect + MeanSlope 0.55 – 0.88/ 0.71/ 0.80/ 0.90
11 densest	Aspect 0.20 – 0.68/ 0.51/ 0.90/ 0.60

Chapter 6: Synopsis

The study of animal movement requires information on a diverse set of variables to characterise choices and behaviours in relation to a varying physical and biological environment. This in itself is a complex task. One of the things that has become inescapably clear during the course of this thesis is the particular challenge of characterising the aerial environment, which requires an understanding of disciplines beyond biology. In this PhD I had the privilege to work under the supervision of an interdisciplinary team, specialising in animal movement and meteorology. I also drew on my own background in computer science and physical geography. This all underpinned the use of a range of meteorological tools to estimate the movements of the air, namely reanalysis models in chapters 2 and 4, and CFD in chapter 5, which allowed me to visualise the invisible air-scape. These models are freely available, but meteorological expertise is required for the model set-up and the interpretation of the outputs. Chapter 2 is similarly interdisciplinary, particularly in the estimation of turbulence from the anemometer mounted onboard the ultralight. And while the general tendency is to borrow tools from other disciplines to advance biological questions, the development of new turbulence proxies from bird-borne sensors could ultimately provide insight that is relevant for meteorologists. Overall, the interdisciplinary approach allowed me to examine bird responses to the aerial environment across a range of scales, from hourly (used in relation to tropical cyclones), to seconds (which is necessary to understand the influence of chaotic elements of the air). The interdisciplinary aspect has therefore been integral to this PhD, shaping the way it was conceived and has developed, the insights I have gained, and my view of the natural world.

In this synthesis I will consider how the previous chapters sit within the broader field by touching on some of the questions that have arisen from the preceding chapters, analyses it would have been interesting to include had there been more time, and practical applications arising from chapter 5.

Chapters 2 and 3 examined fine-scale variation in turbulence and how this impacted pigeons, as a model flapping flier. Whilst it was exciting to find a marked effect of turbulence on a range of flight parameters, it was rather frustrating not to be able to draw definitive conclusions about how it affects flight effort. Nonetheless, ongoing trials may provide insight here, as pigeons equipped with the same data-loggers are being flown in a wind tunnel, with the aim of deriving biomechanical power from acceleration metrics. It will therefore be interesting

to see whether those results can provide fresh insight into the effects of turbulence on flight power, potentially working in collaboration with aerodynamicists.

Another aspect that it would be fascinating to explore would be how the metabolic costs of flight vary in relation to extreme winds. Many of the GPS units deployed on streaked shearwaters also included accelerometers. Acceleration data from birds flying in storms should allow us to examine the proportion of time spent flapping in relation to the wind vector (Spivey et al., 2014). Whilst flight costs decrease with wind speed for dynamic soaring birds (e.g. Furness and Bryant, 1996), this relationship has only been examined in typical wind conditions. Published data from 7 shearwaters showed that these birds flapped for 1 - 70% of time during foraging (Sato et al., 2009), and a large part of this variability is likely to be due to changes in wind speed. It would be interesting to see whether there is a threshold wind speed, above which, flight effort increases due to the need for increased flight control or speed, when operating in extreme conditions. Such relationships may provide insight into the maximum wind speeds in which these birds are able to operate, and therefore, the wind speeds they need to avoid.

The main focus of this thesis is behavioural responses to airflows, whether they be through adjustments to the flight path, flight speed or kinematics. In order to respond to airflows, birds must be able to detect them, but there are surprisingly few studies on the cues birds and other flying animals use to achieve this, beyond the use of social information (Williams et al., 2018). Turbulence and updraughts are both influenced by surface features (i.e. topography, forest canopy and land cover) (De Visscher, 2013, Stull, 1988). Therefore birds may use information about landscape features to predict the likely distribution of turbulence, irrespective of whether that has a positive or negative impact on flight costs. Sound could also be used to detect turbulence, as pigeons have been shown to respond to local pressure oscillations, or the "wind noise" sometimes called pseudo-sound (Pye and Langbauer, 1998), which is linked to turbulence (Kreithen, 1978, Kreithen and Keeton, 1974). Similarly, infrasound has been proposed as a signal that, together with other environmental cues such as wind strength and direction, may be detected by seabirds to forecast the arrival of tropical cyclones even when these are located hundreds of kilometres away (Weimerskirch and Prudor, 2019).

The results in chapter 4 imply that birds have information on a cyclone's trajectory, as shearwaters adapted their movements according to their position with respect to the cyclone, as

well as the cyclone strength. It would therefore be interesting to examine the fine-scale movements of shearwaters in the Sea of Japan more closely in relation to approaching cyclones (Chacko, 2019, Chen et al., 2020). Previous studies of the impact of tropical cyclones on seabird behavioural states have identified significant changes in activity levels associated with environmental conditions (Wilkinson et al., 2019). Hidden Markov Models could therefore be used to distinguish switches between behaviours (Conners et al., 2021) or identify shifts in their intensity (i.e. more/ less intense searching or foraging) in the shearwater dataset, and assess this in relation to wind speed and direction, pressure, or the possible propagation of infrasound, to provide insight into the particular cues that birds might be using.

Chapter 5 is something of an outlier, in that it deals with the distribution of breeding birds, rather than individual movement trajectories. However, the core theme remains the same, which is how birds deal with strong and/ or unsteady flows. The initial justification for this study was the finding that strong winds impede the ability of auks to land at their nesting sites (Shepard et al., 2019). While this may well be a factor that influences nest site selection, it was not possible to say whether this was more or less important than the need for shelter from storm conditions, which potentially include rain and strong swell.

The wind may play an even more important role in influencing take-off or landing performance for larger seabirds, which often nest in exposed areas that could help them achieve high flight speeds at take-off, and improve control during landing (e.g. by using updrafts). During my PhD I started to investigate some of these links in Northern gannets (*Morus bassanus*) on Ailsa Craig, Scotland, (55°15'10.60"N, 5° 6'57.83"W) where there are location data for nesting birds. Unusually, there are also a relatively high number of records of injured birds found beneath the breeding cliffs that had sustained fractures to their neck or wings, consistent with birds crashing during landing or take-off (Wanless, 1979). Crashes may well occur on other islands, but as breeding colonies tend to terminate in the water, as opposed to the talus slopes seen on Ailsa, they are less likely to be fatal. Nonetheless, the carcasses are an important indication that landing and/ or take-off can be risky, and that gannets may adapt their breeding site selection accordingly.

Gannets on Ailsa breed on the West and South cliffs, which are exposed to the prevailing winds, and likely associated with updrafts. In contrast, the East-facing slopes are avoided, and these would typically be in the “down-curl” i.e. experience downdrafts in prevailing winds. Preliminary analysis of the number of gannet carcasses below the breeding

cliffs pointed to an increase in carcass number under certain wind speeds and directions. I started modelling the airflows around this island (Fig.1B and it seems that the mortality rate is negatively correlated with the wind speed at the breeding cliffs (Fig. 1A). This provides further evidence that not only does the wind directly impact take-off and/ or landing capacity, but critically, this can have fitness consequences.

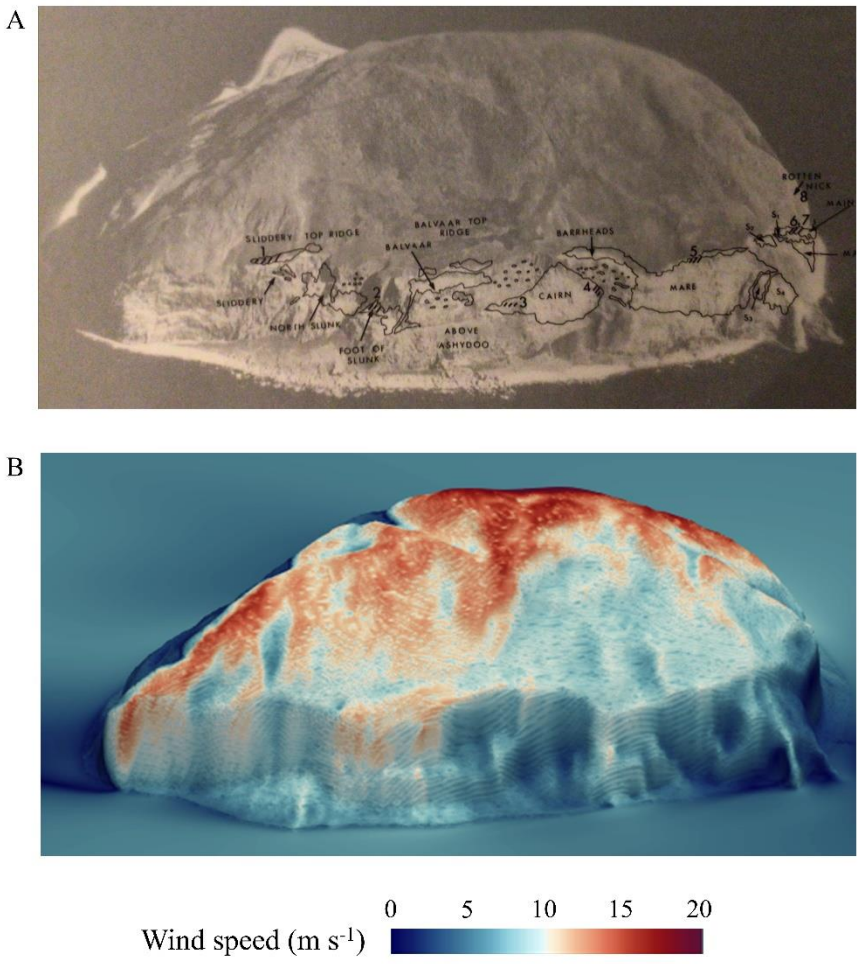

Figure 1. Colony distribution and airflows on Ailsa Craig. A) the distribution of colonies at the West side of Ailsa Craig taken from Wanless (1979), B) the OpenFoam model output of mean wind speed (m s^{-1}) over Ailsa Craig under south-westerly winds. In the lower parts of the cliffs the flow is blocked (similar to Skomer), leading to lower wind speeds compared to the higher parts of the island and the summit where flow is accelerating.

This highlights the importance of understanding the relationship between the aerial environment and habitat quality for nesting birds. This is particularly pertinent for seabirds due to (i) their exposure to strong winds, (ii) their conservation status and (iii) their vulnerability to

expanding human activities such as marine renewable energy devices (Matthiopoulos et al., 2022). Indeed, the ability to predict habitat suitability could be important in identifying locations for species re-introductions or re-establishment. For instance, in the 1700s northern gannets are believed to have bred on the Calf of Man (54° 3'4.64"N, 4°48'50.73"W), a small island off the south coast of the Isle of Man. Here, I am planning to perform CFD simulations to inform the suitability of locations for re-establishing a gannet colony in collaboration with the wardens of the Isle of Man.

In this thesis I have investigated the effects of extreme and variable flows on birds across a range of temporal and spatial scales. Such a range of scales is often necessary if we are to track the impact of the environment from its immediate effects on the locomotion costs and/ or capacities, through to macro-ecological patterns. For example, terrestrial soaring birds distributions and pathways are known to be influenced by the availability of thermals updrafts, and the effects of this form of turbulence on flight costs and long range movement is well described in the literature (e.g. Scacco et al., 2019). But in chapter 2, I found that freestream turbulence also affects a range of path and kinematic variables for a flapping flier, in agreement with previous wind tunnel experiments (Ortega-Jimenez et al., 2014, Ravi et al., 2015) although interestingly there was no suggestion that birds adapted their space-use in response. In the 5th chapter I identified that the distribution of a colonial seabird is affected by a need to shelter from storms/ waves. However this can also be relevant at larger regional scales. As the frequency and intensity of severe storms increases with climate change, the distribution of storms is also affected, and a poleward expansion is already projected (Studholme et al., 2022). This can have implications for seabirds not only in the suitability of breading habitat, but also on their response in-flight. In chapter 4, I identified a surprising strategy from a dynamic soaring bird, but if climate change leads to shifts in the distribution of breeding birds it is not known whether it can add a selective pressure by exposing more species to extreme weather events or species that are less capable in responding to them than for example adult streaked shearwaters (there are no reports of adult streaked shearwater wrecks). Therefore, this thesis suggests that the effects of extreme and variable wind must be examined across scales, in order to form an adequate understanding of different biological processes as these range from fine scale responses to turbulence and storms, to larger scales regional distributions and long range movement.

Overall, one of the main messages I retain from this PhD is how much more there is for us to understand about the aerial environment and its effects on birds. The famous phrase from

Sir Isaac Newton: “what we know is a drop, what we do not is the ocean”, appears to be very true when examining the direct response of flying animals to challenging conditions. For example, chapter 4 revealed a surprising response of shearwaters to cyclones, with birds seemingly flying towards the eye to control the part of the cyclone they were exposed to. But understanding how their behavioural response influences the strength and nature of the systems they can, and cannot, respond to, remains a complex task. The same can be said for understanding responses to turbulence. Nonetheless, I feel fortunate and excited to have been part of this collective journey and I hope that my contribution here will add another “drop” to the understanding of how the aerial world beyond “normal” can affect animal movement and space-use.

References

Chacko, N. 2019. Differential chlorophyll blooms induced by tropical cyclones and their relation to cyclone characteristics and ocean pre-conditions in the Indian Ocean. *Journal of Earth System Science,* 128**,** 1-11.

Chen, M., Pattiaratchi, C. B., Ghadouani, A. & Hanson, C. 2020. Influence of storm events on chlorophyll distribution along the oligotrophic continental shelf off south-western Australia. *Frontiers in Marine Science,* 7**,** 287.

Conners, M. G., Michelot, T., Heywood, E. I., Orben, R. A., Phillips, R. A., Vyssotski, A. L., Shaffer, S. A. & Thorne, L. H. 2021. Hidden Markov models identify major movement modes in accelerometer and magnetometer data from four albatross species. *Movement ecology,* 9**,** 1-16.

De Visscher, A. 2013. *Air dispersion modeling: foundations and applications*, John Wiley & Sons.

Furness, R. W. & Bryant, D. M. 1996. Effect of wind on field metabolic rates of breeding northern fulmars. *Ecology,* 77**,** 1181-1188.

Kreithen, M. L. Sensory Mechanisms for Animal Orientation — Can Any New Ones be Discovered? Animal Migration, Navigation, and Homing: Symposium Held at the University of Tübingen, August 17-20, 1977, 1978. Springer, 25.

Kreithen, M. L. & Keeton, W. T. 1974. Detection of changes in atmospheric pressure by the homing pigeon, Columba livia. *Journal of comparative physiology,* 89**,** 73-82.

Matthiopoulos, J., Wakefield, E., Jeglinski, J. W., Furness, R. W., Trinder, M., Tyler, G., Mccluskie, A., Allen, S., Braithwaite, J. & Evans, T. 2022. Integrated modelling of seabird-habitat associations from multi-platform data: A review. *Journal of Applied Ecology*.

Ortega-Jimenez, V. M., Sapir, N., Wolf, M., Variano, E. A. & Dudley, R. 2014. Into turbulent air: size-dependent effects of von Kármán vortex streets on hummingbird flight kinematics and energetics. *Proceedings of the Royal Society B: Biological Sciences,* 281**,** 20140180.

Pye, J. & Langbauer, W. 1998. Ultrasound and infrasound. *Animal acoustic communication.* Springer.

Ravi, S., Crall, J. D., McNeilly, L., Gagliardi, S. F., Biewener, A. A. & Combes, S. A. 2015. Hummingbird flight stability and control in freestream turbulent winds. *Journal of Experimental Biology,* 218**,** 1444-1452.

Sato, K., Sakamoto, K. Q., Watanuki, Y., Takahashi, A., Katsumata, N., Bost, C.-A. & Weimerskirch, H. 2009. Scaling of soaring seabirds and implications for flight abilities of giant pterosaurs. *PloS one,* 4**,** e5400.

Scacco, M., Flack, A., Duriez, O., Wikelski, M. & Safi, K. 2019. Static landscape features predict uplift locations for soaring birds across Europe. *Royal Society open science,* 6**,** 181440.

Shepard, E., Cole, E.-L., Neate, A., Lempidakis, E. & Ross, A. 2019. Wind prevents cliff-breeding birds from accessing nests through loss of flight control. *Elife,* 8**,** e43842.

Spivey, R., Stansfield, S. & Bishop, C. 2014. Analysing the intermittent flapping flight of a Manx Shearwater, Puffinus puffinus, and its sporadic use of a wave-meandering wing-sailing flight strategy. *Progress in Oceanography,* 125**,** 62-73.

Studholme, J., Fedorov, A. V., Gulev, S. K., Emanuel, K. & Hodges, K. 2022. Poleward expansion of tropical cyclone latitudes in warming climates. *Nature Geoscience,* 15**,** 14-28.

Stull, R. B. 1988. *An introduction to boundary layer meteorology,* Springer Science & Business Media.

Wanless, S. 1979. *Aspects of population dynamics and breeding ecology in the gannet (sula bassana (l.)) of ailsa craig,* University of Aberdeen (United Kingdom).

Weimerskirch, H. & Prudor, A. 2019. Cyclone avoidance behaviour by foraging seabirds. *Scientific reports,* 9**,** 1-9.

Wilkinson, B. P., Satgé, Y. G., Lamb, J. S. & Jodice, P. G. 2019. Tropical cyclones alter short-term activity patterns of a coastal seabird. *Movement ecology,* 7**,** 1-11.

Williams, H. J., King, A. J., Duriez, O., Börger, L. & Shepard, E. L. 2018. Social eavesdropping allows for a more risky gliding strategy by thermal-soaring birds. *Journal of the Royal Society Interface,* 15**,** 20180578.